

The effects of smoking on inflammatory and angiogenic pathways in the retina of mice

Inaugural dissertation

to obtain the degree of doctor of human biology

of the Faculty of Medicine

of the Justus-Liebig-University Giessen

submitted by

Feng Wang

from

Shandong, China

Giessen 2022

From the Department of Ophthalmology

Acting Director (Research and Teaching): Prof. Dr. Dr. Knut Stieger

Faculty of Medicine

Justus-Liebig-University of Giessen, Germany

First Supervisor and Committee Member: Prof. Dr. Dr. Knut Stieger

Second Supervisor and Committee Member: PD Dr. Wadim Bowl

Committee Member: Prof. Bernd Ishaque

Date of Doctoral Defense: 20.06.2022

CONTENTS

CONTENTS	I
ABBREVIATIONS	IV
1 INTRODUCTION.....	1
1.1 The human eye	1
1.2 The structure and function of neural retina	1
1.3 Structure and function of the RPE.....	2
1.4 Structure and function of the choroid.....	3
1.5 The pathological features of age-related macular degeneration.....	4
1.6 The correlation between cigarette smoking and AMD	9
1.7 Electronic cigarette.....	12
1.8 Fibroblast growth factor10	14
1.9 The function of Fgf10	16
1.10 The aims of this study	17
2 MATERIALS AND METHODS	19
2.1 Materials.....	19
2.1.1 Reagents and consumables	19
2.1.2 Equipment.....	21
2.1.3 Buffer preparation.....	21
2.2 Methods.....	22
2.2.1 Conventional cigarette smoke exposure	22
2.2.2 E-cigarette vapor exposure	23
2.2.3 Transgenic mouse generation	25
2.2.4 The C-cigarette smoke exposure for transgenic mice.....	26
2.2.5 Induction of Fgf10 overexpression.....	27
2.2.6 Optical Coherence Tomography scan and retinal images acquisition for the mice of the Fgf10 OE + 12w Re subgroup.	28
2.2.7 Retinal layers thickness measurement for the mice of the Fgf10 OE + 12w Re subgroup.	28
2.2.8 Retinal blood vessel tortuosity measurement for Fgf10 OE transgenic + 12 w Re (no/+ Dox) mice	29

2.2.9	Dissection of neural retina, RPE, choroid/scleral tissues	31
2.2.10	Extraction of total RNA and protein.....	33
2.2.11	Extraction of protein with 1× PBS buffer.....	36
2.2.12	Concentration determination of total RNA and protein samples.....	36
2.2.13	Quality control of total RNA	36
2.2.14	Reverse transcription synthesis of complementary DNA (cDNA).....	37
2.2.15	Real-time PCR (RT-PCR)	39
2.2.16	Enzyme-linked immunosorbent assay (ELISA).....	41
2.3	Data statistics	46
3	RESULTS.....	48
3.1	Neural retinal tissue develops an inflammatory reaction to C-cigarette smoke and E-cigarette vapor in mice	48
3.1.1	The effect of C-cigarette smoke or E-cigarette vapor exposure on neural retina	48
3.1.2	Comparing the effect of C-cigarette smoke with E-cigarette vapor (nicotine-free or nicotine-containing) on neural retinal tissue	50
3.1.3	Comparing the different effects of medium- and long-term exposure of E-cigarette vapor on RPE and choroid	51
3.1.4	The comprehensive effects of medium- or long-term exposure of E-cigarette (nicotine-free vs nicotine-containing) vapor on neural retina, RPE and choroid	53
3.2	Does Fgf10-overexpression have protective effect on the retina of smoking mice model?	55
3.2.1	The Fgf10 mRNA expression in neural retina of Fgf10 OE transgenic (no/ + Dox) mice.	55
3.2.2	Cytokine expression in the neural retina of Fgf10 OE transgenic + 12 w Re (no/+Dox) mice.....	57
3.2.3	Protein expression levels and change with extend of regeneration in the neural retina of Fgf10 OE mice + Re (no/+ Dox).....	59
3.2.4	In vivo retinal layer thickness changes in Fgf10 OE mice + 12 w Re (no/+ Dox) measured by OCT	61
3.2.5	The effect of long-term smoke exposure or Fgf10-overexpression on mouse retinal vasculature tortuosity.....	62
4	DISCUSSION	64

4.1	Neural retinal tissue develops an inflammatory reaction to C-cigarette smoke and E-cigarette vapor in mice	64
4.1.1	The short-term E-cigarette vapor exposure has limited pro-inflammatory effect on neural retina	65
4.1.2	The medium-term E-cigarette vapor (nicotine free and nicotine containing) exposure promotes inflammation and angiogenesis, key pathways in AMD pathogenesis.....	65
4.1.3	The mechanistic effects of E-cigarette vapor on retinal tissue	66
4.1.4	The different effects of C-cigarette smoke and E-cigarette vapor on neural retina	68
4.1.5	The nicotine ingredient in E-cigarette vapor might weaken the harmful effects..	69
4.1.6	The long-term E-cigarette vapor (nicotine containing) exposure can promote angiogenesis in choroid tissue	69
4.2	Does Fgf10-overexpression have a protective effect on retinal tissue in mice exposed to smoke?	71
4.2.1	Both long-term smoking exposure and Fgf10 overexpression do not impact retinal thickness	71
4.2.2	Fgf10 overexpression during regeneration results in changes to the retinal vascular tortuosity induced by smoke exposure	72
4.3	The limitations of the study	73
5	SUMMARY	75
6	ZUSAMMENFASSUNG	77
7	REFERENCES	79
8	ACKNOWLEDGEMENTS	90
9	CURRICULUM VITAE	错误!未定义书签。
10	LIST OF PUBLICATIONS.....	93
11	EHRENWÖRTLICHE ERKLÄRUNG.....	94

ABBREVIATIONS

AMD	Age related macular degeneration
ANOVA	Analysis of variance
bp	Base pair
BRB	Blood-retinal barrier
BrMb	Bruch's membrane
°C	Degree Celsius
C-cigarette	Conventional cigarette
CCS	Conventional cigarette smoke
cDNA	Complementary DNA
CNS	Central nervous system
CNV	Choroidal neovascularization
d	Day
ddH ₂ O	Double-distilled water
dNTP	Deoxyribonucleotide triphosphate
Dox	Doxycycline
E-cigarette	Electronic cigarette
ECV	Electronic cigarette vapor
ELISA	Enzyme linked immunosorbent assay
ELM	External limiting membrane
Fgf10	Fibroblast growth factor10
FgfR	Fibroblast growth factor receptor
Fgfs	Fibroblast growth factors
g	Gram
GCL	Ganglion cell layer
h	Hours
iBRB	Inner Blood-retinal barrier
Ig	Immunoglobulin

IL-1 β	Interleukin 1 beta
ILM	Inner limiting membrane
INL	Inner nuclear layer
iNOS	Inducible nitric oxide synthases
IOP	Intraocular pressure
IPL	Inner plexiform layer
IR	Inner retinal layer
I/OS	Inner/Outer photoreceptor segment
IS	Inner segment of photoreceptor
3 m	3 months
8 m	8 months
mg/kg	Milligram/ Kilogram
Mix	Mixture
Min	Minutes
mL	Milliliter
mM	Mmol/L
MMP-9	Matrix metalloproteinase-9
nAChR	Nicotinic acetylcholine receptors
NF- κ B	Nuclear factor kappa B
NFL	Nerve fiber layer
NO	Nitric oxide
Nrf2	Nuclear factor E2-related factor 2
NT	Nicotine
nt	Nucleotide
oBRB	Outer Blood-retinal barrier
OCT	Optical coherence tomography
O.D.	Optical Density
OE	Overexpressed
ONL	Outer nuclear layer

ONL +	Outer nuclear layer +
OPL	Outer plexiform layer
OR	Outer retinal layer
OS	Outer segment of photoreceptor
PBS	Phosphate buffered saline
PEDF	Pigment epithelium derived factor
PI3K-AKT	Phosphatidylinositol-3 kinase/protein kinase B
PLC γ 1	Phospholipase C gamma 1
RAP	Retinal angiomatous proliferation
RAS-MAPK	RAS-mitogen-activated protein kinase
Re	Regeneration
RNF	Retinal nerve fiber
ROS	Reactive oxygen species
RPE	Retinal pigment epithelium
RT-qPCR	Quantitative real time polymerase chain reaction
SD	Standard deviation
Sec	Seconds
TGF- β	Transforming growth factor- β
TLR4/NF- κ B	Toll-like receptor 4/nuclear factor kappa B
TNF- α	Tumor necrosis factor alpha
μ L	Microliter
VEGF	Vascular endothelial growth factor
Vol.	Volume
2 w	2 weeks
WR	Whole retinal layer
WT	Wild type
wt.	Weight

1 INTRODUCTION

1.1 The human eye

The human eye (Fig. 1) is a complex optical system and enables the perception of optical stimuli by detecting light and converting it into electrochemical impulses in neurons. Light enters the eye through the cornea and lens, passes through the vitreous and focuses on the retina, resulting in a focused two-dimensional image of the visual world.

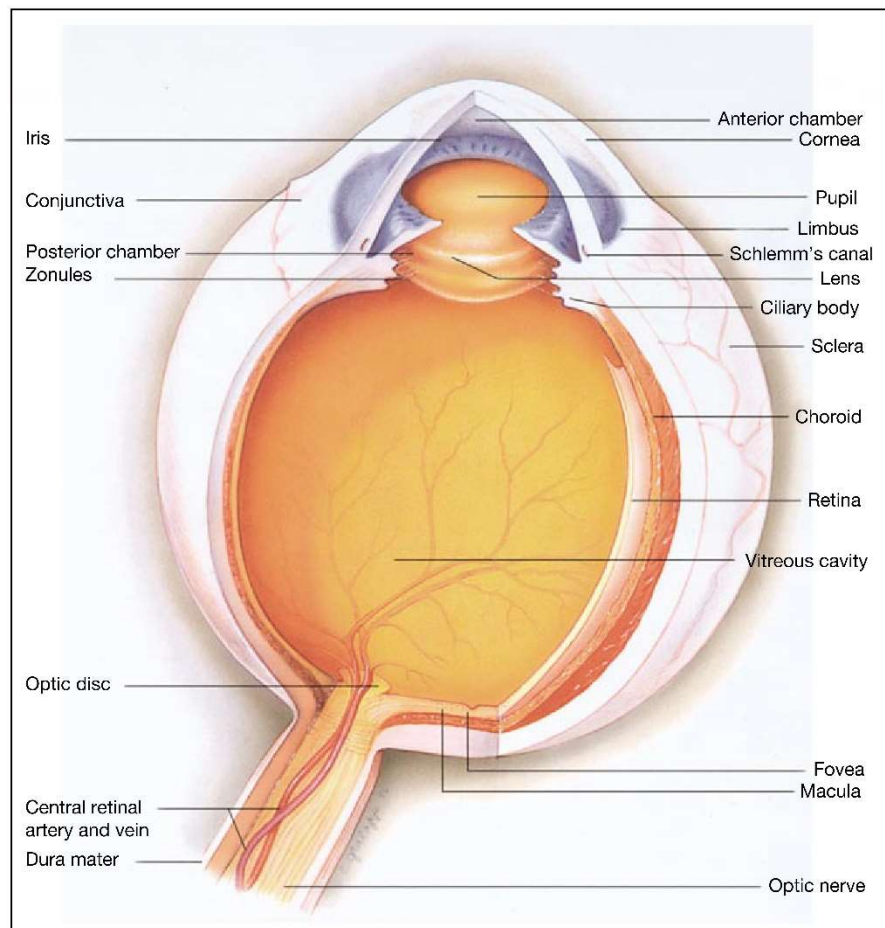


Figure 1. The anatomy schematic diagram of human eyeball (reproduced with permission from Kaplan's paper¹⁾)

1.2 The structure and function of neural retina

The neural retina is a light-sensitive layer that is located in the back of eyeball, upon

which the images are received². It contains several layers of neurons interconnected by synapses, and is supported by the retinal pigment epithelial (RPE) layer (Fig. 2-A, B). The neural retina is comprised of (from inner to outer end): inner limiting membrane (ILM), nerve fiber layer (NFL), ganglion cell layer (GCL), inner plexiform layer (IPL), inner nuclear layer (INL), outer plexiform layer (OPL), outer nuclear layer (ONL), external limiting membrane (ELM), inner segment of photoreceptor (IS), and outer segment of photoreceptor (OS). The outer surface of the neural retina and RPE are tightly connected with the choroid².

In the neural retina, the primary light sensing cells are rods and cones. These two classic photoreceptor cell types mainly contribute to night-time vision (scotopic conditions) and day-time vision (photopic conditions), respectively³. Besides, as a third type of light sensitive cells, intrinsic photosensitive ganglion cells, was discovered during the 1990s^{4,5}. They play a role in the entrainment of the circadian rhythm, pupillary reflex, and response to blue light. The photoreceptors absorb light and then transmit the light signals through the optic nerve to the brain.

The macula is the oval-shaped, pigmented (yellow colour) (Fig 1.) part near the posterior pole of the retina in the human eye, with a diameter of approximately 5.5 mm. The photoreceptor cells in the macula, are mainly cones, which generate sharp, clear, and high-acuity vision. The central area of the macula is called the fovea, which contains exclusively cones. Hence, as the key part of the retina, the fovea generates the highest visual acuity⁶.

In the development of the vertebrate embryo, both retina and optic nerve originate as outgrowth of the developing brain. Therefore, the retina is commonly considered as the extension part of the central nervous system (CNS)⁷. Additionally, the retina and CNS display similarities involved in the anatomy and functionality as well as immunology⁸.

1.3 Structure and function of the RPE

The RPE layer is a highly specific and polarized pigmented cell monolayer, which

firmly attaches to the underlying choriocapillaris and overlying photoreceptors (Fig. 2-A, B). The RPE monolayer not only contributes as one part of the outer blood-retinal barrier (oBRB), but also regulates the movement of solutes and nutrients from choroid to the sub-retinal space. It plays critical roles in maintaining the health of the neural retina, such as (1) absorption of excessive light to protect the neural retina from photooxidation, (2) phagocytosis and degradation of the shed photoreceptor outer segments, (3) secretion of various essential mediators and cytokines including vascular endothelial growth factor (VEGF) and pigment epithelium-derived factor (PEDF) to maintain the structural integrity and normal function of neural retina, (4) participation in the visual cycle, (5) transportation of nutrients to the neural retina from choroid tissues^{9,10}. As one part of oBRB, the tight junctions between adjacent RPE cells plays a vital role in preventing molecules from entering the neural retina¹¹.

1.4 Structure and function of the choroid

The choroid (Fig. 1) is a highly vascularized and pigmented tissue layer of the eyeball. It lies between RPE and sclera, and is comprised of blood vessels, resident immunocompetent cells, melanocytes, fibroblasts and supporting collagenous as well as elastic connective tissue. The choroid is multifunctional: it is able to supply oxygen and nutrition to the RPE and outer neuronal retina, it prevents the retina from overheating by heating dissipation, it absorbs excessive light, and it modulates the intraocular pressure (IOP) via vasomotor control of blood flow¹². The dense network of blood vessels in the choroid is named choriocapillaris, which is adjacent to the Bruch's membrane beneath of RPE. The choriocapillaris supplies oxygen and metabolites, and is also responsible for the removal of metabolites from neuronal retina^{13,14}. However, along with aging, the density of choriocapillaris will decrease¹⁵.

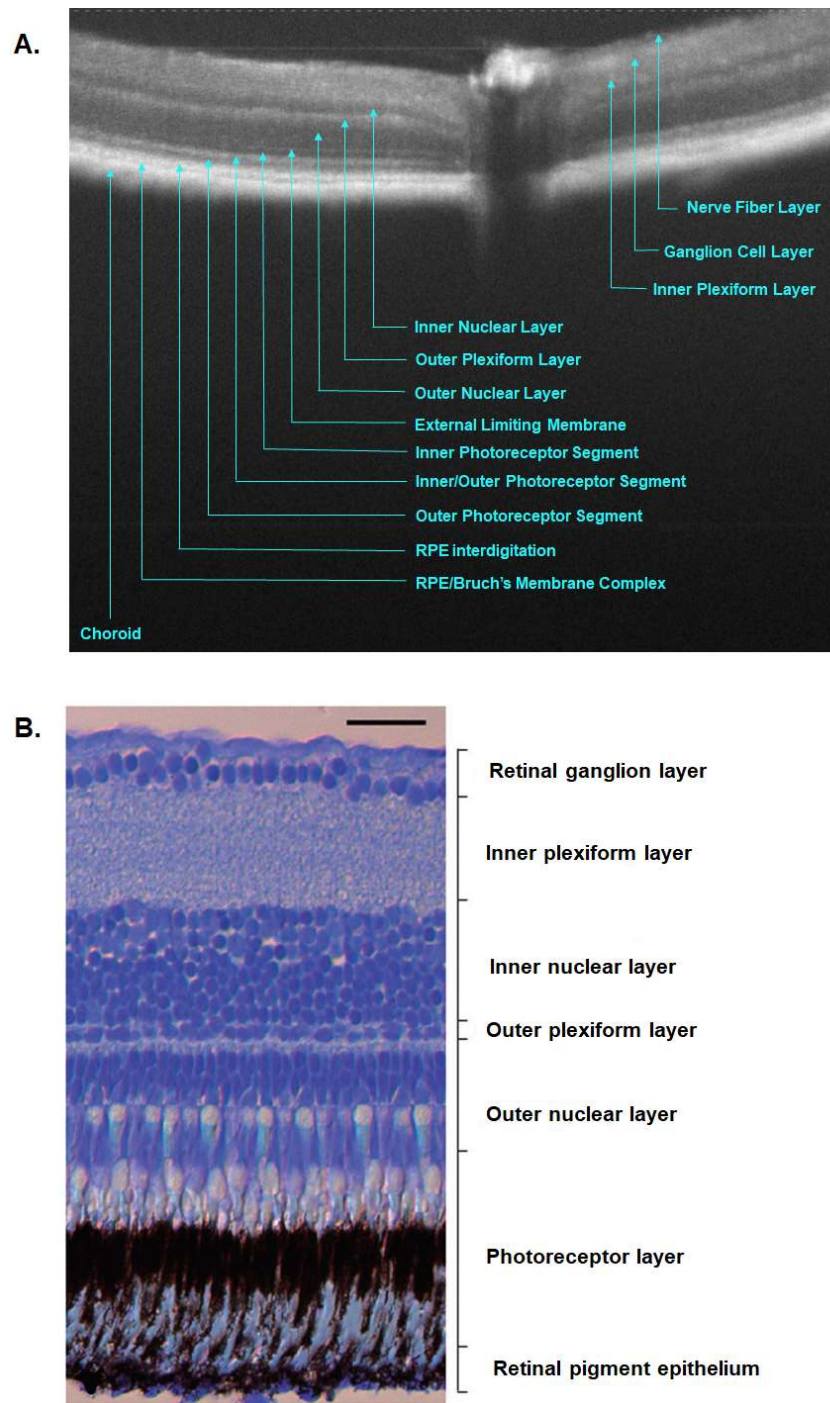


Figure 2. (A) In vivo retinal layer cross-section image generated by optical coherence tomography (OCT) from a healthy mouse. (B) Histological appearance of the neural retina, RPE layers (reproduced with permission from Gramage's paper¹⁶).

1.5 The pathological features of age-related macular degeneration

Age related macular degeneration (AMD) is an extremely complex, multifactorial

disorder characterized by the degeneration of photoreceptors, RPE and choriocapillaris¹⁷. AMD is a leading cause of irreversible blindness in individuals older than 65 years of age around the world, especially in developed countries, and the incidence is increasing along with age¹⁸. With the extension of human life, the number of people suffering from visual impairment caused by AMD is gradually increasing. It is projected that the number of worldwide AMD patients will rise to approximately 300 million by 2040, which will impose a heavy economic burden on the public system¹⁹. Although there are numerous studies probing the aetiology of AMD over the years, the complete and comprehensive underlying pathogenic mechanisms have not yet been identified due to the multifactorial nature, posing a stringent need to understand the pathogenesis of this disorder and further develop effective treatments in the global ophthalmology field.

Based on the presence or absence of blood vessels that have disruptively invaded the neural retina of AMD patients, AMD is mainly classified into a dry (also called non-neovascular or atrophy) and a wet (also named neovascular or exudative) form. The dry form accounts for 80-90% of all AMD cases, and 10-20% of them can develop into wet AMD. The dry form can cause a certain degree of vision loss or impairment slowly. Patients suffering from the wet form of AMD lose vision rapidly if they do not receive effective treatment. Generally, most AMD patients start with dry AMD and then progress to wet AMD at a later stage. Therefore, dry AMD is commonly considered as a risk factor or initial stage of wet AMD²⁰. In recent years, an increasing number of studies on the treatment of wet AMD have been conducted providing various options for decelerating the progress of wet AMD, such as anti-VEGF intravitreal treatment²¹⁻²³. However, up to date, there is still no effective treatments for dry AMD available.

The fundus pathological changes in the two forms of AMD are different. In dry AMD (Fig. 3-B), at the early stage of the disorder, the lipofuscin accumulates in RPE cells together with the appearance/enlargement of yellow drusen between the RPE cell layer and Bruch membrane beneath the macula area. With the development of disease,

the RPE cells get damaged and even lost, causing the formation of geographic atrophy, which leads to the degeneration of photoreceptor over time (Fig. 3-E)²⁴. On the other hand, the wet form of AMD (Fig. 3-C) is mainly characterized by choroidal neovascularization (CNV) and subretinal fibrosis formation (Fig. 3-F). CNV is characterized by newly formed blood vessels that sprout from choroid through breaks in the Bruch membrane (BrMb) into the subretinal space. Moreover, a second form of abnormal new blood vessel exists in patients with wet AMD, which is called retinal angiomatous proliferation (RAP), here, the neovascularization derives from the retinal circulation and reaches into the subretinal space, sometimes it can even anastomose with CNV^{25,26}. Since both CNV and RAP result in the growth of abnormal blood vessels with incomplete vascular wall structure, it frequently causes fluid and protein leakage beneath the macula, leading the retina to bulge or lift up from its normally flat position, ultimately resulting in irreversible damage to the photoreceptors and reduction of central vision¹⁸.

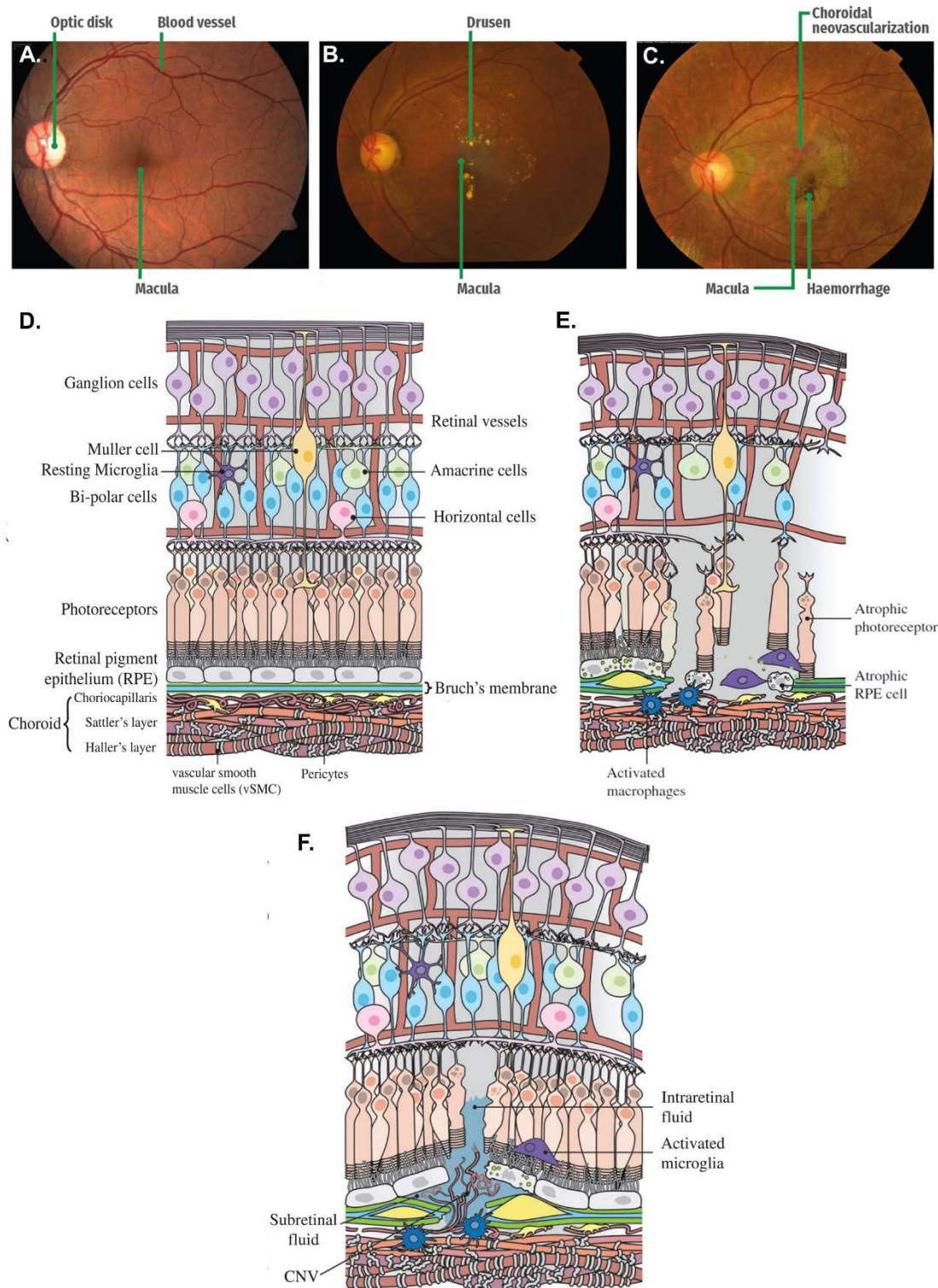


Figure 3. The fundus images and cross section schematic diagram of macula with dry or wet AMD. (A) Normal fundus photograph; (B) the fundus photograph of dry AMD with yellow drusen accumulated under the macular area; (C) the fundus photograph of wet AMD with fluid and protein leakage beneath the macula (A-C are reproduced with permission from Acharya's paper²⁷). The cross-section schematic diagram of normal macula (D) and with dry (E) as well as wet AMD (F). (D-F are reproduced with

permission from van Lookeren Campagne's paper²⁸).

In AMD, the mutual symbiotic relationship of the photoreceptor/RPE/BrMb/choriocapillaris complex is damaged²⁹. While the question of which component of the complex is affected first can vary in both types of AMD, the RPE dysfunction and damage is at the core of both types of AMD pathogenesis. In addition, the damage of RPE is considered as the hallmark of AMD^{18,20}. Since the RPE layer plays a critical role in maintaining the health of the neural retina^{9,10}, the functional deterioration of the RPE normally leads to impaired maintenance of the sensory neural retina, which results in a decreased vision in advanced AMD²⁴.

Although the exact pathogenesis of AMD has not yet been satisfactorily explained, some pathological mechanisms have been demonstrated to be involved in this disease, such as senescence, chronic/para-inflammation, and oxidative stress^{17,30,31}. It was reported that inflammation has a strong association with the pathogenesis of AMD^{32,33}. Numerous previous studies have confirmed that pro-inflammatory cytokines and inflammatory enzymes have a promotive effect in the occurrence and progression of AMD. For instance, there is a certain correlation between the onset of this disorder and elevated levels of interleukin-1 β (IL-1 β), tumour necrosis factor- α (TNF- α) and inducible nitric oxide synthesis enzymes (iNOS)^{24,34-36}. The IL-1 β and TNF- α can induce RPE cells to secrete excessive VEGF to promote the sprout and growth of CNV, which cause the onset and progression of wet AMD. In addition, both IL-1 β and TNF- α can damage oBRB by destroying the structure and function of RPE cells, and undermine the inner blood-retinal barrier (iBRB) by their direct cytotoxic effect on endothelial cells, thereby leading to the degeneration of RPE and photoreceptors. In general, the expression of inflammatory enzyme iNOS is induced under oxidative environment or in the presence of cytokines (e.g., inflammatory cytokines IL-1, TNF, IL-6). The expressed iNOS enzyme could further catalyse the production of large amounts of Nitric oxide (NO), and this catalysis process would last for a long time. NO is an important cellular signalling molecule, and is commonly involved in blood flow modulation, thrombosis, and some neural activities. In eyes, the proper level of NO not

only inhibits retinal neuron apoptosis by a signalling pathway, but also plays important roles in the regulation of blood flow, which benefits the eye keeping homeostasis^{37,38}. On the contrary, excessive NO can evoke oxidative damage, and react with superoxide anions to produce peroxynitrite, which would result in the neurodegeneration and cell apoptosis as well as vascular damage, and further induce retinopathy³⁸⁻⁴⁰. Sennlaub's study suggested that the expression of iNOS was involved in ischemic proliferative retinopathy by inducing the apoptosis of cells in the INL of the avascular retina⁴¹.

Numerous experimental studies (in vivo and vitro) have confirmed that VEGF, as a pro-angiogenic factor, plays a key role in regulating the formation of new blood vessels and the permeability of blood vessels. It is thus demonstrated as an important participant in the generation of CNV and the progression of wet AMD. Besides that, clinical evidences and Cochrane reviews both confirmed that intravitreal injection of anti-VEGF agents (e.g. ranibizumab, aflibercept, and bevacizumab) is one safe and effective treatment option for wet AMD^{42,43}. On the other hand, unlike those deleterious cytokines mentioned above, PEDF is a secreted protein with anti-angiogenic, anti-inflammatory, anti-tumorigenic, and neurotrophic functions. It participates in many physiological and pathophysiological mechanisms. Importantly, overexpressed PEDF can inhibit the development of retinal neovascularization and endothelial cell proliferation⁴⁴. In addition, PEDF is considered as the main endogenous angiogenesis inhibitor, suggesting a neutralizing effect over the pro-angiogenic potential of VEGF. Some studies have found that the expression levels of PEDF in RPE and choroid tissues from AMD patients are significantly reduced^{45,46}. Therefore, it was presumed that, once the VEGF expression increased or PEDF expression decreased, the balance between VEGF and PEDF would be impaired resulting in the development of CNV and wet AMD.

1.6 The correlation between cigarette smoking and AMD

The risk factors of AMD include among others age, genetics and environmental factors,

gender, and race⁴⁷. Concerning environmental factors, cigarette smoke is the strongest and the only avoidable factor. Some epidemiological studies have demonstrated a close correlation between smoking and the progression of AMD, as well as the potential of cigarette smoke to promote the occurrence and the development of early AMD into advanced states (geographic atrophy or neovascular leakage)⁴⁸⁻⁵⁰. Although these are robust evidences indicating a strong association between cigarette smoking and AMD, the exact mechanism to explain how and why cigarette smoking contributes to the pathophysiology of AMD has not yet been totally identified. The following hypothesis are currently discussed in the field:

- [1] **Oxidative stress.** Cigarette smoke generates numerous free radicals, which enter the systemic circulation and further induce oxidative damage in human tissues. The oxidative damage has been verified as one damage mechanism involved in the AMD progression. Experimental studies in animals showed that long-term exposure of mice to cigarette smoke would result in oxidative damage on fundus, which would further cause the ultrastructural degeneration of RPE and BrMb, and even induce the apoptosis of RPE^{51,52}. The dysfunction and degeneration of RPE causes a reduction of metabolic support from RPE to neural retina, which induces the apoptosis of the photoreceptors, and further promotes the progress of AMD^{53,54}.
- [2] **Hemodynamic changes and neovascularization.** The vascular model of AMD proposed by Friedman and co-workers showed that the change in choroidal vasculature is similar to those observed in atherosclerosis, and is one of the main reasons for the progression of AMD⁵⁵. Cigarette smoking promotes the process of atherosclerosis in blood vessels, including pathological processes such as vasculitis, vascular endothelial cell dysfunction, thrombus formation, and abnormal blood lipid accumulation⁵⁶. Other studies found that nicotine and other chemicals in cigarette smoke cause acute effects on the choroidal vascular tissue around the macula, leading to significant decrease of both blood flow rate and perfusion pressure in the choroidal capillary region⁵⁷. Furthermore, the nicotine ingredients in smoke with specific angiogenic properties further promote the development of

AMD⁵⁸. Noticeably, the gas phase of cigarette smoke also contains dioxins. By interacting with cytoplasmic dioxin receptors^{59,60}, the dioxins exhibit toxic effect in eyes, and promote the production of VEGF in neural retinal tissues and RPE cells, thereby facilitating the progression of advanced AMD and the onset of wet AMD⁶¹.

[3] **Inflammatory response and complement activation.** Inflammation plays an important role in the pathogenesis of AMD, which is probably caused by local cell damage, the accumulation of verrucous deposits in the BrMb, and/or the invasion of inflammatory cells⁶². Reactive oxygen species (ROS) can cause oxidative damage to tissues, and partially regulate the immune system by increasing the expression of pro-inflammatory genes⁶³. Meanwhile, the inflammatory response would in turn enhance the oxidative stress. In an experimental study concerning chronic lung disease, it was found that the increased secretion of pro-inflammatory cytokine (TNF- α etc.) and transforming growth factor- β (TGF- β) reduced the synthesis of antioxidant glutathione and further decreased the level of glutathione in cells, thereby leading to increased sensitivity of cells to oxidative damage⁶⁴. Moreover, cigarette smoke can also promote immune cells to activate the nuclear factor kappa B (NF- κ B) pathway, and produce and release inflammatory cytokines⁶⁵. Overall, the mutual promotion of oxidative stress and inflammatory response would amplify the tissue damage. Therefore, it is assumed that smoking increases the burden of RPE oxidative stress, induces an inflammatory response, and further promotes the progression of AMD.

In addition, a study has found that the inhibitor of the alternative complement pathway in smokers is lower compared to non-smokers⁶⁶. Although it is still unsure how the cigarette smoking increases the risk of AMD, it is assumed that complement-related genetic risk factors and cigarette smoke-induced complement cascade activation may synergistically promote the onset and development of AMD⁶². In general, the high concentrations of free radicals and the variety of toxic compounds contained in cigarette smoke not only deplete the antioxidant substances in RPE cells and harm the cells, but

also cause direct oxidative stress damage to RPE and other fundus tissues^{67,68}. Meanwhile, cigarette smoke can also promote the inflammatory response in fundus tissues⁶⁹. The oxidative stress damage and inflammatory response have a mutually promoting circulation effect, which would enhance the damage effect^{70,71}. The comprehensive effects of the various damages described above can eventually cause RPE degeneration and the formation of drusen, resulting in the development of dry AMD⁷¹. On the other hand, not only the cigarette smoke destroys BRB, nicotine and dioxins ingredients in smoke also have promotive effect in the production of CNV in choroid, thereby contributing to the progression of advanced AMD and the onset of wet AMD⁶¹.

Interestingly, by comparing the retinal layer thickness in smoker and non-smoker, the chronic smokers (≥ 25 years) have a thinner retinal (ganglion cell complex) thickness⁷². It suggests that smoking might also change the thickness of different retina layers. Since the retina is one of the body tissues with the highest metabolic activity and the highest rate of oxygen consumption per unit weight, the function of the retina is sensitive to oxygen tension, which is easily affected by the change of perfusion pressure of the eye^{73,74}. Additionally, it has been shown that smoking can significantly reduce the blood flow index of the macular area and causes hypoxia⁵⁷. Since increased retinal vessel tortuosity is one of the early signs of hypoxia-implicated retinopathies, it is speculated that smoking might result in increased retinal vessel tortuosity⁷⁵.

1.7 Electronic cigarette

Due to the known harmfulness of the conventional cigarette (C-cigarette) smoke, more and more alternative products have been developed in recent years. Among them, the electronic cigarette (E-cigarette) (Fig. 4-A, B) is one of the most popular alternatives. The use of E-cigarettes is commonly promoted as a “low-risk”, “less dangerous” alternative to C-cigarettes, and is supposed to avoid the high concentration of toxicants and hence reduce the harm. E-cigarettes consist of a battery-powered device, in which

the e-liquid vaporizes by heating, then the vapor is delivered to the human body to imitate the taste and feeling of C-cigarette smoke. The e-liquid usually contains ingredients such as propylene glycol, vegetable glycerol, different doses of nicotine, and various flavourings, wherein the nicotine and flavouring agents are not essential. The concentration of nicotine and the types of flavouring agents vary in different brands and products⁷⁶.

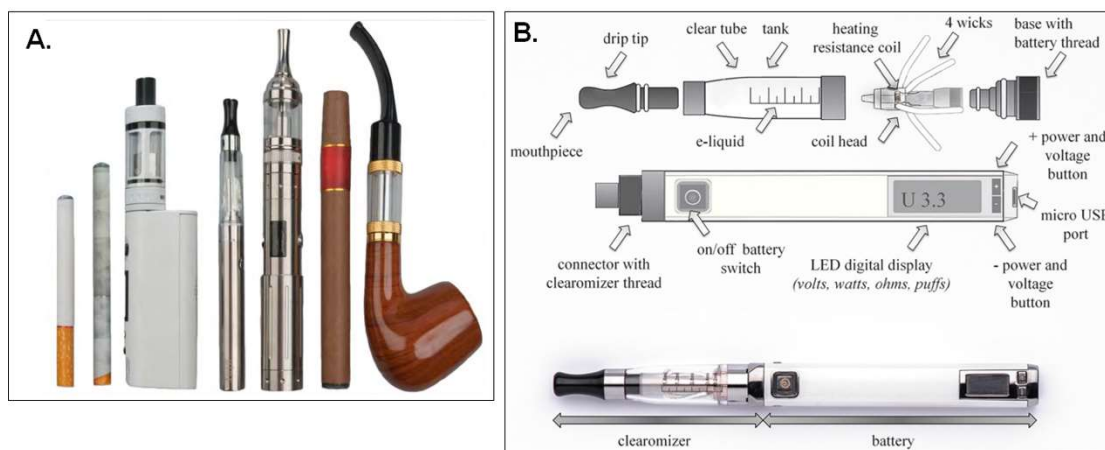


Figure 4. (A) Electronic cigarettes in different shapes (image adapted from the web page of *Wikipedia*)⁷⁷; (B) the basic structure of a conventional E-cigarette (image adapted from the web page of *Wikipedia*)⁷⁷.

The advertisements and market slogans usually state that E-cigarettes are healthier products, which are useful for smoking cessation and can even be used everywhere. Thereby, since the E-cigarette entered the market as a "less harmful" alternative to C-cigarette, the number of products has increased dramatically. It is especially popular among adolescent, and even pregnant women may be persuaded to use it without any scruples because of the belief that E-cigarettes are harmless or safe⁷⁸. But the voice of doubts about its safety is now attracting people's attention. Currently, the quality control of E-cigarettes by various brands has become a controversial issue, concerning its safety and toxicity. Recently, the European Union has formulated a regulation, which clearly stipulates that the upper limit of the nicotine concentration in E-cigarette e-liquid is 20 mg/mL⁷⁹. The nicotine concentration in e-liquid varies greatly in different E-cigarette products, normally, from 0 mg/mL to 25 mg/mL. The most popular nicotine concentration is 18 mg/mL⁷⁶. However, the way, the speed and the level of nicotine

absorption are all important determinants of the efficacy of E-cigarette as an alternative of C-cigarette and the risk of nicotine-related diseases⁸⁰.

With the widespread use of the E-cigarettes, its safety and related disease risk research becomes more and more urgent and extremely important in the field of public health. Although some people in the medical profession or related organizations believe that the alternative use of E-cigarettes can reduce the negative effects of C-cigarette consumption, there is a growing number of studies on the negative health effects of E-cigarettes reported, such as the toxicity for lung and other organs⁸¹⁻⁸³. Overall, there is still a lack of reliable evidence on the effects of E-cigarette vapor on human body after medium- and long-term usage. In 2014, Valacchi et al. reported a control study that compared and analysed the pathological toxicity of E-cigarette vapor and C-cigarette smoke in vitro⁸⁴. The results suggested that although E-cigarette vapor is less toxic than C-cigarette smoke, both the contained nicotine and the unique flavour ingredients have deleterious effects on human cells, and even the basic humectant in e-liquid also has certain harmful effects, such as promoting the release of pro-inflammatory cytokines. Besides, some studies have shown that the e-liquid would produce many ultrafine particles after heating, and these particles with biological activity could further activate inflammatory responses, contribute adverse effects to the cardiovascular system, and even cause acute cardiovascular diseases^{85,86}. In addition, the results from animal experiments indicated that exposing mice to nicotine-containing E-cigarette vapor would promote the occurrence of lung inflammation and oxidative stress damage, as well as the dysfunction of pulmonary vascular endothelial cells⁸⁷⁻⁸⁹. However, up to date, there is still no any related research of the impact of E-cigarette usage on neural retina or fundus reported.

1.8 Fibroblast growth factor10

The human or mouse fibroblast growth factors (Fgfs) belong to a family that contains at least of 22 members, namely Fgf1 to Fgf23 (Fgf15 and Fgf19 are orthologs)⁹⁰. The

mammalian Fgf receptor (FgfR) gene family contains four genes (FgfR1-FgfR4), which encode at least seven prototype receptors, and each FgfR gene contains three main parts: the extracellular domain (assembled of two or three immunoglobulin-like (Ig) loops), the transmembrane segment, and the intracellular tyrosine kinase. Actually, the specific interaction of Fgfs with their specific receptor is mediated mainly by the second and third Ig-loop of the extracellular domain. For FgfR1-FgfR3, selective splicing of exons encoding the C-terminal half of the third Ig loop generate two receptor isoforms, namely IIIb and IIIc^{91,92}. Fgfs are secreted through paracrine or endocrine pathway and mediate the pleiotropic functions in the development (proliferation, migration, differentiation) and adult organism (tissue homeostasis and metabolism) by interaction with their specific receptors and activation of the signalling pathways⁹³.

Fibroblast growth factor10 (Fgf10) comprises 215 amino acids and is specifically expressed in mesenchymal tissue. Fgf10 is secreted in a paracrine manner to specifically activate receptors FgfR2b and FgfR1b with heparin/heparan sulfate^{94,95}, the activated signalling then participates in the bidirectional signalling pathways across epithelial–mesenchymal boundaries, which plays critical roles in the regulation of cell mitogenesis, proliferation, differentiation, and migration^{96,97}. It is well known that Fgf10 plays quite important roles in the outgrowth of limb bud and branch morphogenesis of the lung. Furthermore, it is also indispensable in the development of the gastrointestinal tract during embryonic stages^{98,99}. Fgf10 knockout mice cannot survive after birth due to multiple serious dysplasia phenotypes, such as the agenesis of lungs, limb, thyroid, salivary glands and the dysgenesis of kidney, glandular stomach, pancreas. Interestingly, the phenotypes of FgfR2b knockout mice highly resemble those of the Fgf10 knockout mice. Therefore, it is concluded that FgfR2b is the main receptor of Fgf10⁹⁵. Fgf10 specifically binds with FgfR2b by its co-factor heparan sulfate and forms the Fgf10-FgfR2b-heparan sulfate (2:2:2) ternary signalling complex. Upon activation of FgfR2b, it induces the activation of the intracellular RAS-mitogen-activated protein kinase (RAS-MAPK), phosphatidylinositol-3 kinase/protein kinase B (PI3K-AKT), and Phospholipase C gamma 1 (PLCg1) signalling pathways (Fig. 5)⁹⁵.

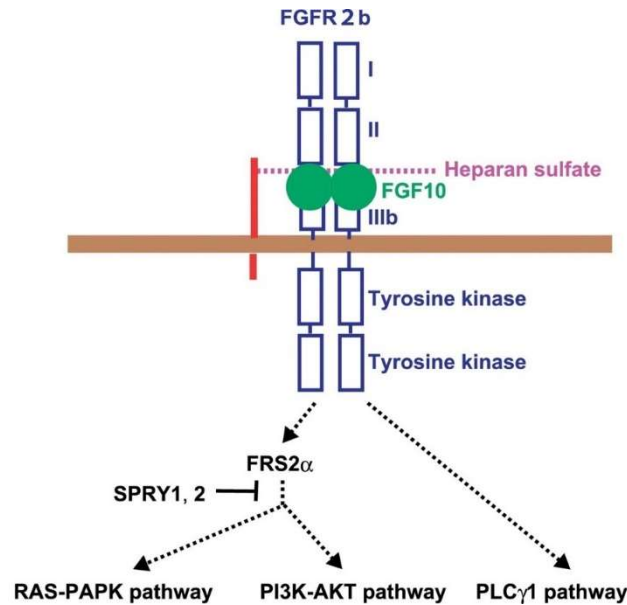


Figure 5. The mechanism of FGF10 action (reproduced with permission from Itoh's paper⁹⁵).

1.9 The function of Fgf10

As a multifunctional growth factor, Fgf10 not only plays critical roles in multiple organs and tissue patterning in the embryo^{99,100}, but also has effects on tissue repair and regeneration by mediating wound healing and tissue homeostasis in adult mammals. In cardiovascular diseases, Fgf10 promotes stem cell differentiation and cell reprogramming towards the cardiogenic lineage or adult cardiomyocyte cell cycle re-entry, which demonstrates that Fgf10 signaling is probably involved in the cardiac regeneration¹⁰¹. In peripheral nerve injury, Fgf10 is likely involved by suppressing excessive oxidative stress and inhibiting Schwann cells apoptosis to provide neuroprotection and promote the regeneration of peripheral nerves. Moreover, Fgf10 can also provide neuroprotective effects and promote functional recovery after spinal cord injury and cerebral ischemia brain injury by activating the PI3K/AKT signaling pathway and suppressing Toll-like receptor 4/ nuclear factor kappa B (TLR4/NF-κB) mediates neuroinflammation^{102,103}. Furthermore, animal experiments have shown that the overexpression of Fgf10 attenuates the extent of inflammation responses and fibrosis in the mouse model of bleomycin induced lung inflammation and fibrosis¹⁰⁴.

Nevertheless, whether the overexpressed Fgf10 has potential protective or regenerative effects on neural retina has not been reported.

1.10 The aims of this study

It has been shown that C-cigarette smoke significantly increase the incidence of AMD and promote its progress. However, as an alternative to conventional smoke, the effects of E-cigarette vapor on neural retina, RPE or choroid have not been investigated. Moreover, there is also no report on the correlation between the use of E-cigarette and the occurrence or development of AMD. It poses the question whether the exposure effect of E-cigarette vapor on fundus is similar to C-cigarette smoke. If E-cigarette vapor can increase the incidence of AMD and promote its progression as well, what would be the role of nicotine ingredient, and what will happen to the neural retinal tissue along with an extension of the E-cigarette vapor exposure? In order to further shed light on a potential correlation between E-cigarette vapor exposure and the onset of inflammatory and angiogenic stimuli reminiscent to the occurrence and development of AMD in humans, in the first part of this study, an in vivo study in mice was carried out by: (1) comparing the effect of C-cigarette smoke and E-cigarette vapor on the neural retina; (2) T.

Second, as mentioned above, Fgf10 has neuroprotective and regenerative effects in nerve injury disease by suppressing excessive oxidative stress and reducing neuroinflammation. On the other hand, it is known that cigarette smoking induces the progression of AMD mainly by similar pathological routes such as induction of oxidative stress and onset of an inflammatory response, and eventually ends in the degeneration and loss of photoreceptor cells in the neural retina. Taking account that the neural retina tissue is one part of the central nervous system¹⁰⁵, therefore, it is hypothesized that the overexpressed Fgf10 also has protective effects on the neural retina upon damage caused by cigarette smoke exposure. In order to verify this hypothesis, in the second part of this study, we investigated the long-term effect of

cigarette smoke exposure on mouse retina, by measuring the retinal vascular morphology and the retinal layer thickness as well as the molecular expression in neural retina. Simultaneously, we used mice engineered for the inducible overexpression of Fgf10 in the retina to probe the protective and regenerative effects of Fgf10 overexpression in the smoke exposure mouse retina.

2 MATERIALS AND METHODS

2.1 Materials

2.1.1 Reagents and consumables

Table 1. Reagents and consumables used in this chapter.

Reagent/Consumable	Model /Article No.	Company and place of origin
RIPA lysis buffer ^a	/	/
AllPrep RNA/Protein Kit (50)	80404	QIAGEN (Germany)
10× Phosphate buffered saline (PBS) buffer, pH 7.4 ^b	/	/
PrimeScript™ 1st strand cDNA Synthesis Kit	6110A	TaKaRa (China)
GoTaq® G2 Flexi DNA polymerase	M7805	Promega (USA)
Mouse IL-1beta/IL-1F2 DuoSet ELISA Kit	DY401-05	R&D Systems (USA)
Mouse VEGF DuoSet ELISA Kit	DY493-05	R&D Systems (USA)
Mouse TNF-α DuoSet ELISA Kit	DY410-05	R&D Systems (USA)
Inducible Nitric Oxide Synthase (iNOS) ELISA Kit	MBS030771	My BioSource (USA)
Mouse Pigment epithelium-derived factor (PEDF) ELISA Kit	KTE70449	Abbkine (China)
Mouse fibroblast growth factor 10 (Fgf10) ELISA Kit	MBS702692	My BioSource (USA)
C-cigarette	3R4F	Kentucky Tobacco Research and Development Center (USA)
E-cigarette liquid (free nicotine) ^c	/	Avoria GmbH (Germany)
E-cigarette liquid (containing 18mg/mL nicotine) ^d	/	Avoria GmbH (Germany)

^{a, b} Manual preparation, see the details in 2.1.3 buffer preparation section.

^{c, d} Both liquids containing 55% propylene glycol, 35% glycerol and 10% water, without flavors.

Table 2. Composition and content of 10× RIPA buffer solution (addition with 1000 mL ddH₂O).

Solute	Quantity
50 mM Tris-HCl, PH 7.4	5.0 mL (1.0 M)
150 mM NaCl	15.0 mL (1.0 M)
1 mM EDTA	0.2 mL (0.5 M)
1% Triton-100	1.0 g
1% sodium deoxycholate	0.1 g

Table 3. Composition and content in 1.0 L of 10× PBS buffer solution (addition with 1000 mL ddH₂O, adjusting pH to 7.4 with HCl).

Solute	Quantity (g)
NaCl	80.0
KCl	2.0
Na ₂ HPO ₄	14.4
KH ₂ PO ₄	2.4

Table 4. Characteristics of gene primers used for qPCR analysis.

Gene name	Species	Primer sequence (forward, reverse)	Product size (bp)
GAPDH	Mouse	GGTCGGTGTGAACGGATTGG	199
	Mouse	GTTGCTGTTGATGGCTTTGA	
Fgf10 ¹⁰⁶	Mouse	GATTGAGAAGAACGGCAAGG	115
	Mouse	GTTGCTGTTGATGGCTTTGA	

2.1.2 Equipment

Table 5. Equipment used in this chapter

Equipment	Model/Article number	Company and place of origin
Clean air workbenches	13-261-500	Thermo Fisher Scientific (USA)
Homogenizer	Precellys®24	Bertin (France)
Reinforced tubes 2.0 mL	Precellys lysing kits	Bertin (France)
Centrifuge	1-15PK	Sigma (Germany)
Heating block	TB2	Biometra (Germany)
Micropipette	1µL/10µL/20µL/100µL/ 200µL/1000µL	Transferpette® S (Germany)
Photometer	Mettler Toledo	Eppendorf Research (Germany)
–80 °C Freezers	Hera Freeze	Hanau (Germany)
PCR thermocycler	T-professional	Biometra (Germany)
RNA quality analysis system	QIAxcel System	QIAGEN (Germany)
Real-time PCR System	Realplex mastercycler	Eppendorf (Germany)
Gel electrophoresis	PS 305T	Biometra (Germany)
C-cigarette smoke generator and exposure chamber	SM2000	Burghart (Germany)
E-cigarette vapor generator	Joyetech eVic-VTC Mini e-cigarettes	Joyetech (China)
E-cigarette vapor exposure chamber	inExpose inhalation exposure system	SCIREQ (Canada)

2.1.3 Buffer preparation

RIPA buffer solution

The solutes described in Table 2 were mixed and dissolved with ddH₂O into a 1.0 L clear solution.

RIPA lysis buffer solution

To a 10.0 mL RIPA buffer solution (Table 2), 1 tablet protease inhibitor was added. The mixture was stirred until it was clear. The obtained RIPA lysis buffer solution was stored

in -20°C refrigerator before use.

10× PBS buffer solution

To the mixture of required solutes (Table 3), 1000 mL of ddH₂O was added to dissolve them into a clear solution, in which the pH value was then adjusted to 7.4. The buffer was sterilized and stored at room temperature before use.

1× PBS buffer solution

1× PBS buffer solution was prepared by diluting 10× PBS buffer solution into one tenth concentration with ddH₂O.

2.2 Methods

All animal experiments were approved by the local ethics committee for animal welfare (Regierungspräsidium, Giessen, Germany) and performed in accordance with the Association for Research in Vision and Ophthalmology statement for the use of animals in ophthalmic and vision research. Mice used in the experiments were C57BL/6J from the colony at the cardiopulmonary institute or directly purchased from Charles River Deutschland, Sulzfeld, Germany. Animals were housed under a 12: 12 h, light: dark cycle and given standard rodent food and water supply ad libitum during experiment. All analyses/exposures were done in a blinded, randomized fashion. For the study design sample size estimation was performed prior to the experiments.

2.2.1 Conventional cigarette smoke exposure

48 male C57BL/6J (wild type, WT) mice (14 ± 2 weeks old) were randomly distributed to the experimental and control subgroups of the medium-term and long-term exposure groups (Fig. 6-A), ensuring that each subgroup has 12 mice. Whole body exposure to the mainstream smoke of 3R4F cigarettes (Kentucky Tobacco Research and Development Centre, USA, containing 0.7 mg nicotine per cigarette) generated by a smoke generator (Burkhart, Wedel, Germany) (Fig. 7-A&B) was performed as

previously described^{107,108}. The particle concentration was set as 200 mg/m³ during the exposure. Mice were exposed for 6 hours per day, 5 days per week for a period of 3 (medium-term) or 8 (long-term) months¹⁰⁹. Mice in the control subgroup were kept under in the room air environment, while the other conditions were the same as the corresponding experimental subgroup. In the 24 h after the end of the C-cigarette smoke, the mice were sacrificed and the neural retina were harvested.

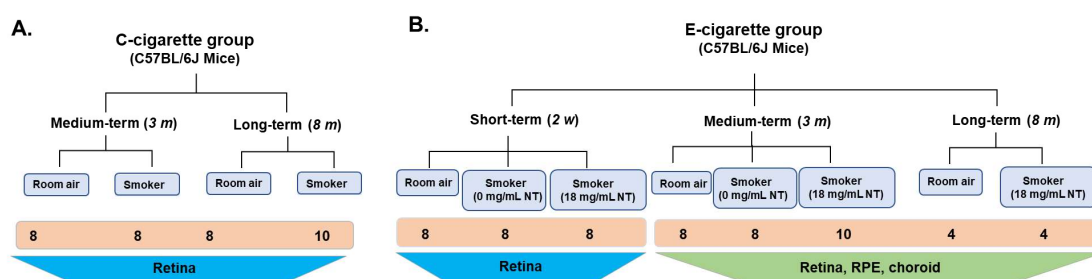


Figure 6. The experimental scheme (adapted from Wang's paper¹¹⁰). (A) C-cigarette exposure group with medium-term and long-term subgroups and the corresponded control mice model; (B) E-cigarette exposure group with short-term, medium-term and long-term subgroups, wherein nicotine-free E-cigarette and 18 mg/ml of nicotine-containing E-cigarette were used besides the long-term subgroup using nicotine-containing E-cigarette only. NT: nicotine.

2.2.2 E-cigarette vapor exposure

120 male WT mice (14 ± 2 weeks old) were randomly divided into the experimental and control subgroups of short-term (2 w), medium-term (3 m) and long-term (8 m) exposure groups (Fig. 6-B), ensuring that each group contains 15 mice. In order to evaluate the effect of nicotine on neural retina/RPE/choroid, additional control experiments by the comparison of nicotine-free E-cigarette and nicotine-containing E-cigarette were performed in the short-term and medium-term exposure groups (Fig. 6-B). The e-liquid (Aavoria GmbH, Nuremberg, Germany) used in both smoker subgroups did not contain any flavoring reagents, and the basic components inside (containing 55% propylene glycol, 35% glycerol and 10% water) were completely the same besides nicotine content. In the long-term exposure group, 18 mg/mL nicotine-containing E-cigarette was used in smoker subgroup to evaluate the long-term effect of E-cigarette.

In the exposure experiment, the mice were exposed in a whole-body manner to E-cigarette vapor for 6 hours per day, 5 days per week, using InExpose inhalation exposure system (SCIREQ, Montreal, Canada) (Fig. 7-C). The e-liquid was vaporized at 2 puffs per min (2 sec evaporation per puff) and hence 720 puffs in total for one day (6 hours). According to the manual from the manufacturer, 1.5 mL of e-liquid can be evaporated every 400 breaths, so that 5.4 mL of e-liquid would be evaporated every 6 hours in the smoke generator, which is close to the daily intake of e-liquid by human smokers (the average amount). Except for the smoke exposure time, the mice in the experimental groups were transferred to a standard indoor air environment. Mice in the control groups were kept in a standard indoor air environment all the time, while the other conditions were the same as the corresponding experimental subgroup. In the 24 h after the end of E-cigarette vapor exposure, the mice were sacrificed for tissue dissection. For the mice in the short-term exposure group, only neural retinal tissue was harvested; while for the mice in both medium-term and long-term exposure groups, all neural retinal, RPE and choroid/scleral tissues were harvested.

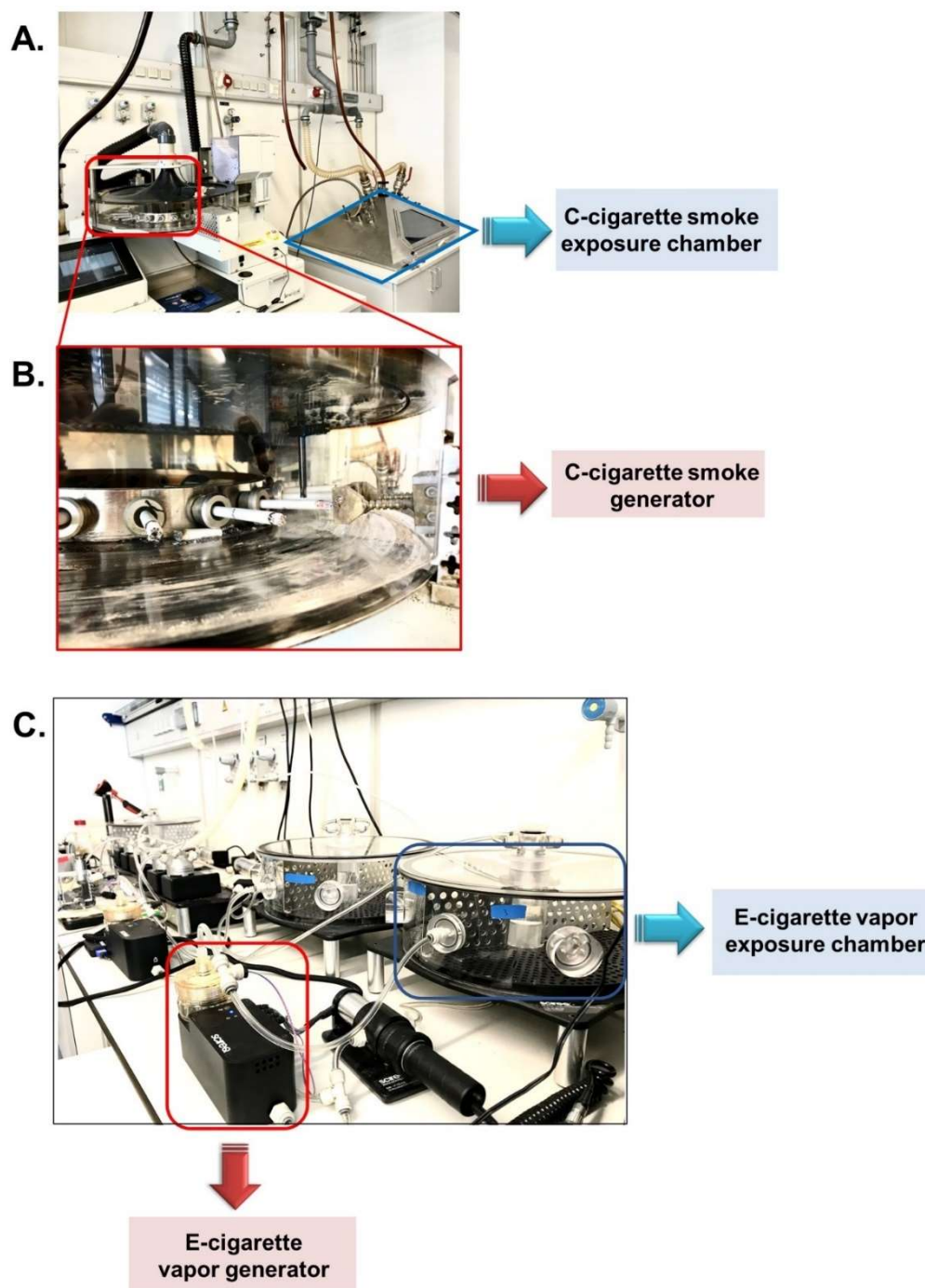


Figure 7. Smoke and vapor exposure equipment. (A) C-cigarette smoke exposure chamber; (B) C-cigarette smoke generator; (C) E-cigarette vapor generator and E-cigarette vapor exposure chamber.

2.2.3 Transgenic mouse generation

The experimental procedures were approved by the governmental ethics committee for animal welfare (Regierungspräsidium, Giessen, Germany). The generation of double transgenic R26rtTA; tet (o)Fgf10 mice are the same as described in previous reports^{93,98}.

All animals were housed under a 12: 12 h, light: dark cycle with food and water supply ad libitum during experiment.

2.2.4 The C-cigarette smoke exposure for transgenic mice

Experimental scheme is displayed as Fig. 8-A, 150 male doubles transgenic R26rtTA; tet(o)Fgf10 mice (14 ± 2 weeks old) were randomly divided equally into experimental (smoker) and control (room air) groups, ensuring that each subgroup has 75 mice. Each 15 male WT

mice for experimental and control subgroups were set as the control of Fgf10 OE transgenic mice. The experimental subgroup mice were exposed to the mainstream smoke of 3R4F cigarettes by whole-body way for a period of 8 months (long-term), and the specific details are described in the **section of 2.2.1**. In addition, the mice in the control group were kept under in the room air environment, while the other conditions were the same as the corresponding experimental subgroup.

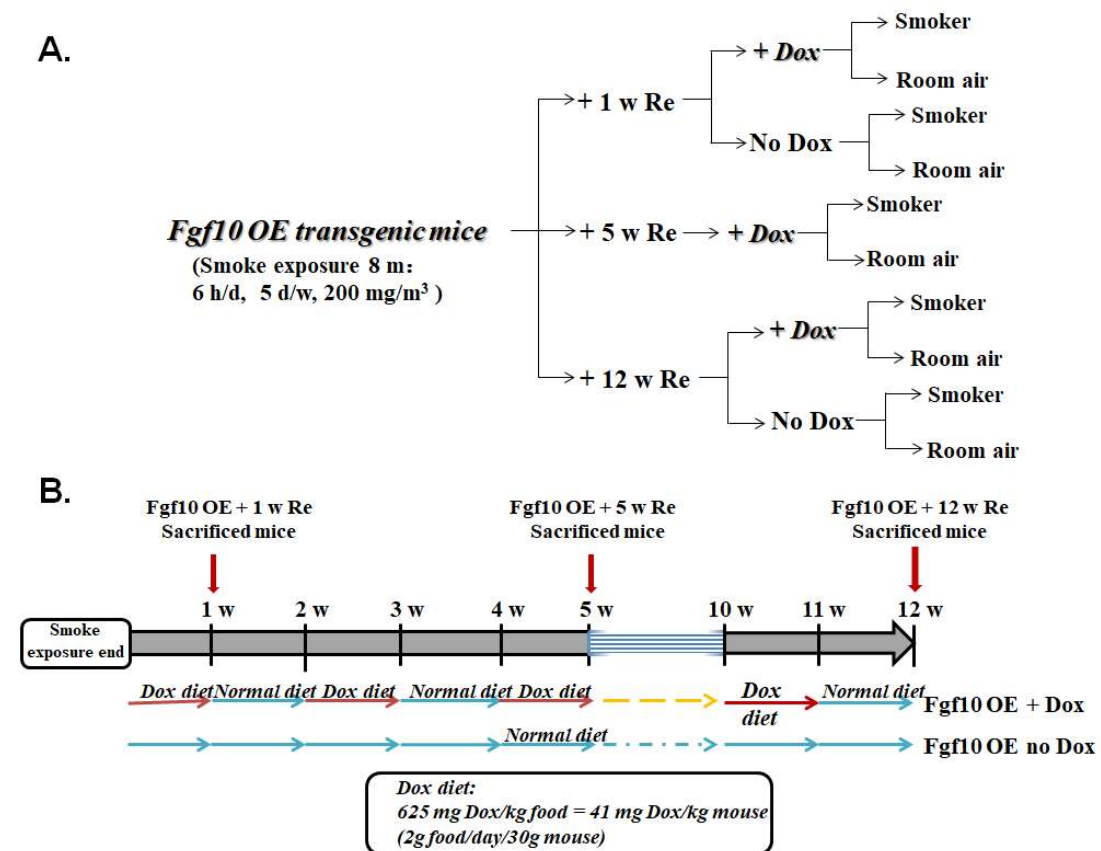


Figure 8. The experimental scheme. (A) The experimental subgroup of Fgf10-overexpression (OE) transgenic mice were exposed to cigarette smoke in a manner of whole-body exposure. The particle

concentration in the smoking chamber was adjusted to 200 mg/m³ and mice were exposed for 6 h/d, 5 d/w. After 8 m of exposure, both smoker and control (room air) mice were placed in the normal room air environment for different periods (1 w/5 w/12 w) as the phase of regeneration. **(B)** Doxycycline was applied to induce the overexpression of Fgf10 gene during the diet cycles (1 w Dox diet given: 1 w normal diet given). For the mice of “Fgf10 OE + Dox” subgroup, the diet cycle started at the second day after the smoke exposure finished. The mice of “Fgf10 OE no Dox” subgroup were fed only with normal diet. 0.0625% of doxycycline was contained in Dox diet.

2.2.5 Induction of Fgf10 overexpression

The regeneration (Re) phases started at the second day after the smoke exposure finished, as shown in Fig. 8-B. During the regeneration periods, doxycycline containing diet (diet with 0.0625% doxycycline, we call it "Dox diet") was applied to induce the overexpression of Fgf10 in double transgenic rtTA; tet (O)Fgf10 mice (namely Fgf10 overexpressed (OE) transgenic mice).

During the phases of regeneration, the mice in Fgf10 OE + Dox subgroup were fed with Dox diet for 1 w, followed by normal diet for the second week. Such a diet cycle ran for six times and completed at the end of twelfth week. Per kilogram of such Dox diet contains 625 mg Dox which equals to 41 mg Dox/kg mice (2g food/day/30g mice). At the timepoints of 1 w, 5 w and 12 w of regeneration, each 12 mice from both smoker and room air subgroups were sacrificed separately. The retinal tissues were harvested (according to the protocol in the section of 2.2.9), and analysed by qPCR and ELISA. In addition, the mice of Fgf10 OE no Dox group were fed only with normal diet, and at the timepoints of 1 w and 12 w of regeneration, each 12 mice of both smoker and room air subgroups from this group were also sacrificed to harvest the neural retinal tissues. It is worth noting that, at the timepoint of 12 w of regeneration, Micron III microscope was applied to get the both retinal optical coherence tomography (OCT) scan and retinal images in vivo before the mice were sacrificed. The thickness of different retinal layers and the retinal vessels tortuosity metrics were evaluated, to analyse the vascular morphology and potential layers thickness changes.

2.2.6 Optical Coherence Tomography scan and retinal images acquisition for the mice of the Fgf10 OE + 12w Re subgroup.

Within twenty-four hours after 12 w regeneration finished, the mice were anesthetized with a mixture of dexmedetomidine (0.5 mg/kg) and ketamine (50 mg/kg), and the OCT scan imaging and retinal image acquisition were performed. Mydriasis was achieved by dropping topical mydriatic solutions (1% tropicamide), and GenTeal TM lubricant gel was applied to maintain corneal clarity and moist during imaging. Micron III intraocular imager (Phoenix Research Labs; Pleasanton, CA) (Fig. 9) was used to perform the image-guided OCT scan (across the retinal papilla and periphery regions) and retinal imaging acquisition on both eyes of each mouse. The retinal image of the peripheral retina is a section with a minimum distance of 3-5 mm from the optic disc. The status of retinal vessels can be assessed by retinal images combined with further analysis.

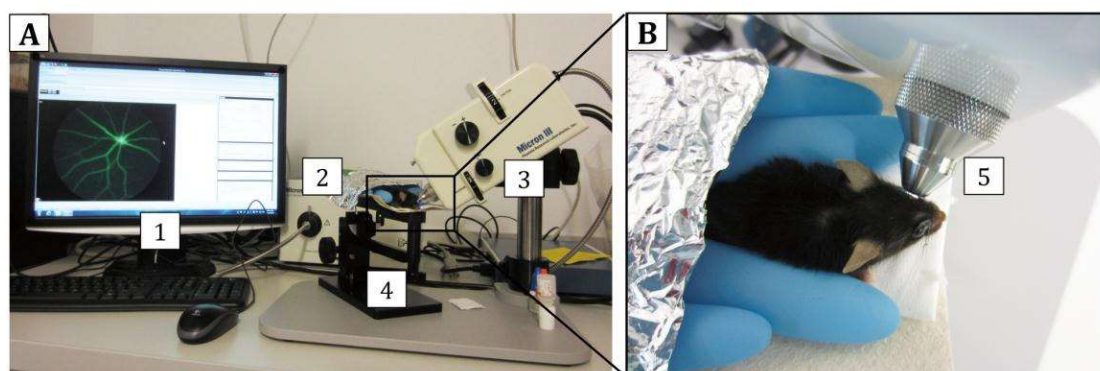


Figure 9. Micron III retinal imaging microscope. (A) the various components of the experimental setup: 1. computer, 2. lightbox, 3. microscope, 4. platform, 5. objective lens. The Micron III camera is connected to the light box and the computer. The mouse was fixed on the height-adjustable platform. (B) With the objective lens touching the mouse cornea, the mice eye remains still. The display presents both the bright field mouse retina image with a guide beam and the OCT scan image. (With permission from Dr. Röhl¹¹¹)

2.2.7 Retinal layers thickness measurement for the mice of the Fgf10 OE + 12w Re subgroup.

InSight software (Phoenix Research Labs) was used to segment and measure the

thickness of different retinal layers. The retinal OCT images were segmented into four layers groups (Fig. 10-A-D): the inner retina layer (IR): ILM + RNF + GCL + IPL + INL + OPL), the ONL+ layer: ONL + ELM + IS, the outer retina layer (OR): I/OS + OS + RPE, and the whole retina (WR). The retinal thickness across the papilla (Fig. 10-A, B) and periphery (Fig. 10-C, D) regions were measured separately. In order to reduce or avoid error, the data of optic disc region was excluded.

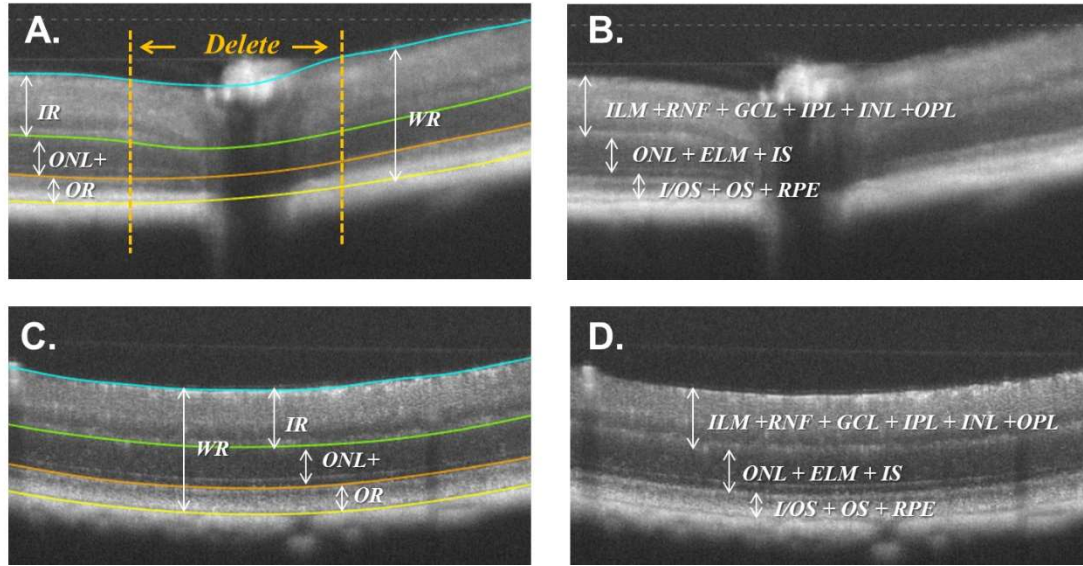


Figure 10. The retinal OCT scan images of Fgf10 OE transgenic + 12 w Re (no/+ Dox) mice. The OCT images which scan across retinal papilla (A, B) and periphery region (C, D). In order to reduce error, the data of optic disc region weren't used for measurement and analysis. WR: whole retinal layer, IR: inner retinal layer, ONL+: outer nuclear layer + layer, OR: outer retinal layer, ILM: inner limiting membrane, RNF: retinal nerve fiber, GCL: ganglion cell layer, IPL: inner plexiform layer, INL: inner nuclear layer, OPL: outer plexiform layer, ONL: outer nuclear layer, ELM: external limiting membrane, IS: inner photoreceptor segment, I/OS: inner/Outer photoreceptor segment, OS: outer photoreceptor segment, RPE: retinal pigment epithelium.

2.2.8 Retinal blood vessel tortuosity measurement for Fgf10 OE transgenic + 12 w Re (no/+ Dox) mice

In the group of Fgf10 OE transgenic + 12 w Re (no/+ Dox) mice, the retinal image that centred on the optic disc in each right eye was selected. The lasso tool in photoshop was applied to quantitatively analyse all arterial and venous tortuosity within 240 μ m diameter from the optic disc. The retinal images from room air (no Dox), room air (+ Dox), smoker (no Dox) and smoker (+ Dox) subgroups are presented in Fig. 11 (A-D,

respectively), wherein, the yellow arrow shows the arterial tortuosity and the blue arrow shows the venous tortuosity. The retinal image from smoker no doxycycline subgroup was taken as example to illustrate the area measurement method (Fig. 11-E). The red area and blue area reflect the arterial and venous tortuosity covered area respectively. Schematic diagram (Fig. 11-F) displays the statistical methods: it is supposed that there were three vessels in a retina, the tortuosity numbers of each vessel were $N_a = 7$, $N_b = 1$, $N_c = 3$ respectively, and the corresponding tortuosity total covered area were a , b and c respectively. Thus, the average tortuosity numbers of each blood vessels in this retina would be $\frac{N_a + N_b + N_c}{1 + 1 + 1} = \frac{7 + 1 + 3}{3} = 3.67$, and the average covered area of each tortuosity should be $\frac{a + b + c}{N_a + N_b + N_c} = \frac{a + b + c}{7 + 1 + 3} = \frac{a + b + c}{11}$.

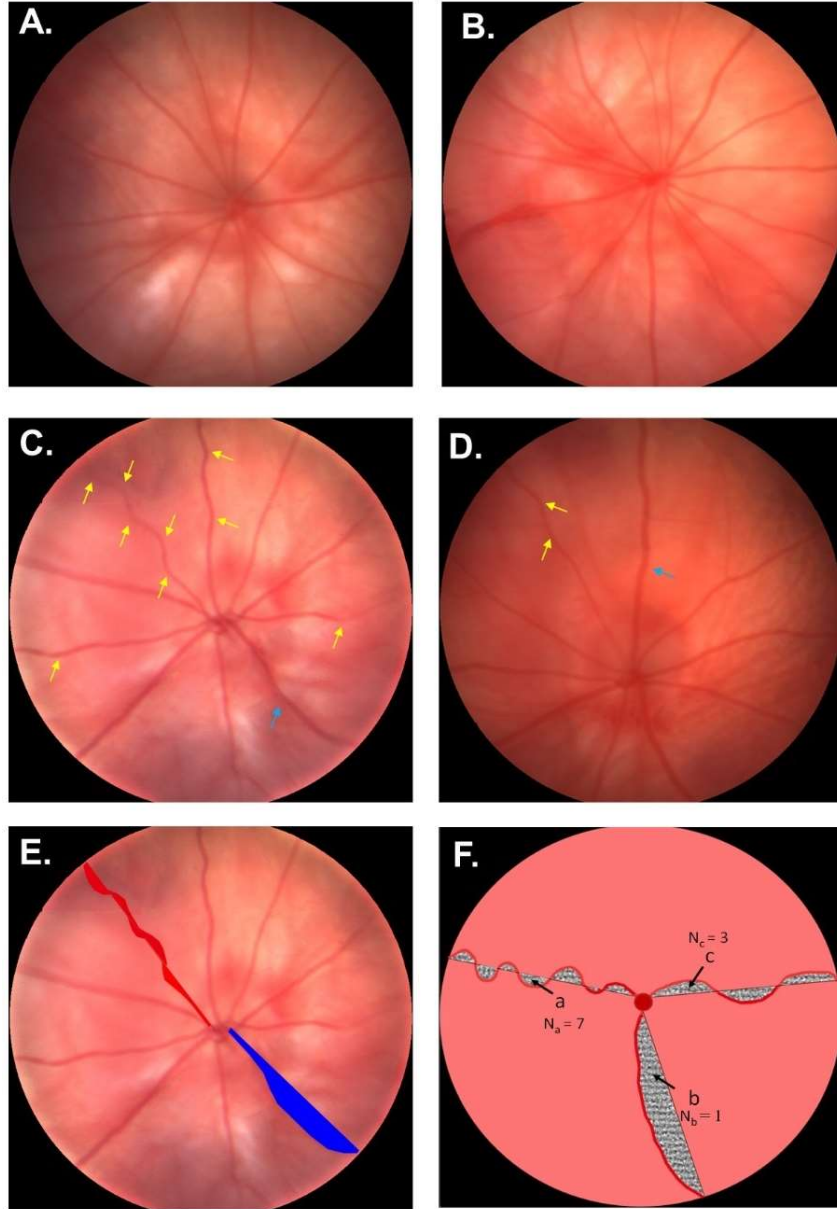


Figure 11. The retinal images of Fgf10 OE transgenic + 12 w Re (no/+ Dox) mice (n=12 for each group). Images of (A), (B), (C), (D) represent the room air (no Dox), room air (+ Dox), smoker (no Dox), smoker (+ Dox) subgroups respectively. Yellow arrows indicate arterial tortuosity, and blue arrows show venous tortuosity. Diagram (E), using the image of smoker (no Dox) subgroup to show the measure method of tortuosity covered area, red area indicates arterial tortuosity covered area, and blue area displays venous tortuosity covered area. (F) the schematic diagram of statistical methods.

2.2.9 Dissection of neural retina, RPE, choroid/scleral tissues

The dissection operation was performed following the procedure reported by Wei *et al*¹¹²:

- [1] Following euthanasia, eyeballs were removed and put into ice bath-cooled $1\times$ PBS buffer.
- [2] The eyeballs were washed with $1\times$ PBS buffer 3 times to get rid of the blood. The cleaned eyeballs were then transferred to a petri dish which contained fresh $1\times$ PBS buffer, and was put under a dissecting microscope.
- [3] Using tweezers to fix the eyeball, a small hole was made at the area between limbus and sclera with a hypodermic needle. A circle along the outside of cornea was cut subsequently, followed by the removal of all the anterior eyeball tissues (cornea, iris, lens and vitreous) with dissecting scissor. Afterward, the optic nerve was removed carefully, and the neural retinal tissue was separated and quickly placed in a 1.5 mL centrifuge tube (marked with important information in advance) and temporarily stored in liquid nitrogen.
- [4] The cup-shaped half eyeball (composed by the remained RPE, choroid (sclera) tissues) was cut into four small flaps from the edge to the direction of the optic nerve vertically. The remaining tissue was flattened, and transferred into a 1.5 mL centrifuge tube which contained ice bath-cooled 100 μ L of RIPA protein lysis buffer with protease inhibitor. The tissues were able to immerse completely in the lysis buffer, and the centrifuge tubes were placed on ice for incubation for 1 hour. The centrifuge tubes were tapped several times to help RPE layer be separated from choroid/sclera. In the later stage of incubation, a brown clump (i.e. RPE layer) could be observed as detached from the choroid/sclera.
- [5] After the separation of RPE layer, the remaining choroidal (scleral) tissue was transferred into a new 1.5 mL centrifuge tube which contained ice bath-cooled 100 μ L RIPA protein lysis buffer (with protease inhibitor). The schematic diagram of RPE and choroid/sclera tissue dissection process is shown as Fig. 12.
- [6] Finally, the centrifuge tubes containing the neural retina/RPE/choroid (sclera) tissues were stored in a -80°C refrigerator before use.

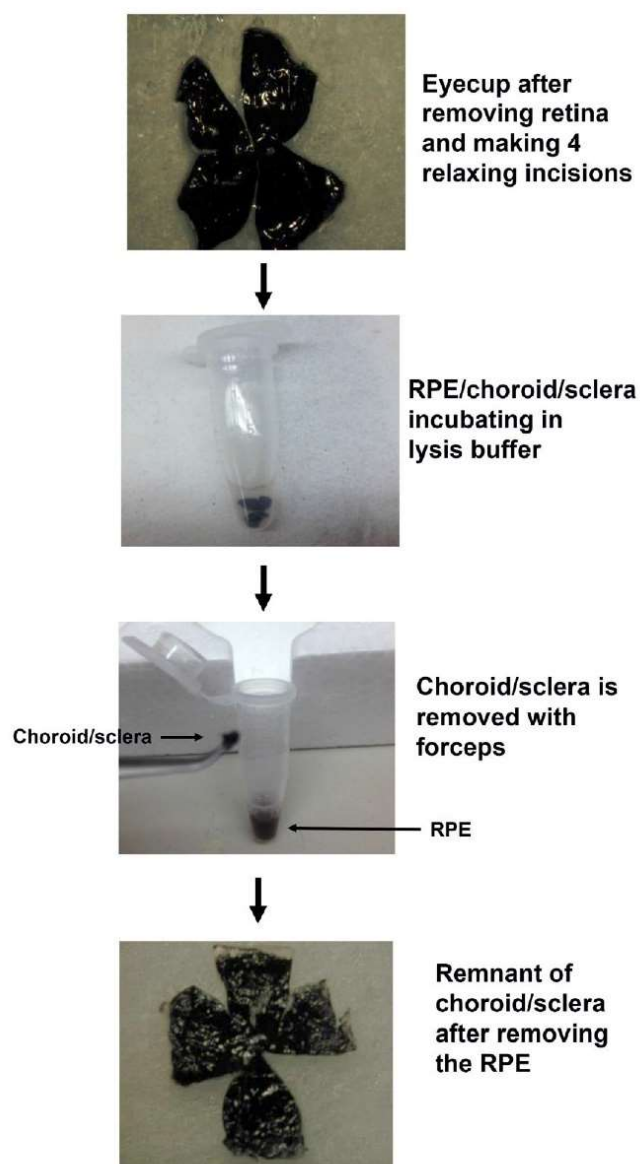


Figure 12. Schematic diagram of RPE separation (with permission from Wei's paper¹¹²).

2.2.10 Extraction of total RNA and protein

Total RNA and protein in neural retinal/RPE/choroid (sclera) tissues were extracted with AllPrep RNA/Protein kit. The operations were performed according to the manual provided by the manufacturer, and the procedure was shown as below.

Preparation before the extraction:

- 1) Addition of 2-mercaptoethanol (10 μ L) to RLT buffer (1.0 mL).

- 2) Dilution of the RPE buffer. The RPE buffer in the kit (concentrated) was 1:5 diluted with pure alcohol (96~100%) before use.

Experimental procedure:

- [1] The Protein Cleanup spin column was vortexed gently for 5 sec to resuspend the resin in it. The cap of the spin column was 1/4 turn rotated counterclockwise to ensure no vacuum state inside the column. The bottom closure of the Protein Cleanup spin column was snapped off to make the bottom open, and the spin column was placed in a 2 mL centrifuge tube, which was then centrifuged for 3 min at 750× g (there would be a small gap between the wall of column and gel bed after centrifuge). 0.5 mL of 1× PBS buffer was added to the Protein Cleanup spin column to equilibrate the resin gel inside. The Protein Cleanup spin column was vortexed gently and centrifuging it at 750× g for 3 min again, then the gel bed in the spin column would be inclined. The spin column was transferred carefully into a new 2 mL centrifuge tube for reserve.
- [2] **Tissues homogenization:** 4 centrifuge tubes which contained neural retinal tissues (from 4 mice of same subgroup) were taken out from the −80°C refrigerator and placed on ice immediately. All the neural retinal tissues in the tubes were transferred into one 2 mL reinforced tube. 250 μL APL buffer (containing RNA stabilizer) was added into the reinforced tube to lyse these neural retinas. Subjecting the tissues to homogenization at 6000-2×20-060 mode. If the homogenization was not completely after one process, the homogenize process was repeated. Afterward, the reinforced tube was centrifuged at 10,000× g for 5 min, and stood for another 5 min to precipitate the ions insight.
- [3] **Extraction and purification of the protein:** The supernatant in the reinforced tube obtained from the previous step was pipetted to the AllPrep spin column (built-in a 2 mL centrifuge tube) carefully, and centrifuged at 8000× g for 1 min to purify the protein solution. RNA bounded to the silica membrane in the AllPrep spin column during centrifuge process, (keep the column at room temperature for the

next step use), and the flow-through contained total protein. Then, the flow-through onto center of the slanted gel bed was pipetted in Protein Cleanup spin column slowly (dropwise). The column was centrifuged at $240\times g$ for 3 min to purify the protein solution. The flow-through in the bottom of centrifuge tube was the purified total protein solution. Subsequently, the Protein Cleanup spin column was discarded and the corresponding amount of protease inhibitor and glycerin was added to the obtained purified protein solution to protect the stability of protein. The solution was mixed well and divided it into one small sample (10 μL) and three aliquots samples. The aliquoted protein solution was stored in -80°C refrigerator before use, and the small sample was placed on ice and used for the subsequent protein solution concentration determination.

- [4] **Purification of RNA:** The AllPrep spin column (from step 3) was placed in a new 2 mL collection tube. RLT buffer (350 μL) was added to the column, which was then centrifuged at $8000\times g$ for 1 min to elute the RNA bounded to the silica membrane. Ethanol (350 μL , 70 vol.%) was added to the flow-through and pipetted up and down several times to mix the solution fully until the solution became opaque. The mixed solution was pipetted to the RNeasy spin column in a 2 mL collection tube, which was then centrifuged at $8000\times g$ for 1 min to make RNA bound to the silica membrane in spin column. Then, the flow-through was discarded. RW1 buffer (700 μL) was added to the RNeasy spin column, followed by the centrifuging at $8000\times g$ for 30 sec to wash the spin column membrane. RPE buffer (500 μL) was added to the RNeasy spin column and the column was centrifuged at $8000\times g$ for 30 sec to wash the spin column membrane. The spin column membrane was washed by RPE buffer (500 μL) again. Then the RNeasy spin column was centrifuged at full speed for 1 min to completely remove the remaining wash buffer in the silica membrane. The RNeasy spin column was then transferred into a new 1.5 mL collection tube. RNase-free water (50 μL) was pipetted onto the spin column membrane, followed by the centrifugation at $8000\times g$ for 1 min to elute RNA. The flow-through was obtained as purified total RNA solution, from which 3 μL RNA solution was taken out for concentration

determination while the remained solution was divided into 3 aliquots and stored in a -80°C refrigerator before use.

2.2.11 Extraction of protein with $1\times$ PBS buffer

4 centrifuge tubes containing neural retinas (from 4 mice of same subgroup) were taken out from the -80°C refrigerator and placed on ice immediately. All neural retinas were transferred into a 2 mL reinforced tube. Pre-cooled $1\times$ PBS buffer (200 μL) containing protease inhibitors was added to the reinforced tube, which was then subjected to the homogenization at 6000-2 \times 20-060 mode. After the homogenization was complete, the reinforced tube was then subjected to centrifugation at $5000\times g$ for 5 min. The supernatant was then aliquoted to 4 centrifuge tubes, and stored in a -80°C refrigerator before use.

2.2.12 Concentration determination of total RNA and protein samples

The concentration of total RNA and protein within the samples was determined by use of a spectrophotometer (Eppendorf, Germany). The total RNA solution was calculated by determining the ratio of OD260/OD280, and considered to be appropriate when located between 1.8 and 2.0, and was therefore used for downstream applications.

2.2.13 Quality control of total RNA

Quality of total RNA after extraction was verified using the QIAxcel liquid chromatography device, which allows assessment of very small quantities of RNA.

- [1] Samples of total RNA solution were taken out from -80°C refrigerator and placed on ice for later use.
- [2] 1 μL of sample solution was pipetted into the corresponding tube of the 12-tube strip (0.2 mL).
- [3] 1 μL of QX RNA size marker (200–6000 nt) was pipetted into the last tube of the 12-tube strip.

- [4] QX RNA denaturation buffer (1 μ L) was added into each sample tube and QX RNA size marker tube, and the solution was mixed well by pipetting up and down many times, then the 12-tube strip was covered with cap to seal.
- [5] The 12-tube strip was put into a heating block to heat at 70°C for 2 min, afterward, the 12-tube strip was placed on ice for 1 min.
- [6] The 12-tube strip was centrifuged at 1000 \times g for 30 sec to collect any condensation.
- [7] QX RNA diluent buffer (8 μ L) was added into each sample tube and QX RNA size marker tube to bring the total volume reach 10 μ L (the empty tubes were filled with 10 μ L QX RNA dilution buffer to protect the capillaries of QIAxcel machine from damage).
- [8] The 12-tube strip was brought into the QIAxcel that had been set up in advance to run and analyze.
- [9] After the program running finished, the ratio of 28S: 18S ribosomal RNA bands in the analysis results was checked. If the ratio was 2:1, it means that the quality of extracted RNA was high and had not degraded. Therefore, only those samples with ratio of 28S: 18S ribosomal RNA bands close to 2:1 was chosen for downstream applications.

2.2.14 Reverse transcription synthesis of complementary DNA (cDNA)

PrimeScript TM 1st Strand cDNA Synthesis Kit (6110A, TaKaRa, China) and total RNA solutions were used for reverse transcription according to the following protocol.

- [1] The kit solvents were removed from the -20°C refrigerator and thawed on ice.
- [2] The volume of RNA solution and ddH₂O required were calculated according to the amount of 80 ng total RNA and the specific RNA solution concentration of each group, and the mixture 1 (Mix 1) was then prepared according to the reagents and volumes as shown in Table 6. Three replicate PCR samples were prepared for each RNA sample. In addition, in order to synthesize cDNA more efficiently, we used the same amount of Random 6mers and Oligo dT primers for amplification in this

experiment.

Table 6. Reagents and volumes required for Mix 1 solution.

Reagent	Volume (μL)
ddH ₂ O	8 – X
dNTP mixture	1
Random 6mers (50 μM) + Oligo(dT) (50 μM) primers	0.5 + 0.5
Total RNA solution	X
Total volume	10

- [3] The PCR tubes which contain Mix 1 solution were incubated in the heater at 65°C for 5 min to fully denature the RNA. Afterward, the PCR tubes were placed on ice immediately to cool down. The reaction Mix 2 was then prepared according to the reagents and volumes as shown in Table 7, and mixed well.

Table 7. Reagents and volumes required for Mix 2 solution.

Reagent	volume (μL)
ddH ₂ O	4.5
5×PrimeScript buffer	4
RNase inhibitor (40 U/ μL)	0.5
PrimeScript RTase (200 U/ μL)	1
Total volume	10

- [4] the Mix 2 (10 μL) solution was added into each PCR tube which contains Mix 1 solution, and mixed well by pipetting up and down several times. Afterward, PCR amplification was performed to generate cDNA. The PCR steps is shown in Table 8.

Table 8. The PCR steps for cDNA synthesis.

Temperature (°C)	Time (min)
30	10
42	60

70	15
10	Pause

2.2.15 Real-time PCR (RT-PCR)

[1] Preparation of RT-qPCR reaction system

In order to avoid contamination, except for the cDNA solution, all the solutions which were shown in Table 9 were prepared on the ultra-clean workbench (3 qPCR tubes for 3 cDNA solutions of each RNA sample). Afterward, the qPCR tube was taken out from ultra-clean workbench and placed on a clean workbench to add the corresponding cDNA solutions, mixed thoroughly by pipetting up and down several times (placed the qPCR tube on ice throughout the operation to prevent the formation of primer dimers). The qPCR tubes were centrifuged at $\times 1000$ g, 4°C for 30 sec to remove bubbles in solution and accumulate solution to the bottom of qPCR tubes. A positive control and negative control were set for each time RT-qPCR performed. One external cDNA carrying the target of interest was used as exogenous positive control, to determine whether or not the qPCR reaction conditions were optimal as well as to verify if false negatives were being detected in the experiment. The same volume ddH₂O was used instead of the template cDNA solution namely no template control, which served as a general control for extraneous nucleic acid contamination and also as an important control for primer dimer formation. The characteristics and sequences of the primers which were used in the qPCR are shown in table 9. Primers were diluted in RNA-free water.

Table 9. Reagents and volume required for RT-qPCR.

Reagent	Volume (μL)
ddH ₂ O	1.6
5× GoTaq Flexi Buffer	2.0
dNTPs (1.25 mM)	1.6
MgCl ₂ (25 mM)	1.2

Forward primer (10 pmol/μL)	0.4
Reverse primer (10 pmol/μL)	0.4
10% DMSO	0.4
SYBR Green (1:1000)	0.3
cDNA	2.0
GoTaq-polymerase	0.1

[2] RT-qPCR detection

The RT-qPCR running parameters of the Realplex mastercycler instrument (Eppendorf, Germany) was set in advance: pre-denaturation (93°C, 2 min), denaturation (95°C, 1 min), annealing (60°C, 30 sec), extension (72°C, 30 sec), in which annealing and extension processes are repeated in 40 cycles. The prepared qPCR tubes were placed into Realplex mastercycler instrument and the run started. After the run ended, the resulting data were obtained from the device and further analyzed. In addition, a 2% agarose gel was used for electrophoresis to assess whether the quantity and size of the amplified products were correct or not. If the amplification result was incorrect or there were non-characteristic products, the experimental conditions should be improved and repeated, even redesigned the primer sequence until the correct amplification products were produced.

[3] Relative quantification of mRNA

After the relevant data were obtained, $2^{-\Delta\Delta C_t}$ method was used for statistics. The value of the control group was set as 1.00, and data of experimental group was the corresponding multiple of control group. The relative mRNA level was expressed by means \pm SD, $n = 4$. If the SD values of some groups was found be greater than 20% after statistics, the corresponding experiment shall be repeated until the available data was obtained.

2.2.16 Enzyme-linked immunosorbent assay (ELISA)

The proteins that were isolated by using AllPrep RNA/Protein Kit (50) (80404, QIAGEN, Germany) was used to quantify the levels of cytokine IL-1 β and VEGF, which would be further analyzed by mouse IL-1beta/IL-1F2 DuoSet and mouse VEGF DuoSet ELISA kits (R&D Systems). The proteins that were lysed in 1 \times PBS buffer (with protease inhibitor), were used to quantify the levels of PEDF and iNOS, TNF- α proteins by using Mouse PEDF ELISA Kit (KTE70449, Abbkine, China), iNOS, ELISA Kit (MBS030771, My Biosource, USA) and mouse TNF- α DuoSet ELISA kits (R&D Systems) respectively. All the operation was performed according to the related manufacturer's protocol.

2.2.16.1 R&D Systems ELISA kit (IL-1 β , TNF- α , VEGF) related experimental protocol

Before the experiment, the reagents were taken out from 4°C refrigerator and warmed to room temperature (kept at least 15 min). The standard antibody (ELISA kits of IL-1 β , TNF- α and VEGF) was 1:2 diluted 10 times serially, as shown in Fig. 13.



Figure 13. Preparation of R&D Systems ELISA kit (IL-1 β , TNF- α , VEGF) standard antibody reference.

2.2.16.1.1 96-Well microplate preparation

[1] The capture antibody was diluted to working concentration with 1 \times PBS buffer without carrier protein. The diluted capture antibody was then coating on the 96-well microplate (100 μ L per well). The coated microplate was sealed and incubated

overnight at room temperature.

- [2] On the second day, the liquid in wells was removed and 400 μL $1\times$ washing buffer was added to each well for washing (totally 3 times). The remained washing buffer was removed by inverting the microplate onto clean paper towels.
- [3] Reagent diluent (300 μL) was added to each well to block the microplate. Then the blocking microplate was incubated at room temperature for 2 h.
- [4] The washing process described in step 2 was repeated 3 times.

2.2.16.1.2 Assay Procedure

- [1] The standard antibody with 10 increasing concentrations prepared in advance (Fig. 13) were added into 10 wells serially (100 μL per well, duplicated wells), to establish a concentration gradient. The sample solutions to be determined were added into the wells (100 μL per well, duplicated wells) according to the marks made in advance. Reagent diluent was added to blank wells (100 μL per well, duplicated wells). Afterward, the microplate was sealed and incubated at room temperature for 2 h.
- [2] The washing process described in section **2.2.16.1.1-[2]** (step 2 of microplate preparation) was repeated 3 times.
- [3] The detection antibody was diluted with reagent diluent according to the manufacturer's protocol, and was added into each well to be determined (100 μL per well). The microplate was then covered with a new adhesive strip and incubated for 2 h at room temperature.
- [4] The washing process (step 2 of microplate preparation) was repeated 3 times.
- [5] The working dilution of Streptavidin-HRP (100 μL) was added into each well. The microplate was then sealed and placed in a dark box to incubate for 20 min at room temperature.
- [6] The washing process (step 2 of microplate preparation) was repeated 3 times.
- [7] The substrate solution A (50 μL) and substrate solution B (50 μL) were added to each well and mixed well. The microplate was sealed and placed in a dark box to

incubate for 20 min at room temperature. The solution turned blue gradually during the incubating process.

- [8] The stop solution (50 μL) was added to each well. The microplate was tapped gently to ensure the solution mixed thoroughly. The solution color turned to yellow from blue immediately.
- [9] The optical density value of each well was determined immediately, using a microplate reader, in which the absorbance was set to 450 nm and the wavelength correction was set to 540 nm.
- [10] According to the optical density value in standard wells and the corresponded standard antibody concentration gradient, the standard curve was created as shown in Fig. 14.
- [11] The optical density value of the determined sample was substituted into the corresponding equation obtained in the previous step, to calculate the concentration of the determined protein solution. Afterward, the amount of protein (IL-1 β , TNF- α , VEGF) in 80 μg total protein would be calculated according to the determined concentration. If the standard deviation (SD) of two data obtained from a same sample was more than 20%, the assay experiment would be repeated until the SD is less than 20%. The two groups of data were then statistically compared for further analysis.

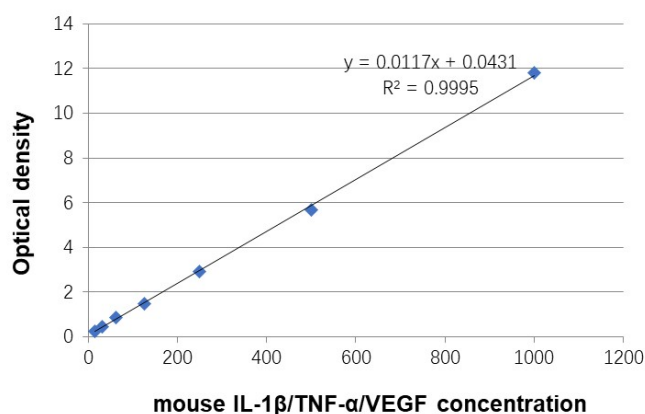


Figure 14. The standard curve model of mouse IL-1 β /TNF- α /VEGF concentration

2.2.16.2 iNOS (My BioSource) ELISA kit experimental protocol

All reagents were placed at room temperature for 30 min before use. The standards, samples and blank wells (control wells) were set up in advance. All standards and samples were assayed in duplicate.

- [1] The standard antibody or the sample solutions (50 μ L) were added into the corresponding wells, while the diluent (50 μ L) was added to blank wells.
- [2] HRP solution (100 μ L) was added into each well, and the microplate was covered with membrane and was incubated in an incubator at 37°C for 60 min.
- [3] The solution in the wells was aspirated out. 1 \times washing buffer (350 μ L) was then added into each well, and kept for 1 min. The washing buffer was removed, and the microplate was placed on a clean absorbent paper and drained by tapping. This washing process was repeated 4 times.
- [4] The substrate solution A (50 μ L) and substrate solution B (50 μ L) were added to each well (including blank control well), and tapped the microplate gently to mix the solution well. The microplate was covered with strip and incubated in a dark incubator at 37°C for 20 min. The solution would turn blue during the process.
- [5] The stop solution (50 μ L) was added into each well including blank control well, and tapped the microplate gently to mix the solution well. The solution color would turn yellow from blue immediately.
- [6] The optical density was determined with a microplate reader at 450 nm immediately.
- [7] According to the optical density value in the standard wells and the corresponded standard antibody concentration gradient, the standard curve was created. The optical density values of the determined samples were substituted into the corresponding equation, to calculate the concentrations of iNOS protein in the sample solutions. The amount of iNOS protein in 80 μ g total protein was then calculated according to the concentration.

2.2.16.3 PEDF (Abbkine) ELISA kit experimental protocol

All reagents were taken out from fridge and warmed to room temperature before use. The standard antibody was 1:2 diluted 5 times following the steps shown in Fig. 15 to the lowest concentration of 10 $\mu\text{g/L}$. The washing solution was diluted to the desired concentration with ddH₂O. The Standard wells, testing sample wells, blank wells were set in advance. All standard antibody solutions, test samples and blank control were equipped with double wells to enable the determination in duplicate.

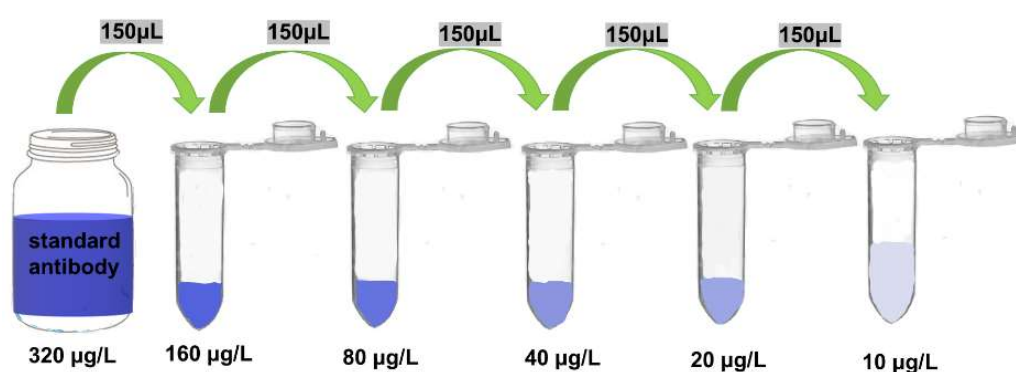


Figure 15. Standard antibody dilution steps of PEDF ELISA kit.

- [1] The diluted standard solutions were added into standard wells (50 μL per well). 10 μL sample solution together with 40 μL of sample diluent were added to each sample well. The blank wells were left empty.
- [2] The microplate was sealed and incubated at 37°C for 45 min.
- [3] The solution in the wells was aspirated out, and 250 μL of 1 \times washing buffer was added into each well and kept for 1.5 min. The washing buffer was then removed, and the microplate was placed on a clean absorbent paper and drained by tapping. This washing process was repeated 4 times.
- [4] The HRP conjugated detection antibody (50 μL) was added into each well except the blank ones.
- [5] The microplate was sealed and incubated in a dark incubator at 37°C for 30 min.
- [6] The washing process described in step 3 was repeated.

- [7] The chromogen solution A (50 μ L) together with chromogen solution B (50 μ L) were added into each well and mixed gently, followed by incubating the microplate in a dark incubator at 37°C for 15 min.
- [8] The stop solution (50 μ L) was added into each well and tapping the microplate gently.
- [9] The optical density (O.D.) was determined by using a microplate reader at 450 nm immediately.
- [10] According to the optical density values in the standard wells and the corresponded standard antibody concentrations gradient, the standard curve was created. The optical density values of the determined samples were substituted into the corresponding equation, to calculate the concentrations of PEDF protein in the sample solutions. The amount of PEDF protein in 80 μ g total protein was then calculated according to the concentration.

2.2.16.4 Fgf10 (My BioSource) ELISA kit experimental protocol

The proteins that were extracted by using $1\times$ PBS buffer was used to quantify the level of cytokine Fgf10, which was analyzed by mouse fibroblast growth factor 10 ELISA Kit (My BioSource, USA). All the operation was performed according to the related manufacturer's protocol. And the exact processes please refer to PEDF ELISA performing in the **section 2.2.16.3**.

2.3 Data statistics

The levels of proteins (IL-1 β , iNOS, TNF- α , VEGF, PEDF, Fgf10) in 80 μ g total proteins from different little groups were compared and analysed. The ratios of VEGF vs PEDF proteins was also analysed. Values were expressed as mean \pm SD. One or two-way analysis of variance (1 or 2 way-ANOVA) or multiple *t*-tests were used to determine statistical significance. All statistics were carried out using GraphPad Prism

7 (GraphPad Software Inc, SanDiego, CA, USA), *P* value less than 0.05 was defined as statistically significant.

3 RESULTS

3.1 Neural retinal tissue develops an inflammatory reaction to C-cigarette smoke and E-cigarette vapor in mice

3.1.1 The effect of C-cigarette smoke or E-cigarette vapor exposure on neural retina

In the medium-term C-cigarette smoke exposure subgroup, the level of pro-inflammatory cytokines TNF- α (Fig. 16-C) is reduced in neural retina, the level of anti-angiogenic cytokines PEDF (Fig. 16-E) slightly increased, and the ratio of VEGF over PEDF (Fig. 16-F) decreased by about 40% compared to control mice. Whereas, after long-term exposure, only the level of IL-1 β (Fig. 16-A) is higher in C-cigarette smoke exposure mice than control mice (about 1.8 folds).

In short-term E-cigarette vapor exposure groups, compared to control mice, the expression of iNOS (Fig. 16-H) in nicotine-free subgroup increased, however, both the levels of TNF- α (Fig. 16-I) and the ratio of VEGF over PEDF (Fig. 16-L) decreased significantly. Data of the nicotine-containing E-cigarette subgroup showed low levels of TNF- α (Fig. 16-I) and down-regulated VEGF over PEDF ratio (Fig. 16-L) in vapor exposure mice compared to control mice.

In medium-term exposure groups, the level of iNOS (Fig. 16-H,) and the ratio of VEGF over PEDF (Fig. 16-L) are increased significantly in the nicotine-free E-cigarette subgroup. In contrast, the data from the nicotine-containing subgroup indicate that the expression of IL-1 β (Fig. 16-G) decreased, but TNF- α (Fig. 16-I) increased significantly. Although there are higher levels of PEDF, there is no significant difference between nicotine-containing subgroup and control mice with regard to the ratio of VEGF to PEDF.

Interestingly, long-term nicotine-containing E-cigarette vapor exposure can reduce the expression of TNF- α (Fig. 16-I) in neural retina, and the ratio of VEGF over PEDF (Fig. 16-L) is decreased as well.

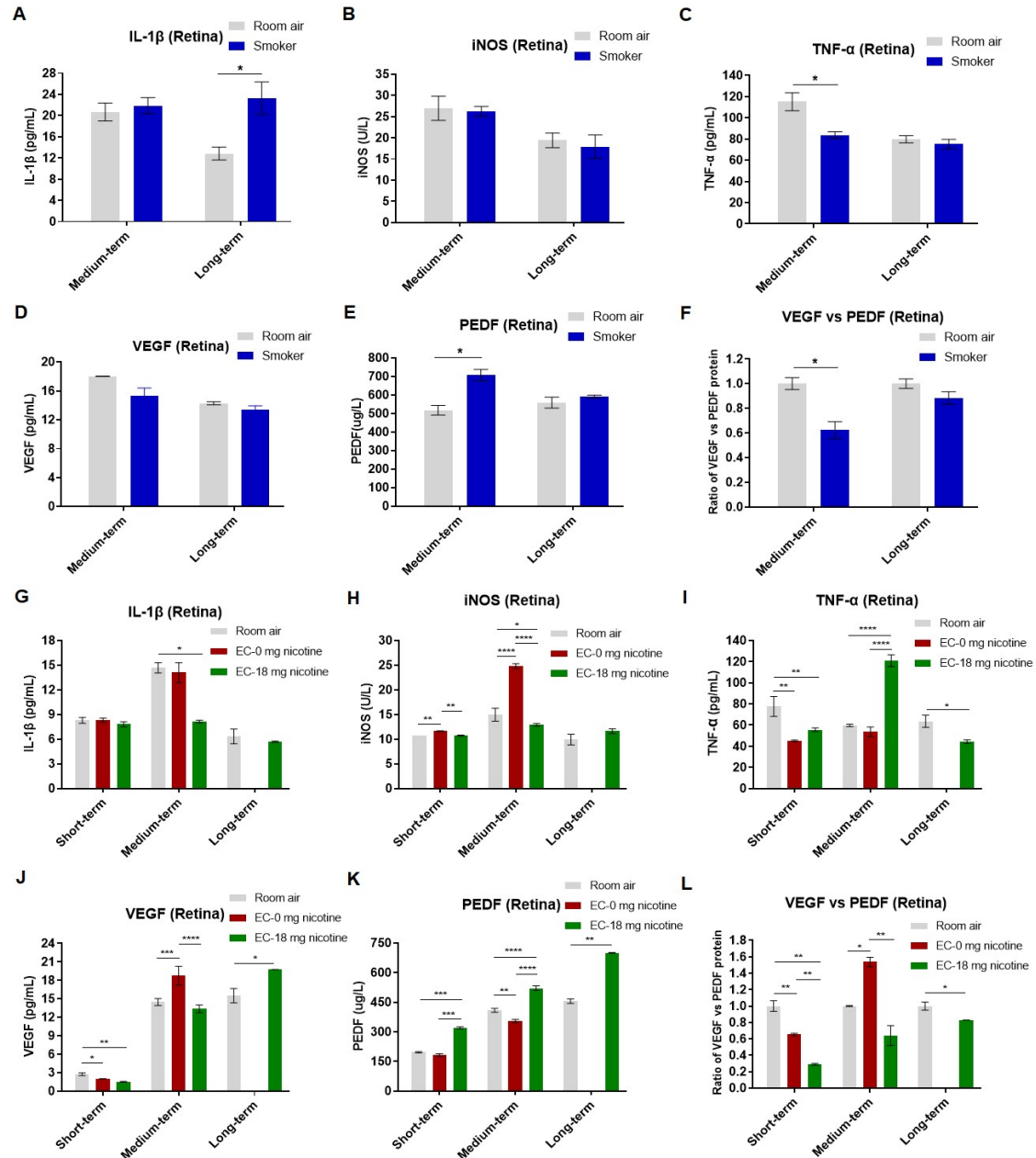


Figure 16. Protein levels in the neural retina of animals from the C-cigarette smoke or E-cigarette vapor exposure subgroups. Data presented are from factors IL-1 β (A, G), iNOS (B, H), TNF- α (C, I) and VEGF (D, J), PEDF (E, K). The ratio of VEGF over PEDF proteins (F, L) reflects the comprehensive effect of pro-angiogenic. Histograms A-F were from C-cigarette smoke exposure groups; histograms G-L were from E-cigarette vapor exposure groups. EC-0 mg nicotine: E-cigarette (nicotine free) vapor; EC-18 mg nicotine: E-cigarette (nicotine containing) vapor. Data are presented as mean \pm SD. * $P < 0.05$, ** $P < 0.01$, *** $P < 0.001$, **** $P < 0.0001$.

3.1.2 Comparing the effect of C-cigarette smoke with E-cigarette vapor (nicotine-free or nicotine-containing) on neural retinal tissue

In medium-term exposure groups, in neural retinal tissues from mice exposed to C-cigarette smoke, the protein level of the pro-inflammatory mediator TNF- α (Fig. 17-C) is decreased by 27%, and there is a decreased ratio of VEGF vs. PEDF (Fig. 17-F) by 38%. Surprisingly, most of the investigated factors in the nicotine free E-cigarette subgroup changed in an opposite trend with regard to the C-cigarette subgroup, except TNF- α (Fig. 17-C). In the nicotine-containing E-cigarette subgroup, the expression level of IL-1 β (Fig. 17-A) decreased by 44% after exposure, while TNF- α (Fig. 17-C) increased by 103%. Besides, the regulation trends of iNOS, VEGF and PEDF were similar to the C-cigarette subgroup.

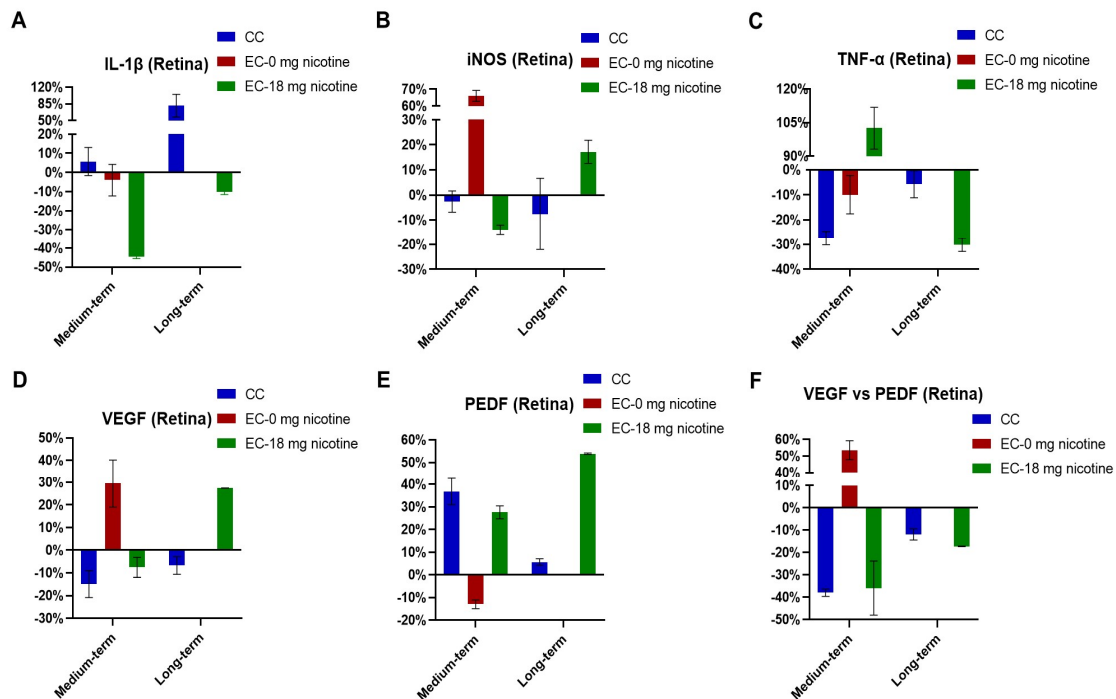


Figure 17. Comparison of the percentage changes in protein concentration between C-cigarette smoke and E-cigarette vapor exposure subgroups. Presented is the percentage change in protein concentration for cytokines IL-1 β (A), iNOS (B), TNF- α (C), VEGF (D), PEDF (E), and the ratio of VEGF to PEDF (F) in neural retinal tissue of each experimental subgroup after smoke or vapor exposure. Ratio of VEGF vs PEDF reflects the changes to the equilibrium of both factors at the RPE/neural retina interface. CC: C-cigarette smoke; EC-0 mg nicotine: E-cigarette (nicotine free) vapor; EC-18 mg nicotine: E-cigarette (nicotine containing) vapor.

In long-term exposure group, the changes in the C-cigarette exposure subgroup were similar to the medium-term group. The most significant change is the increase of the IL-1 β protein level by 81% (Fig. 17-A), while the change of the ratio of VEGF to PEDF (Fig. 17-F) is less. In the nicotine-containing E-cigarette group, IL-1 β and TNF- α both were down-regulated by 10% and 30% respectively, while the iNOS level was up-regulated by 17%. In addition, the protein levels of VEGF (Fig. 17-D) and PEDF (Fig. 17-E) both increased simultaneously, resulting in a decreased ratio of VEGF to PEDF (Fig. 17-F) by 17%.

3.1.3 Comparing the different effects of medium- and long-term exposure of E-cigarette vapor on RPE and choroid

In RPE, after medium-term nicotine-free E-cigarette vapor exposure, the protein levels of IL-1 β (Fig. 18-A), iNOS (Fig. 18-B), and VEGF (Fig. 18-D) were up-regulated, the ratio of VEGF to PEDF (Fig. 18-F) increased significantly as well. Simultaneously, data from the nicotine-containing subgroup indicated that IL-1 β (Fig. 18-A) and TNF- α (Fig. 18-C) levels increased significantly. The increase of the ratio of VEGF vs PEDF (Fig. 18-F) is more significant compared to the nicotine-free subgroup. In the long-term nicotine-containing exposure subgroup, the changes of protein levels of pro-inflammatory mediators are similar to but less significant than the medium-term exposure group, and there is no significant difference for the ratio of VEGF vs PEDF anymore.

In the choroid, after medium-term nicotine-free E-cigarette vapor exposure, the levels of IL-1 β (Fig. 18-A), TNF- α (Fig. 18-C), and VEGF (Fig. 18-D) all increased significantly. Nevertheless, the data from nicotine-containing subgroup showed a slight increase of IL-1 β , while the ratio of VEGF over PEDF (Fig. 18-F) decreased significantly. Additionally, the long-term effect of nicotine-containing E-cigarette vapor on the choroid resulted in higher levels of IL-1 β , iNOS, and in the ratio of VEGF vs. PEDF.

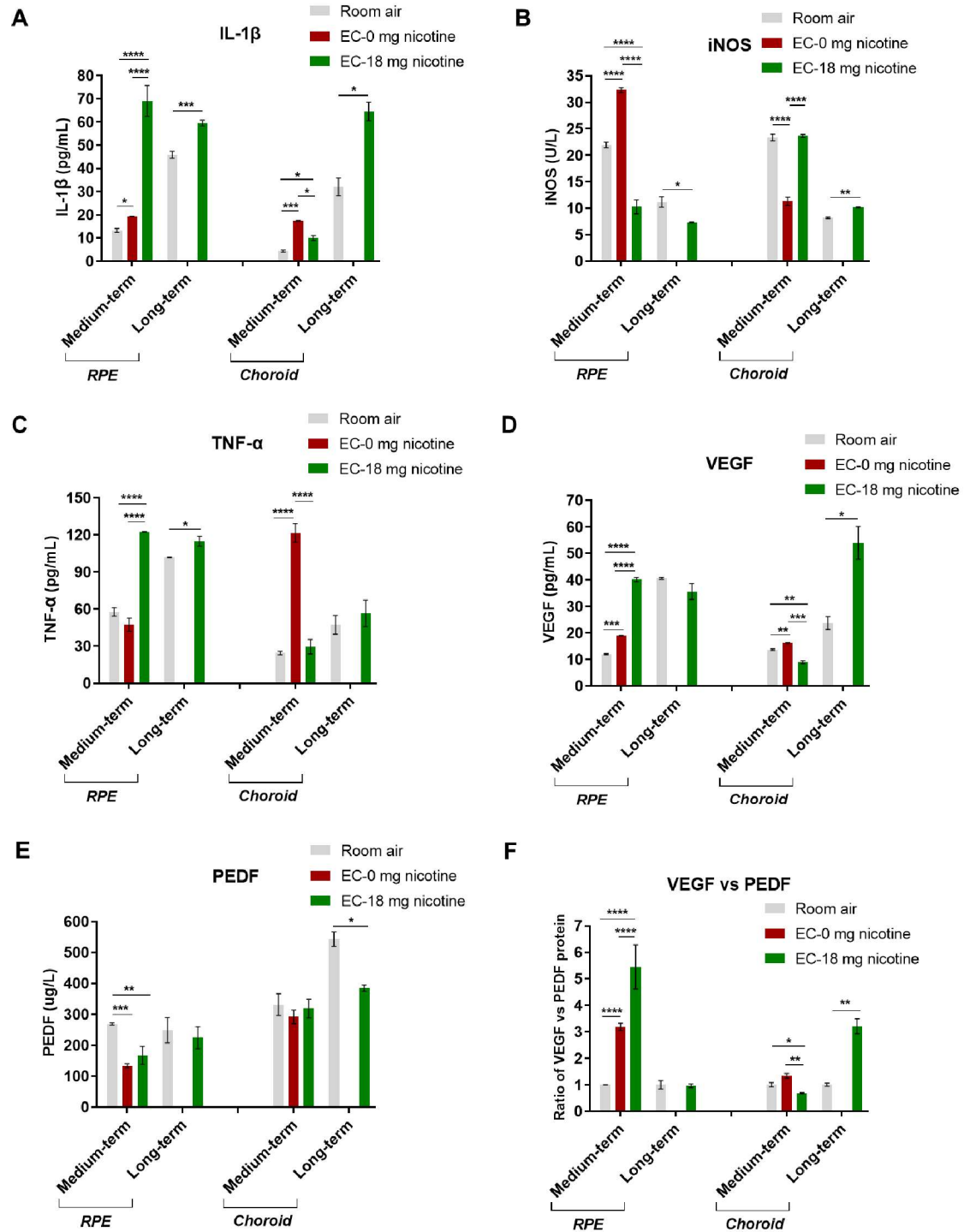


Figure 18. Protein levels in RPE and Choroid of animals from the E-cigarette vapor exposure subgroups. Data presented are from factors IL-1 β (A), iNOS (B), TNF- α (C), VEGF (D), and PEDF (E) protein secreted by RPE and choroid in mice. The ratio of VEGF over PEDF (F) protein of each control was set as 1.0, this ratio reflects the changes to the equilibrium of both factors at the RPE/neural retina interface. All the data are presented as mean \pm SD. EC-0 mg nicotine: E-cigarette (nicotine free) vapor; EC-18 mg nicotine: E-cigarette (nicotine containing) vapor. * $P < 0.05$, ** $P < 0.01$, *** $P < 0.001$, **** $P < 0.0001$.

3.1.4 The comprehensive effects of medium- or long-term exposure of E-cigarette (nicotine-free vs nicotine-containing) vapor on neural retina, RPE and choroid

In mice that were exposed to nicotine-free E-cigarette vapor for the medium-term period, only the levels of iNOS (Fig. 19-B) increased in the neural retina. In RPE tissue, surprisingly, the ratio of VEGF to PEDF (Fig. 19-F) increased by 219%. However, the concentrations of mediators in choroidal tissue are different compared to the neural retina and RPE, the levels of IL-1 β (Fig. 19-A) and TNF- α (Fig. 19-C) increased by 298% and 398% dramatically.

In the nicotine-containing E-cigarette subgroup of medium-term exposure, the level of TNF- α (Fig. 19-C) increased by 103% in neural retina. Surprisingly, in RPE tissue, the level of IL- β (Fig. 19-A) and TNF- α (Fig. 19-C) dramatically increased by 421% and 113% respectively, and a significantly increased ratio of VEGF to PEDF (Fig. 19-F) by 445% was also observed. But the cytokines level change in the choroid was not as obvious, only IL- β (Fig. 19-A) was upregulated by 130%.

In long-term nicotine containing E-cigarette vapor exposure subgroups, the cytokine level changes were not significant in both, neural retina and RPE. However, in the choroid, the level of VEGF (Fig. 19-J) was upregulated by 128%, accompanied with the downregulated level of PEDF (Fig. 19-K) by 29%, and hence the ratio of VEGF to PEDF (Fig. 19-L) was increased dramatically (221%).

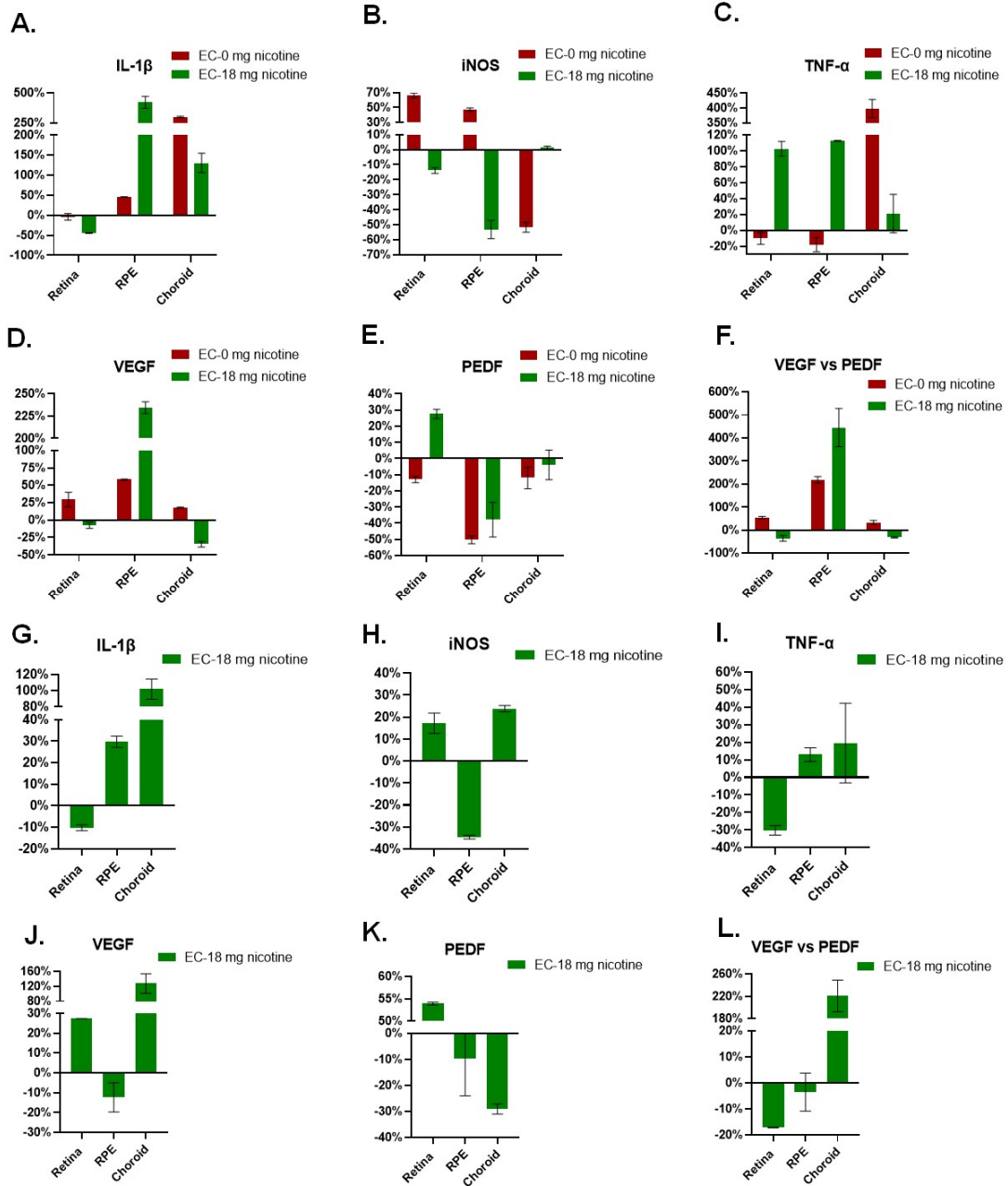


Figure 19. Comparison of percentage changes in protein level in neural retina, RPE, and choroid in the E-cigarette medium-term or long-term exposure subgroups. Data sets are presented for factors IL-1 β (A, G), iNOS (B, H), TNF- α (C, I), VEGF (D, J), PEDF (E, K), and the ratio of VEGF to PEDF (F, L). Ratio of VEGF vs PEDF reflects the changes to the equilibrium of both factors at the RPE/neural retina interface. Histograms A-F were from medium-term exposure groups; histograms G-L were from long-term exposure groups. EC-0 mg nicotine: E-cigarette (nicotine free) vapor; EC-18 mg nicotine: E-cigarette (nicotine containing) vapor.

3.2 Does Fgf10-overexpression have protective effect on the retina of smoking mice model?

Fgf10 overexpressing (OE) mice were placed into the smoke incubator apparatus according to the experimental scheme (Fig. 8, Material and Methods). After 8 months of exposure, both smoker and control (room air) mice were placed in the normal room air environment for different periods (1 week (w)/5 w/12 w) as the phase of regeneration (Re), during which Fgf10 overexpression was induced by oral doxycycline application (+ dox) or not.

3.2.1 The Fgf10 mRNA expression in neural retina of Fgf10 OE transgenic (no/+ Dox) mice.

The Fgf10 mRNA expression in the neural retina of Fgf10 OE transgenic (no/+ Dox) mice relative to WT mice both in room air group is shown in Fig. 20-A. The Fgf10 mRNA expression in neural retina of Fgf10 OE transgenic mice (no Dox) increased at 1 w regeneration timepoint, was about 4.3 times over WT mice. Nevertheless, after 12 w of regeneration, the level fell back again, and there was no significant difference with WT mice. However, Fgf10 mRNA expression in neural retina of Fgf10 OE transgenic (+ Dox) mice all increased significantly at three timepoints (1 w, 5 w, 12 w). Interestingly, the expression reached a peak at 1 w Re timepoint, when it was 130-fold higher than in WT mice. With the extension of regeneration time, the doxycycline induced overexpression of Fgf10 was downregulated gradually, it was only 2.8-fold over WT mice at 12 w regeneration timepoint. These results indicated that Doxycycline successfully induced the Fgf10 gene overexpression in the neural retina.

In Fig. 20-B, the Fgf10 mRNA expression levels in the neural retina of smoker mice are presented. Comparing with WT smoking mice, in Fgf10 OE transgenic (no Dox) smoker mice, the Fgf10 mRNA expression increased, and the trend was similar with the room air group. It was 5.0 times over WT smoker mice at 1 w regeneration

timepoint, and 2.6 times at 12 w regeneration timepoint, the difference with significant. Moreover, the relative Fgf10 mRNA expression in neural retina of Fgf10 OE transgenic (+ Dox) smoker mice was always significantly higher than WT smoker at all three regeneration timepoints.

Fig. 20-C shows the comparative analysis between smoker and control in different subgroups. In the neural retinas of smoker mice in both the WT and Fgf10 OE transgenic (no Dox) group, the Fgf10 mRNA expression was significantly upregulated compared to control mice. However, in the neural retina of Fgf10 OE transgenic (+ Dox) mice, the Fgf10 mRNA expression levels in smoker mice were lower than control mice at 1 w and 5 w regeneration timepoints, but upregulated dramatically at 12 w regeneration (30.9-fold).

Fig. 20-D displays the relative percentage change of Fgf10 mRNA expression in neural retina from mice of the smoke exposure groups comparing with control mice.

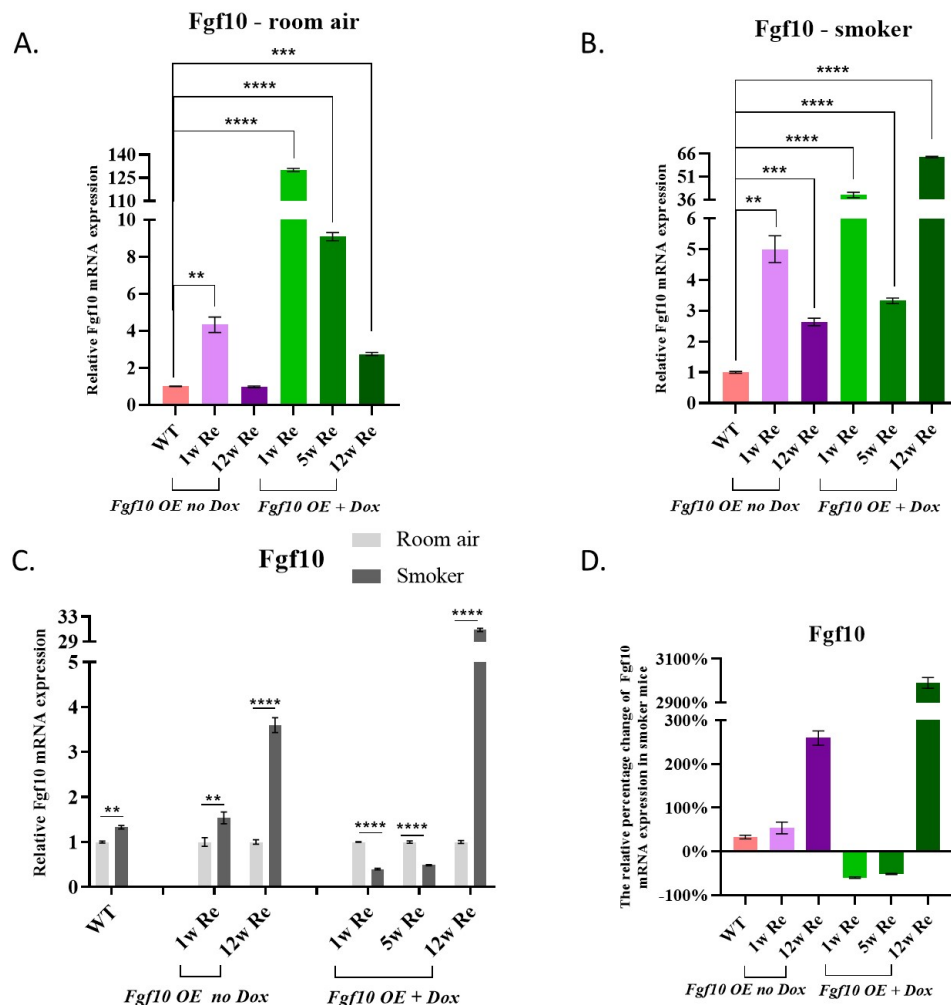


Figure 20. The Fgf10 mRNA expression in the neural retina of Fgf10 OE (no/+ Dox) mice. **(A)** In the control (room air) subgroup, relative to WT mice, the Fgf10 mRNA relative fold expression in Fgf10-overexpression (no/+ doxycycline) mice. **(B)** In the smoker subgroup, relative to WT mice, the Fgf10 mRNA relative fold expression in Fgf10-overexpression (no/+ doxycycline) smoker mice. **(C)** The Fgf10 mRNA relative fold expression of smoker mice relative to control mice in different gene groups. **(D)** the relative percentage change of Fgf10 mRNA expression of smoker relative to control mice in different gene groups. Data (n = 12) are presented as mean \pm SD. * P < 0.05, ** P < 0.01, *** P < 0.001, ****P < 0.0001.

3.2.2 Cytokine expression in the neural retina of Fgf10 OE transgenic + 12 w Re (no/+ Dox) mice

Fig. 21 shows that the Fgf10 (A) protein level in the neural retina of Fgf10 OE +12 w Re (+ Dox) mice is significantly higher compared to both WT and Fgf10 OE + 12 w Re (no Dox) mice, and that there is no significant difference between WT and Fgf10 OE + 12 w Re (no Dox) mice. Additionally, Fig. 21-B indicates that, both in room air and smoker subgroups, the Fgf10 protein levels in neural retina of mice receiving doxycycline via the food during regeneration phase are much higher than non-Fgf10 overexpressing mice (no Dox in the food), which further demonstrates that doxycycline administration successfully induced Fgf10 overexpression.

In animals exposed to smoke but not receiving doxycycline, protein levels of Fgf10 (C), TNF- α (E), VEGF (G), and the ratio of VEGF vs PEDF (I) was lower in the neural retina compared to control mice (Fig 21). In animals exposed to smoke and receiving doxycycline (Fgf10 overexpressed), protein levels TNF- α (E), and the ratio of VEGF vs PEDF (I) were lower, while the levels of IL-1 β (D), iNOS (F) and PEDF (H) all increased significantly. Fig. 21-J displays the percentage change of protein levels and the VEGF vs. PEDF ratio in animals exposed to smoke and with an Fgf10 overexpression (+ Dox) or without (no Dox), in correlation to control mice.

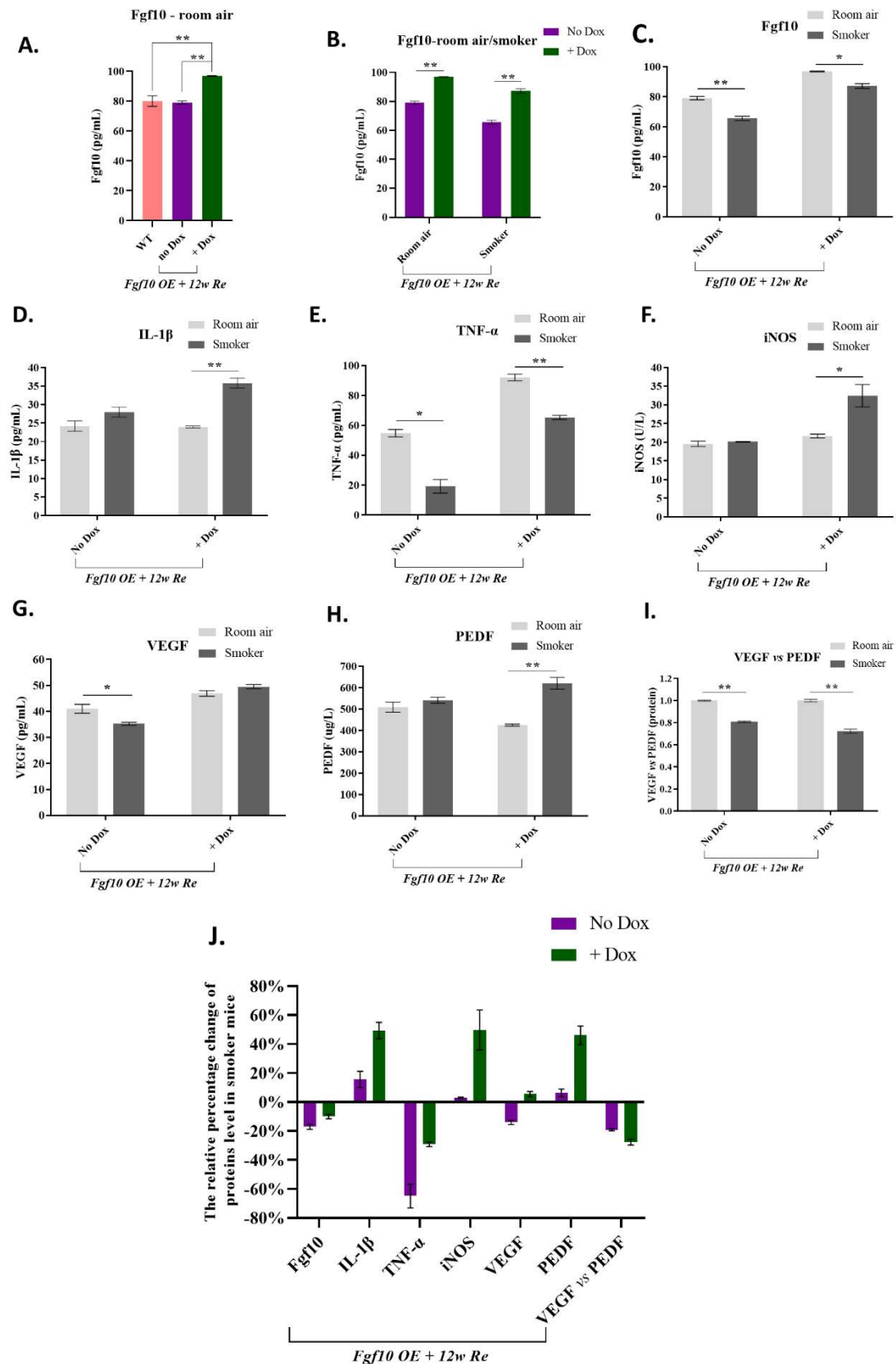


Figure 21. The cytokines protein levels in the neural retina of Fgf10 OE (no/+ Dox) mice. (A) In room air subgroups, the Fgf10 protein expression levels in the neural retina of WT and Fgf10 OE transgenic + 12 w Re (no/+ Dox) mice. (B) the Fgf10 protein expression levels difference in mice which given normal

(no Dox) or doxycycline diet (+ Dox) during the 12 w regeneration period, in room air and smoker subgroups. After Fgf10 OE transgenic mice experienced long-term smoke exposure followed by 12 w regeneration (no/+ Dox), the proteins of Fgf10 (C) and inflammation-related cytokines IL-1 β , TNF- α , iNOS (D, E, F) as well as pro-angiogenic related cytokines VEGF(G), PEDF (H) expression levels in the neural retina. VEGF vs PEDF (I) reflects the comprehensive pro-angiogenic effect, the ratio of control mice was set as 1.00. (J) In neural retina of Fgf10 OE + 12 w Re (no/+ Dox) smoker subgroup, relative to corresponding room air subgroups, the percentage change of proteins (Fgf10, IL-1 β , TNF- α , iNOS, VEGF, PEDF) expression as well as VEGF vs PEDF ratio. Data (n = 12) are presented as mean \pm SD. * P < 0.05, ** P < 0.01, *** P < 0.001, **** P < 0.0001.

3.2.3 Protein expression levels and change with extend of regeneration in the neural retina of Fgf10 OE mice + Re (no/+ Dox)

In the neural retina of animals exposed to smoke but not receiving doxycycline (Fig. 22), protein levels of Fgf10 (A) and VEGF (C) were lower than control mice at 1 w and 12 w Re timepoints. Besides, there was no significant difference observed between smoker and control mice at both timepoints for IL-1 β (B).

On the other hand, in the neural retina of animals exposed to smoke and receiving doxycycline during regeneration, Fgf10 protein levels (A) were lower than control mice at all three regeneration timepoints (1 w, 5 w and 12 w). These results are similar with that those from animals exposed to smoke but not receiving doxycycline. Surprisingly, the protein level of IL-1 β (B) in the retina of animals exposed to smoke receiving doxycycline was lower at 1 w regeneration timepoint, and then increased dramatically at 5 w regeneration timepoint (7.3 times over control mice), and was still higher than control mice (1.5-fold) at 12 w timepoint. Moreover, the VEGF protein (C) levels in retina of smoker mice receiving doxycycline were both higher than non-smoker at 1 w and 5 w timepoints, especially at 5 w (1.9-fold). Nevertheless, there is no significant difference between smoker and non-smoker at 12 w timepoint. Interestingly, in the non-smoker subgroup, Fgf10 (A) and VEGF (C) have opposite protein level trends throughout regeneration phase. Considering the results from the non-overexpression (no Dox) subgroup, the data indicate that long-term smoke exposure could reduce Fgf10 and VEGF protein expression, whereas the induction of transgenic Fgf10 expression

via doxycycline administration generates an inducing effect on IL-1 β and VEGF expression in the retina.

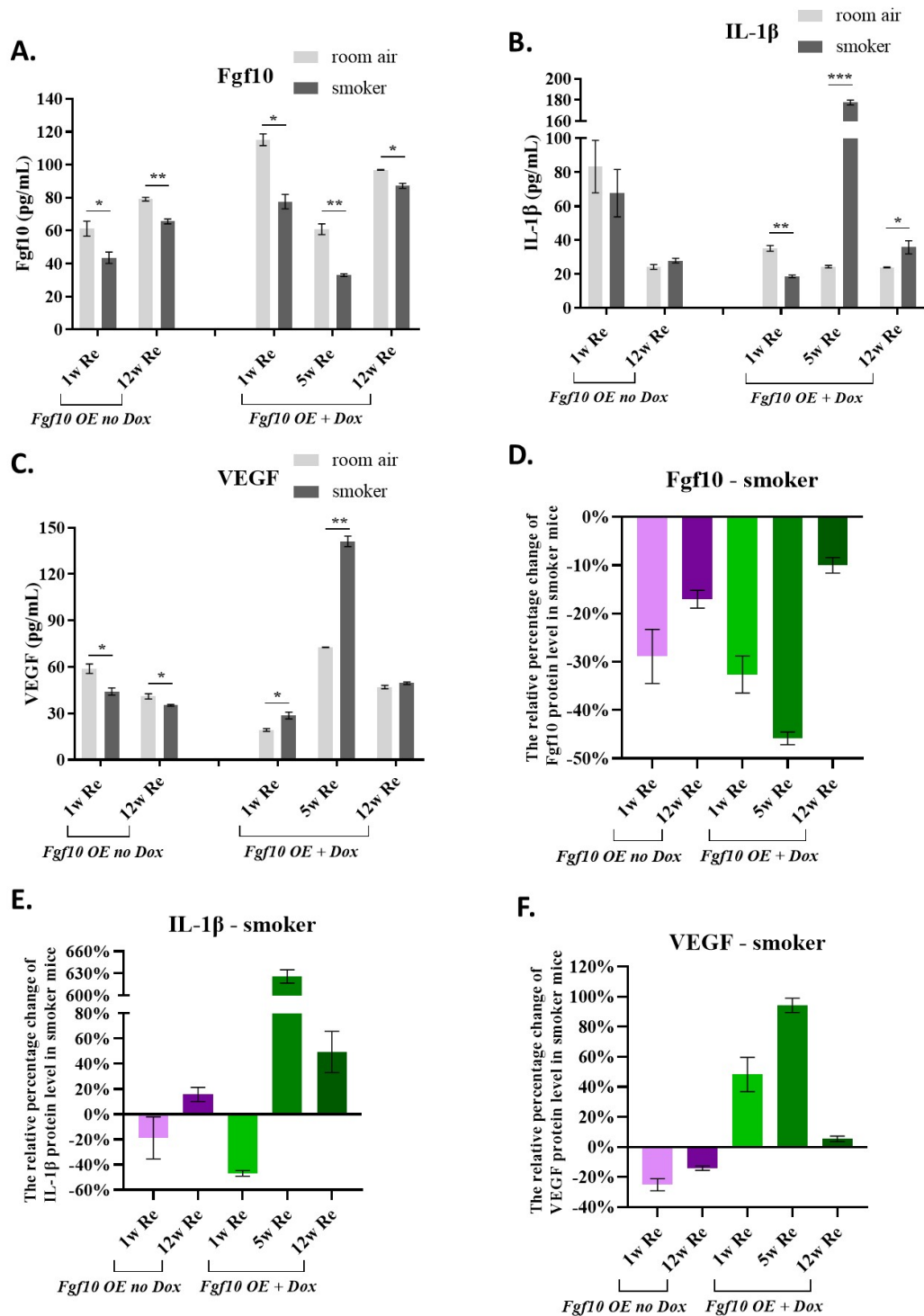


Figure 22. At different regeneration (no/ + Dox) timepoints, the protein levels of Fgf10 (A) and IL-1 β (B) as well as VEGF (C) in neural retina of Fgf10 OE transgenic smoker and non-smoker. The Fgf10 (D), IL-1 β (E) and VEGF (F) protein levels percentage change in smoker neural retina, relative to non-smoker. Data (n = 12) are presented as mean \pm SD. * P < 0.05, ** P < 0.01, *** P < 0.001, **** P < 0.0001.

0.0001.

Fig. 22-(D), (E) and (F) display the protein level percentage changes of Fgf10 and IL-1 β as well as VEGF in animals exposed to smoke and receiving doxycycline (+ Dox) or not (no Dox) in comparison to control animals. It is worth to note that in the Fgf10 overexpression subgroup, the 5 weeks regeneration timepoint is the prominent changing point for Fgf10, IL-1 β , VEGF protein concentrations.

3.2.4 In vivo retinal layer thickness changes in Fgf10 OE mice + 12 w Re (no/+ Dox) measured by OCT

Fig. 23 (A, B) shows the comparative results of retinal layer thickness in smoker and non-smoker mice either receiving doxycycline (+ Dox, Fgf10 overexpression) or not (no Dox). There were no significant differences in layer thickness observed between smoker and non-smoker mice regardless of whether Fgf10 was overexpressed or not for all analysed retinal layers (WR, IR, ONL+, OR).

In addition, the retinal layers thickness that across papilla or peripheral areas were also compared between mice with doxycycline (+ Dox, Fgf10 overexpression) and without doxycycline (not Dox) (Fig. 23-C, D). Similarly, no significant differences were observed between both groups.

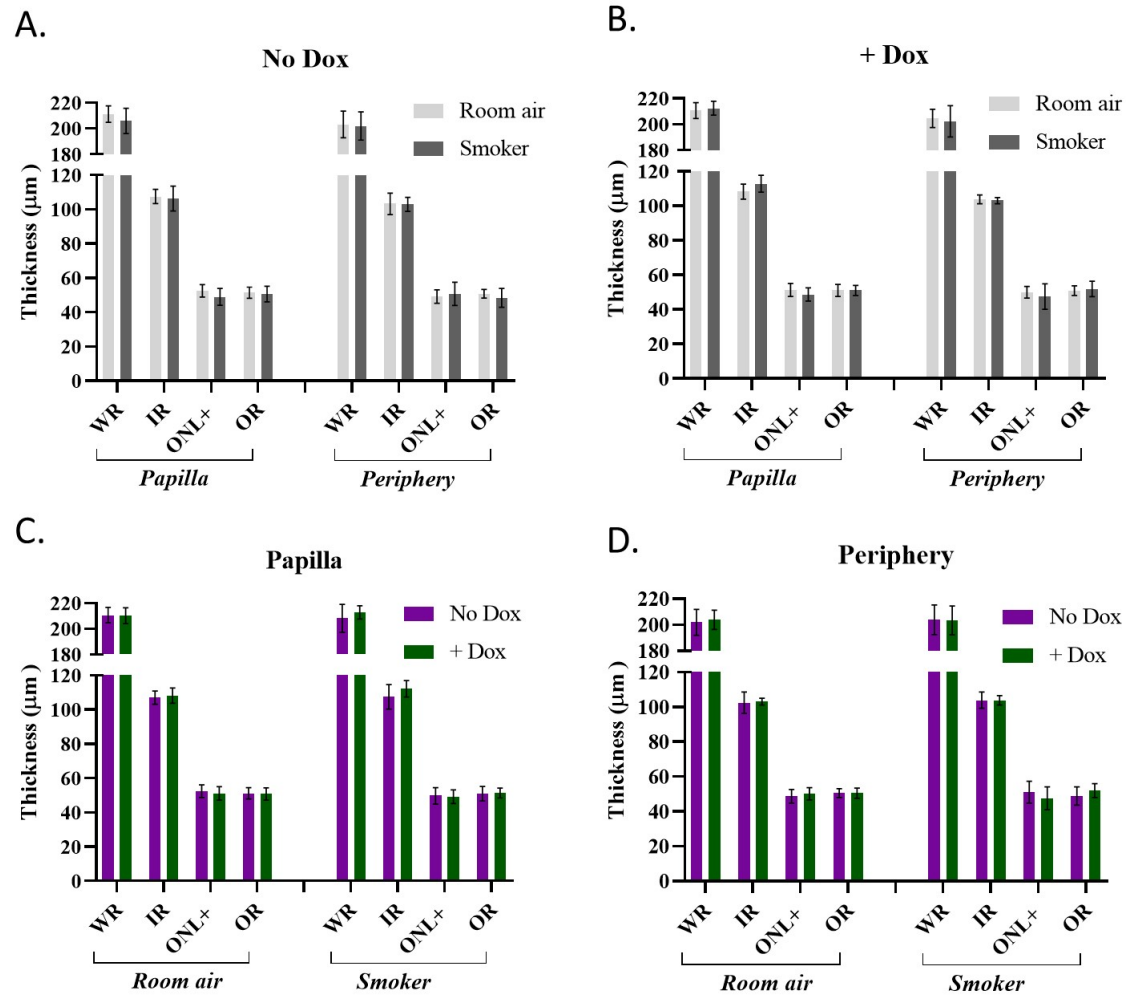


Figure 23. The different retinal layers (across papilla or periphery regions) thicknesses in Fgf10 OE transgenic + 12 w Re no Dox (A) and + Dox (B) mice. The different retinal layers thicknesses across papilla (C) and periphery (D) regions in the Fgf10 OE transgenic + 12 w Re (no/ + Dox) non-smoker and smoker mice. Data ($n = 12$) are presented as mean \pm SD. * $P < 0.05$, ** $P < 0.01$, *** $P < 0.001$, **** $P < 0.0001$.

3.2.5 The effect of long-term smoke exposure or Fgf10-overexpression on mouse retinal vasculature tortuosity

The influences of smoke exposure and presence of Fgf10 during regeneration phase was also assessed with regard to retinal vessel tortuosity and area covered by the tortuosity (Fig. 24). For a description of how tortuosity and area of tortuosity was calculated, please see Methods section 2.2.8 and Fig. 11.

In mice exposed to smoke, tortuosity of arteries was significantly increased in those mice not receiving doxycycline (no Dox) (Fig 24-C) comparing to those receiving doxycycline (+ Dox), while the covered area of tortuosity was significantly less (Fig 24-D). However, mice not exposed to smoke did not show any different behaviour of the vein, regardless of Fgf10 overexpression or not (Fig 24-A, B, C, D). This implies that the presence of Fgf10 in smoker animals during regeneration phase had an effect on the tortuosity of retinal arteries but not veins.

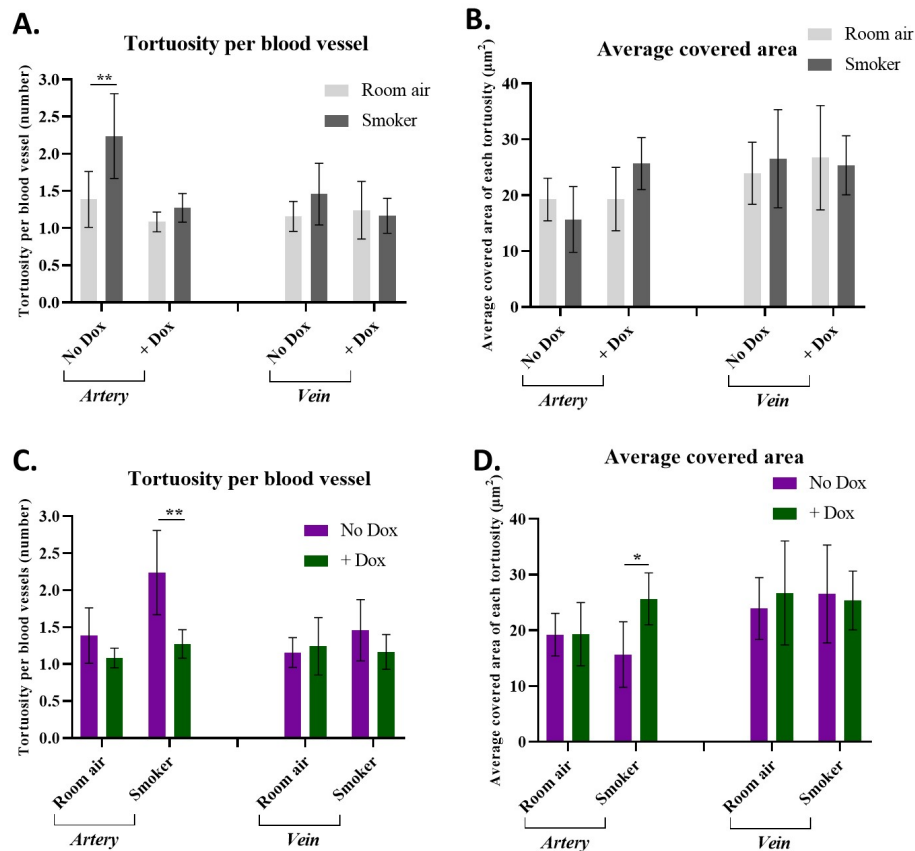


Figure 24. The tortuosity per retinal vessel, and the average covered area per tortuosity. (A) the comparison of retinal tortuosity over blood vessels quantities between smoker and non-smoker (room air) from non-Fgf10 overexpression (no Dox) and Fgf10 overexpression (+ Dox) subgroups. (B) the comparison of average covered area of per retinal blood vessel tortuosity between smoker and non-smoker from two subgroups. (C) the comparison of retinal tortuosity over blood vessels quantities between two subgroups. (D) the comparison of average covered area of per retinal blood vessel tortuosity between two subgroups.

4 DISCUSSION

4.1 Neural retinal tissue develops an inflammatory reaction to C-cigarette smoke and E-cigarette vapor in mice

Most of the past reported studies about the association of smoking with AMD were mainly focused on the effect of smoking on RPE but scarcely on the neural retina. In order to uncover the impact of C-cigarette smoke on neural retina and to distinguish the differential influences of C-cigarette smoke and E-cigarette vapor, in this present study, the effect of smoking towards the neural retina was investigated by comparing the effects of medium-/long-term exposure of C-cigarette smoke with E-cigarette vapor on retinal tissue in mice. In addition, the short-/medium-/long-term effects of E-cigarette vapor exposure on mice's neural retina, RPE, choroid tissues were also evaluated. Herein, the medium- and long-term exposure were conducted to simulate vaping habits of the human population and unveil the association of E-cigarette vapor exposure with increased inflammation and angiogenesis pathways involved in the onset of AMD in humans as well. The short-term exposure was performed as well to assess the immediate adverse effects of E-cigarette vapor on neural retina.

The pathogenesis of two types AMD is not alike. In dry AMD, it is presumably beginning with the RPE dysfunction followed by the dysfunction or loss of photoreceptors and choriocapillaris. In wet AMD, it starts with the dysfunction and loss of the choroidal vasculature alone or together with the RPE layer, followed by the accumulation of pro-inflammatory mediators in choriocapillaris and the subsequent production of excessive angiogenic substances by the RPE because of hypoxia²⁹. Unfortunately, to date, the mechanistic effect of cigarette smoking on neural retina/RPE/choroid is still unknown. Nevertheless, some reviews have summarized that cigarette smoking can increase the oxidative stress burden and hence induce the inflammation response on RPE and choroid, causing the damage to both³¹. Furthermore,

impairing the choroidal blood flow and decreasing the perfusion pressure could result in hypoxia and promote angiogenesis, and eventually cause the development of AMD^{113,114}. Another review elaborated that E-cigarette vapor exposure not only disrupts pulmonary homeostasis but also can increase the inflammatory response and oxidative stress¹¹⁵. Although there are no specialized studies regarding the mechanism of E-cigarette vapor on the retina, in studies with regard to the respiratory system it is assumed that the vapor could also cause the inflammatory response and oxidative stress similar to C-cigarette smoke⁸⁷⁻⁸⁹, which both play key roles in the progression of AMD.

4.1.1 The short-term E-cigarette vapor exposure has limited pro-inflammatory effect on neural retina

In the present study, our results indicated that after short-term exposure to E-cigarette vapor (nicotine-free or nicotine-containing), in neural retina tissue, the anti-angiogenic pathway was activated and no obvious change occurred in the expression of pro-inflammatory mediators. This suggests that the short-term exposure to E-cigarette vapor only had limited pro-inflammatory effect in neural retina. However, AMD is a complicated disease, in which the pathology involves the change of photoreceptor/retinal pigment epithelium/Bruch's membrane/choriocapillaris complex, and the pathological changes of the complex components are changing over time^{29,116}. Therefore, if we want to probe the association of E-cigarette vapor exposure with AMD, it is essential to investigate the neural retina/RPE/choroid tissues simultaneously instead of neural retina alone.

4.1.2 The medium-term E-cigarette vapor (nicotine free and nicotine containing) exposure promotes inflammation and angiogenesis, key pathways in AMD pathogenesis

The comprehensive results from neural retina, RPE and choroid after medium-term

exposure to E-cigarette vapor revealed that both nicotine-containing and nicotine-free E-cigarette vapor could stimulate the expression of pro-inflammatory and angiogenic mediators in RPE and choroid tissues. It is presumably the cause that led to inflammatory response in these tissues and generate CNV. Interestingly, such results are in line with the pathogenesis of wet AMD as mentioned above, which suggests that even without nicotine or flavoring agents, the E-cigarette vapor that is only generated from basic humectants still can promote the occurrence and progression of wet AMD.

In addition, we found that the adverse effects which are stimulated by nicotine-containing E-cigarette vapor on the RPE (choroid) are stronger than those of nicotine-free vapor. Since the only difference between two E-cigarette vapors is the presence of nicotine component, thereby, our results suggest that the nicotine component can enhance the harmful effect of vapor which derives from basic solvents on RPE (choroid). As shown in Fig. 19-F (red-line vs. green-line), in RPE tissue, the relative change of the ratio of VEGF to PEDF in the nicotine-containing subgroup (445%) is about 2 times higher than the value from nicotine-free subgroup (219%). This result is consistent with a study by Pon and colleagues, wherein they confirmed that nicotine could increase the ratio of VEGF to PEDF by interacting with nicotinic acetylcholine receptors (nAChR) on RPE cells, which is critical in the development of wet AMD for second-hand smokers¹¹⁷. Previous studies have demonstrated that nicotine is an agent with pro-angiogenic effect and can stimulate the proliferation of CNV⁵⁸, and the impact of nicotine on the expression of pro-angiogenic and inflammatory mediators has also been reported¹¹⁸. All these reported findings could rationalize our results of nicotine-containing E-cigarette vapor exposure.

4.1.3 The mechanistic effects of E-cigarette vapor on retinal tissue

It is known that the basic humectants (propylene glycol and vegetable glycerin) in e-liquid are used as solvents for nicotine and flavoring agents¹¹⁹. The study by Bekki and colleagues showed that heating the mixture of propylene glycol and vegetable glycerol

could generate carbonyl compounds such as formaldehyde, acetaldehyde, acetone, and acrolein¹²⁰. Additionally, Higham et al. found that the acrolein present in the vapor extract might originate from the heated glycerol¹²¹. The United States department of labor indicates that the first-time exposure to formaldehyde agent triggers the immune system of the body; in addition, the acute exposure of formaldehyde can cause strong irritation to the eyes, nose and throat, and might induced cough and even asthma, while the subsequent chronic exposure might cause severe allergic reactions in the skin, eyes and respiratory tract¹²². Nevertheless, the toxicity of acrolein is far more severe than formaldehyde (about 10-1000 times)¹²³. Acrolein reacts with sulfhydryl groups and leads to the oxidative stress damage of cells, which is cause by increased production of oxidative substances, by oxidative damage to proteins and DNA, by consumption of antioxidants and antioxidant enzymes, and by inactivation of nuclear factor-E2-related factor 2 pathways (Nrf2)¹²⁴. Furthermore, acrolein causes mitochondrial dysfunction (by reducing membrane potential, activating mitochondrial complex group, etc.), which in turns results in a reduced cell viability¹²⁵. Some studies suggest that acrolein could also induce an inflammatory reaction from macrophages and epithelial cells^{126,127}. For instance, Higham and colleagues found that the acrolein level that can be detected in E-cigarette vapor induces neutrophils to release matrix metalloproteinase-9 (MMP-9)¹²¹, which indirectly proves that the acrolein is one of the components in E-cigarette vapor with underlying pro-inflammatory potential.

Heating of four different kinds of E-liquid ((1) propylene glycol, (2) glycerin, (3) commercial e-liquid (no nicotine), (4) Vape Dudes Classic tobacco flavor (containing 24mg/mL nicotine)) generated all high levels of Reactive oxygen species (ROS), with the third type of commercial e-liquid (no nicotine) produced the highest level of ROS⁸⁹. Thereby, this study confirmed that the heating process can produces ROS itself, and the nicotine ingredient in the e-liquid is not the only source of ROS. Moreover, it can even be speculated that the presence of nicotine might reduce the amount of ROS produced. On the other hand, this study also found that after exposing the mice to E-cigarette vapor (containing nicotine) for 3 days, the level of IL-6, IL-1 α , IL-13 and other pro-

inflammatory mediators present in the alveolar lavage fluid significantly increased. The authors of this study consider that such phenomenon might be caused by oxidative stress and inflammatory reactions, which are mediated by Nano-scale toxic particles and heavy metals in e-cigarette vapor reaching into the alveolar epithelium⁸⁹.

Based on these reports, with regard to our results of nicotine free E-cigarette vapor exposure, it is speculated that the acrolein or other relative carbonyl compounds in the vapor from humectants induce the expression of pro-inflammatory mediators from RPE cells and the choroidal capillary endothelial cells or some special inflammatory cells. However, although some studies reported that E-cigarette vapor exposure could induce angiogenesis¹²⁸, it still cannot be judged whether the angiogenic effect is induced by nicotine or not. Future studies are needed to probe the exact mechanisms of how the nicotine free E-cigarette vapor causes angiogenesis.

4.1.4 The different effects of C-cigarette smoke and E-cigarette vapor on neural retina

The ingredients present in C-cigarette smoke are different from those in E-cigarette vapor. C-cigarette smoke is produced by burning tobacco, which contains more than 4700 toxic substances, including tar, nicotine, carbon monoxide, carbon dioxide, acrolein and nitric oxide etc.¹²⁹. Even though E-cigarette vapor has fewer toxic components than C-cigarette smoke, E-cigarette vapor contains some especially harmful substances not detected in C-cigarette smoke, such as heavy metals, volatile carcinogens (acrylamide, benzene and propylene oxide)¹³⁰.

In an animal model established by Reinikovaite and co-workers, E-cigarette vapor and C-cigarette smoke effects were studied with regard to lung injury, and it was found that the destructive damage of E-cigarette vapor on the pulmonary structure was very similar to that of C-cigarette smoke. The result showed that both groups of rats all had significant emphysema, although the serum nicotine/cotinine levels in rats from the C-

cigarette smoke subgroup was higher than in the E-cigarette vapor subgroup, while the destruction of lung structure in both subgroups was similar. Regarding the results in the E-cigarette subgroup, it was speculated that the fine particulate matter (with a hydrodynamic diameter of 2.5 μm or less) present in the E-cigarette vapor caused the drastic negative effect on the rat lung morphology^{131,132}.

4.1.5 The nicotine ingredient in E-cigarette vapor might weaken the harmful effects

In the present study, after medium-term exposure, there was no significant difference between C-cigarette smoke and nicotine-containing E-cigarette vapor subgroups with regard to cytokines levels of pro-inflammatory or pro-angiogenic cytokines in neural retina. However, it is surprising that nicotine free E-cigarette vapor has an even stronger effect on the promotion of both aspects. Since it is the only difference between both vapor, nicotine is crucial and can be considered to attenuate the adverse effect of E-cigarette vapor generated from basic humectants on the neural retina. However, this speculation is not in line with the conclusion of previous studies that nicotine has a pro-angiogenic and pro-inflammatory effects^{58,118,133}. Nevertheless, it is worth to mention that the neural retina is a part of the central nervous system¹⁰⁵, and previous studies have shown that nicotine has protective effects on the nervous system¹³⁴. Therefore, it can be inferred that nicotine also has protective effects on neural retina by weakening the harmful effects of E-cigarette vapor formed by the basic humectants on the neural retina.

4.1.6 The long-term E-cigarette vapor (nicotine containing) exposure can promote angiogenesis in choroid tissue

By analyzing the data from Fig. 18 and Fig. 19, it can be deduced that the tissues that are most affected by smoke exposure initially are both, RPE and choroid, while with increasing exposure duration only the choroid displays severe changes in cytokine

profile. Moreover, the levels of VEGF and PEDF decreased dramatically in the PRE, and turned even lower than in related control mice. According to the pathological progression of wet AMD, it is assumed that with the extension of the exposure period, the damage to the RPE might become more serious, and the layer of RPE becomes dysfunctional or even apoptotic/necrotic, leading to a decreased ability to produce pro-inflammatory and angiogenic factors. On the other hand, due to the increasing loss of choroidal blood vessels, the hypoxia of choroidal capillaries becomes more serious²⁹, which in turn stimulates the choroidal capillary endothelial cells to produce more angiogenic substances such as VEGF, and hence the expression of the antiangiogenic mediator PEDF decreases, promoting the generation of CNV in lesions of the neural retina and RPE interface, which is a hallmark sign in the development of AMD in humans.

4.2 Does Fgf10-overexpression have a protective effect on retinal tissue in mice exposed to smoke?

Fgf10 exerts protective and regenerative effects on tissues by inhibiting inflammation and mediating antioxidant response as well as mobilizing stem cells, and plays important roles in the regeneration of acute lung injury, cerebral ischemia, spinal cord/peripheral nerve injury and wound healing^{101-103,135-137}. However, the potential protective role of Fgf10 in the retina is not yet clear. In the present study, we investigated the potential effects of Fgf10 overexpression in the retina of mice that were exposed to smoke and experienced different periods of regeneration afterwards. Cytokine levels, retinal layer thickness and retinal vessel tortuosity were measured in order to detect potential changes.

4.2.1 Both long-term smoking exposure and Fgf10 overexpression do not impact retinal thickness

As described in the results section, without the administration of doxycycline, Fgf10 OE transgenic mice did not overexpress the Fgf10 cytokine, whereas under administration of doxycycline, Fgf10-overexpression was clearly detectable during the regeneration phase.

In both subgroups of 12 weeks regeneration phase with or without Fgf10 overexpression, no significant change in retinal layers (IR, ONL+, OR, WR) thickness was observed between smoker and non-smoker mice (Fig. 23). These results are consistent with previous reports that there is no significant difference between long-term smoker and non-smoker (healthy individuals) for retinal thickness in humans^{138,139}. Few studies focused only on the acute effects of smoking on the choroidal thickness with contradictory results. For instance, Sizmaz et al. showed that the mean choroidal thickness at the fovea significantly decreased at 1h and 3h later after smoking¹⁴⁰. In contrast, another study assessed both the acute and long-term effects of smoking on the

choroidal thickness of young smoker with a history of more than 10 years of smoking, and showed that cigarette smoking leads to an increase in the choroidal thickness, which was recovered to normal level after 1h. Furthermore, they observed no difference between smoker and non-smoker for the thickness of retina and choroid¹⁴¹. In the present study, data were obtained at 12 weeks after smoking exposure ended. Therefore, these are not acute changes but chronic effects of smoke after experienced 12 weeks regeneration phase. The long-term exposure to smoke does not change retinal layer thickness in papilla and periphery areas. Besides that, it is obvious that Fgf10 overexpression also has no effect on the thickness of retinal layers.

4.2.2 Fgf10 overexpression during regeneration results in changes to the retinal vascular tortuosity induced by smoke exposure

Even though various measurement methods have been reported to quantify vascular tortuosity, there is no standard method generally agreed upon¹⁴²⁻¹⁴⁶. In this study, we evaluated for the first time the tortuosity by calculating the average tortuosity number per vascular and the average covered area per tortuosity.

We observed alterations to the retinal vascular morphology after long term smoke exposure (Fig. 24). In particular, the retinal arterial tortuosity was significantly increased. It has been demonstrated that the increased retinal vessel tortuosity has an inverse relationship with vascular oxygenation, and hence, the increased retinal blood vessels tortuosity is an early sign of hypoxia in some retinopathies⁷⁵. Furthermore, previous studies suggested that the possible mechanisms that cause retinal vascular tortuosity are associated with hemodynamic changes (such as increased retinal blood flow velocity)¹⁴⁷⁻¹⁴⁹, endothelial dysfunction¹⁵⁰, tissue hypoxia¹⁵¹, and angiogenesis¹⁵². On the other hand, smoking not only decreases the perfusion pressure of the choriocapillaris and reduces retinal blood flow¹¹³, but the nicotine composition in smoke can promote the neovascularization in choroid and retina¹⁵³. In addition, the mitochondrial oxidative stress and inflammatory response induced by smoking can

further contribute to vessel endothelial dysfunction¹⁵⁴. The interplay between the diverse mechanisms triggered by smoke exposure might contribute to the incidences of an increased vessel tortuosity in the retinas of mice in this model.

Interestingly, our data show that the severity of retinal arterial tortuosity is lower in smoker mice that overexpressing Fgf10 during the regeneration compared to smoker mice not overexpressing Fgf10, which indicates a protective effect of Fgf10 in retinal tissue exposed to smoke. It might neutralize the hypoxia mediated effects caused by smoking. One recent study showed that exogenous Fgf10 treatment could activate the PI3K/AKT signalling and stimulate the overexpression of antioxidant proteins by mediating antioxidant response, which further promoted the regeneration of damaged peripheral nerves¹⁰². Some studies on lung injury also demonstrated that Fgf10 has an effect of promoting the damaged lung epithelial regeneration¹⁰¹. In addition, another animal study suggested that the overexpression of Fgf10 could attenuate the extent of lung fibrosis by suppressing the inflammation response during both inflammatory and fibrotic phases which was induced by bleomycin¹⁰⁴. Furthermore, Fgf10 could also improve symptoms in an animal ulceration model by decreasing the secretion of inflammatory cytokines (IL-6, TNF- α)¹⁵⁵. Therefore, it can be speculated that the overexpression of Fgf10 attenuates the retinal vascular tortuosity induced by smoking through several possible mechanisms, including the activation of the anti-oxidative stress response, the decrease of the inflammatory response in endothelial cells, and the promotion of migration of epithelial cells (with/without enhanced proliferation)¹⁵⁵. But the exact mechanisms for the effect are not yet fully clarified, it still needs further research to explore.

4.3 The limitations of the study

With regard to limitations of our study, it should be considered that whole-body exposure was performed in this mouse model. The anterior tissue of the ocular surface such as cornea as well as skin surrounding the eye have been exposed to the smoke or

vapor, which might have an impact on our results. However, anterior/posterior diffusion of molecules in the eye is not easily possible due to the presence of physiological barriers. Therefore, since this exposure is also similar to human smoke/vapor exposure, it should not interfere significantly with the data presented here. A second limitation is the relatively low number of eyes analyzed in some of the subgroups (E-cigarette, long-term exposure). This renders the interpretation of the respective data less robust. However, these initial data on a small number of animals provide a first view on these yet under-investigated mechanisms and pave the way for further experiments with an increased number of animals. A third limitation is the fact that values for VEGF and IL-1 β were sometimes very low and below the detection range as published by the manufacturers. In order to generate valuable data also in these samples, we have extended the standard curve of the ELISA and calculated the lower limit of detection separately. This way, we have obtained values that have to be considered with more caution compared to those obtained within the standard curve offered by the manufacturer.

5 SUMMARY

Cigarette smoke has been identified as a major risk factor for the development of age-related macular degeneration (AMD), which can promote the occurrence and progression of AMD mainly by inducing oxidative stress and inflammatory responses. As an alternative to C-cigarette, E-cigarettes have been globally promoted and have been widely used. The increasing usage of E-cigarettes raises concerns with regard to consequences related to neural retinal tissue. On the other hand, as a multifunctional growth factor, fibroblast growth factor10 (Fgf10) exerts its effects of neuroprotection and regeneration in nerve injury diseases by suppressing excessive oxidative stress and reducing neuroinflammation. Taking account that the neural retina tissue is one part of central nervous system, it is hypothesized that high levels of Fgf10 also have protective effects on the neural retina upon damage caused by cigarette smoke exposure.

In this thesis, two controlled studies in mouse models were conducted in order to: (1) probe the comprehensive effects of E-cigarette vapor on the neural retina, RPE and choroidal tissues by measuring the pro-inflammatory and pro-angiogenic mediators in retina/RPE/choroid by ELISA assays; (2) investigate the long-term effect of cigarette smoke exposure on mouse retina, by measuring the retinal vascular morphology and the retinal layer thickness as well as the molecular expression pattern of important factors in the neural retina. Simultaneously, we used mice engineered for the inducible overexpression of Fgf10 in the retina to probe the protective and regenerative effects of Fgf10 overexpression in the smoke exposure in the murine retina.

The results showed that long-term C-cigarette smoke exposure promoted an inflammatory reaction in the neural retina. Mice exposed to E-cigarette (nicotine-free) vapor developed inflammatory and angiogenic reactions more pronounced in RPE and choroid compared to retinal tissue, while nicotine-containing E-cigarette vapor caused even more serious reaction. Both, inflammatory and pro-angiogenic reactions increased with the extension of exposure time. Moreover, the Fgf10-overexpressing smoker mice display less arterial tortuosity compared to smoker mice not overexpressing Fgf10.

However, there was no significant differences in layer thickness observed between smoker and non-smoker in Fgf10-overexpressing mice.

These results demonstrate that long-term exposure to C-cigarette smoke is harmful to the neural retina. Likewise, the exposure to E-cigarette vapor (with or without nicotine) increases the occurrence and progression of inflammatory and angiogenic stimuli in the retina, which might also be related to the onset of wet AMD in humans. Furthermore, the overexpression of Fgf10 has protective and regenerative effects on the retina upon damage caused by cigarette smoke exposure.

6 ZUSAMMENFASSUNG

Zigarettenrauch wurde als Hauptrisikofaktor für die Entwicklung der altersbedingten Makuladegeneration (AMD) identifiziert, welcher das Auftreten und Fortschreiten der AMD hauptsächlich durch Induktion von oxidativem Stress und Entzündungsreaktionen fördern kann. Als Alternative zur klassischen (C)-Zigarette wurden elektronische (E)-Zigaretten weltweit beworben und sind mittlerweile weit verbreitet. Die zunehmende Verwendung von E-Zigaretten wirft Bedenken hinsichtlich der Folgen der Exposition im Zusammenhang mit neuronalem Netzhautgewebe auf. Andererseits hat der Fibroblasten-Wachstumsfaktor10 (Fgf10) als multifunktionaler Wachstumsfaktor eine neuroprotektive und regenerierende Wirkung bei Nervenverletzungskrankheiten, indem er übermäßigen oxidativen Stress unterdrückt und Neuroinflammation reduziert. Unter Berücksichtigung der Tatsache, dass das neurale Netzhautgewebe ein Teil des zentralen Nervensystems ist, wird angenommen, dass überexprimiertes Fgf10 auch eine schützende Wirkung auf die neurale Netzhaut bei Schäden durch Zigarettenrauchexposition hat.

In dieser Arbeit wurden zwei kontrollierte Studien in Mausmodellen durchgeführt, um: (1) die umfassenden Auswirkungen von E-Zigaretten-Dampf auf die neurale Netzhaut, das RPE und das Aderhautgewebe Messung der proinflammatorischen und proangiogenen Mediatoren in der Netzhaut mittels ELISA-Tests zu untersuchen; (2) die Langzeitwirkung von Zigarettenrauchexposition auf die Netzhaut der Maus zu untersuchen, indem die retinale Gefäßmorphologie und die Netzhautschichtdicke sowie die molekulare Expression in der neuralen Netzhaut gemessen werden. Gleichzeitig verwendeten wir Mäuse, die für die induzierbare Überexpression von Fgf10 in der Netzhaut entwickelt wurden, um die schützenden und regenerativen Wirkungen der Fgf10-Überexpression in der rauchexponierten Mausnetzhaut zu untersuchen.

Die Ergebnisse zeigten, dass eine langfristige C-Zigaretten-Rauchexposition eine Entzündungsreaktion in der neuralen Netzhaut förderte. Mäuse, die (nikotinfreien) E-Zigaretten-Dämpfen ausgesetzt waren, entwickelten entzündliche und angiogene

Reaktionen, die bei RPE und Aderhaut im Vergleich zum Netzhautgewebe ausgeprägter waren, während nikotinhaltige E-Zigaretten-Dämpfe noch schwerwiegendere Reaktionen verursachten. Sowohl entzündliche als auch pro-angiogene Reaktionen nahmen mit der Verlängerung der Expositionszeit zu. Darüber hinaus weisen Rauchermäuse mit Fgf10-Überexpression geringere durchschnittliche arterielle Tortuosität auf als Rauchermäuse ohne Überexpression. Es wurden jedoch keine signifikanten Unterschiede in der Schichtdicke zwischen Rauchermäusen und Nichtrauchermausen bei Fgf10-Überexpression beobachtet.

Diese Ergebnisse zeigen, dass eine langfristige Exposition gegenüber C-Zigarettenrauch für die neurale Netzhaut schädlich ist. Ebenso erhöht die Exposition gegenüber E-Zigaretten-Dämpfen (mit oder ohne Nikotin) das Auftreten und Fortschreiten von entzündlichen und angiogenen Reizen in der Netzhaut, die ebenfalls mit dem Beginn einer feuchten AMD beim Menschen zusammenhängen könnten. Darüber hinaus hat das überexprimierte Fgf10 eine schützende und regenerative Wirkung auf die Netzhaut bei Schäden durch Zigarettenrauchexposition.

7 REFERENCES

1. Kaplan, H.J. Anatomy and function of the eye. *Chem Immunol Allergy* **92**, 4–10 (2007).
2. Gray, H. & Lewis, W.H. Anatomy of the Human Body (20th Edition). in *Anatomy of the Human Body (20th Edition)* (Lea & Febiger, US, 1918).
3. Eye, human. in *Eye, human* (Encyclopædia Britannica, Chicago, 2010).
4. Foster, R.G. et al. Circadian photoreception in the retinally degenerate mouse (rd/rd). *J Comp Physiol A* **169**, 39–50 (1991).
5. Zaidi, F.H. et al. Short-wavelength light sensitivity of circadian, pupillary, and visual awareness in humans lacking an outer retina. *Curr Biol* **17**, 2122–2128 (2007).
6. Bedinghaus, T. The Anatomy of the Macula. in *The Anatomy of the Macula* Vol. 2020 (Verywell Health, U.S., 2020).
7. Purves, D., Augustine, G.J. & Fitzpatrick, D. The Retina. in *Neuroscience (2nd edition)* (eds. Purves, D., Augustine, G.J., Fitzpatrick, D. & al., e.) (Sinauer Associates, Sunderland (MA), 2001).
8. London, A., Benhar, I. & Schwartz, M. The retina as a window to the brain—from eye research to CNS disorders. *Nat Rev Neurol* **9**, 44–53 (2013).
9. Campbell, M. & Humphries, P. The blood-retina barrier: tight junctions and barrier modulation. *Adv Exp Med Biol* **763**, 70–84 (2012).
10. Strauss, O. The retinal pigment epithelium in visual function. *Physiol Rev* **85**, 845–881 (2005).
11. Simó, R., Villarroel, M., Corraliza, L., Hernández, C. & Garcia-Ramírez, M. The retinal pigment epithelium: something more than a constituent of the blood-retinal barrier—implications for the pathogenesis of diabetic retinopathy. *J Biomed Biotechnol* **2010**, 190724 (2010).
12. Nickla, D.L. & Wallman, J. The multifunctional choroid. *Prog Retin Eye Res* **29**, 144–168 (2010).
13. Ferrara, D., Waheed, N.K. & Duker, J.S. Investigating the choriocapillaris and choroidal vasculature with new optical coherence tomography technologies. *Prog Retin Eye Res* **52**, 130–155 (2016).
14. Wangsa-Wirawan, N.D. & Linsenmeier, R.A. Retinal oxygen: fundamental and clinical aspects. *Arch Ophthalmol* **121**, 547–557 (2003).
15. Moreira-Neto, C.A., Moul, E.M., Fujimoto, J.G., Waheed, N.K. & Ferrara, D. Choriocapillaris Loss in Advanced Age-Related Macular Degeneration. *J Ophthalmol* **2018**,

- 8125267 (2018).
16. Gramage, E., Li, J. & Hitchcock, P. The expression and function of midkine in the vertebrate retina. *Br J Pharmacol* **171**, 913–923 (2014).
 17. Blasiak, J. Senescence in the pathogenesis of age-related macular degeneration. *Cell Mol Life Sci* **77**, 789–805 (2020).
 18. Somasundaran, S., Constable, I.J., Mellough, C.B. & Carvalho, L.S. Retinal pigment epithelium and age-related macular degeneration: a review of major disease mechanisms. *Clin Exp Ophthalmol* (2020).
 19. Mitchell, P., Liew, G., Gopinath, B. & Wong, T.Y. Age-related macular degeneration. *Lancet* **392**, 1147–1159 (2018).
 20. Ambati, J. & Fowler, Benjamin J. Mechanisms of Age-Related Macular Degeneration. *Neuron* **75**, 26–39 (2012).
 21. De Falco, S. Antiangiogenesis therapy: an update after the first decade. *Korean J Intern Med* **29**, 1–11 (2014).
 22. Martin, D.F. et al. Ranibizumab and bevacizumab for neovascular age-related macular degeneration. *N Engl J Med* **364**, 1897–1908 (2011).
 23. Browning, A.C., O'Brien, J.M., Vieira, R.V., Gupta, R. & Nenova, K. Intravitreal Aflibercept for Retinal Angiomatous Proliferation: Results of a Prospective Case Series at 96 Weeks. *Ophthalmologica* **242**, 239–246 (2019).
 24. Kauppinen, A., Paterno, J.J., Blasiak, J., Salminen, A. & Kaarniranta, K. Inflammation and its role in age-related macular degeneration. *Cell Mol Life Sci* **73**, 1765–1786 (2016).
 25. Brancato, R. et al. Optical coherence tomography (OCT) angiomatous proliferation (RAP) in retinal. *Eur J Ophthalmol* **12**, 467–472 (2002).
 26. Tsai, A.S.H. et al. Retinal angiomatous proliferation. *Surv Ophthalmol* **62**, 462–492 (2017).
 27. Acharya, U.R. et al. Novel risk index for the identification of age-related macular degeneration using radon transform and DWT features. *Comput Biol Med* **73**, 131–140 (2016).
 28. van Lookeren Campagne, M., LeCouter, J., Yaspan, B.L. & Ye, W. Mechanisms of age-related macular degeneration and therapeutic opportunities. *J Pathol* **232**, 151–164 (2014).
 29. Bhutto, I. & Luty, G. Understanding age-related macular degeneration (AMD): relationships between the photoreceptor/retinal pigment epithelium/Bruch's membrane/choriocapillaris complex. *Mol Aspects Med* **33**, 295–317 (2012).
 30. Chen, M. & Xu, H. Parainflammation, chronic inflammation, and age-related macular degeneration. *J Leukoc Biol* **98**, 713–725 (2015).
 31. Datta, S., Cano, M., Ebrahimi, K., Wang, L. & Handa, J.T. The impact of oxidative stress

- and inflammation on RPE degeneration in non-neovascular AMD. *Prog Retin Eye Res* **60**, 201–218 (2017).
32. Ambati, J., Atkinson, J.P. & Gelfand, B.D. Immunology of age-related macular degeneration. *Nat Rev Immunol* **13**, 438–451 (2013).
 33. Rivera, J.C. et al. Ischemic Retinopathies: Oxidative Stress and Inflammation. *Oxid Med Cell Longev* **2017**, 3940241 (2017).
 34. Oh, H. et al. The potential angiogenic role of macrophages in the formation of choroidal neovascular membranes. *Invest Ophthalmol Vis Sci* **40**, 1891–1898 (1999).
 35. Lavalette, S. et al. Interleukin-1 β inhibition prevents choroidal neovascularization and does not exacerbate photoreceptor degeneration. *Am J Pathol* **178**, 2416–2423 (2011).
 36. Lentsch, A.B. & Ward, P.A. Regulation of inflammatory vascular damage. *J Pathol* **190**, 343–348 (2000).
 37. Sierra, A. et al. Expression of inducible nitric oxide synthase (iNOS) in microglia of the developing quail retina. *PLoS One* **9**, e106048 (2014).
 38. Toda, N. & Nakanishi-Toda, M. Nitric oxide: ocular blood flow, glaucoma, and diabetic retinopathy. *Prog Retin Eye Res* **26**, 205–238 (2007).
 39. Lind, M. et al. Inducible nitric oxide synthase: Good or bad? *Biomed Pharmacother* **93**, 370–375 (2017).
 40. Chiou, G.C. Review: effects of nitric oxide on eye diseases and their treatment. *J Ocul Pharmacol Ther* **17**, 189–198 (2001).
 41. Sennlaub, F., Courtois, Y. & Goureau, O. Inducible nitric oxide synthase mediates retinal apoptosis in ischemic proliferative retinopathy. *J Neurosci* **22**, 3987–3993 (2002).
 42. Bakri, S.J. et al. Safety and Efficacy of Anti-Vascular Endothelial Growth Factor Therapies for Neovascular Age-Related Macular Degeneration: A Report by the American Academy of Ophthalmology. *Ophthalmol* **126**, 55–63 (2019).
 43. Solomon, S.D., Lindsley, K., Vedula, S.S., Krzystolik, M.G. & Hawkins, B.S. Anti-vascular endothelial growth factor for neovascular age-related macular degeneration. *Cochrane Database Syst Rev* **3**, Cd005139 (2019).
 44. Farnoodian, M., Sorenson, C.M. & Sheibani, N. PEDF expression affects the oxidative and inflammatory state of choroidal endothelial cells. *Am J Physiol Cell Physiol* **314**, C456–472 (2018).
 45. Yoshida, T. [Molecular mechanism of choroidal neovascularization in age-related macular degeneration]. *Nippon Ganka Gakkai Zasshi* **111**, 881–891 (2007).
 46. Bhutto, I.A. et al. Pigment epithelium-derived factor (PEDF) and vascular endothelial growth factor (VEGF) in aged human choroid and eyes with age-related macular

- degeneration. *Exp Eye Res* **82**, 99–110 (2006).
47. Lambert, N.G. et al. Risk factors and biomarkers of age-related macular degeneration. *Prog Retin Eye Res* **54**, 64–102 (2016).
 48. Klein, R., Klein, B.E., Linton, K.L. & DeMets, D.L. The Beaver Dam Eye Study: the relation of age-related maculopathy to smoking. *Am J Epidemiol* **137**, 190–200 (1993).
 49. Vingerling, J.R., Hofman, A., Grobbee, D.E. & de Jong, P.T.V.M. Age-Related Macular Degeneration and Smoking: The Rotterdam Study. *Arch Ophthalmol* **114**, 1193–1196 (1996).
 50. Joachim, N., Mitchell, P., Burlutsky, G., Kifley, A. & Wang, J.J. The Incidence and Progression of Age-Related Macular Degeneration over 15 Years: The Blue Mountains Eye Study. *Ophthalmol* **122**, 2482–2489 (2015).
 51. Frei, B., Forte, T.M., Ames, B.N. & Cross, C.E. Gas phase oxidants of cigarette smoke induce lipid peroxidation and changes in lipoprotein properties in human blood plasma. Protective effects of ascorbic acid. *Biochem J* **277** (Pt 1), 133–138 (1991).
 52. Fujihara, M., Nagai, N., Sussan, T.E., Biswal, S. & Handa, J.T. Chronic cigarette smoke causes oxidative damage and apoptosis to retinal pigmented epithelial cells in mice. *PLoS One* **3**, e3119 (2008).
 53. Beatty, S., Koh, H.-H., Phil, M., Henson, D. & Boulton, M. The Role of Oxidative Stress in the Pathogenesis of Age-Related Macular Degeneration. *Surv Ophthalmol* **45**, 115–134 (2000).
 54. Cai, J., Nelson, K.C., Wu, M., Sternberg, P. & Jones, D.P. Oxidative damage and protection of the RPE. *Prog Retin Eye Res* **19**, 205–221 (2000).
 55. Friedman, E. The role of the atherosclerotic process in the pathogenesis of age-related macular degeneration. *Am J Ophthalmol* **130**, 658–663 (2000).
 56. Benowitz, N.L. Cigarette smoking and cardiovascular disease: pathophysiology and implications for treatment. *Prog Cardiovasc Dis* **46**, 91–111 (2003).
 57. Ayhan, Z., Kaya, M., Ozturk, T., Karti, O. & Hakan Oner, F. Evaluation of Macular Perfusion in Healthy Smokers by Using Optical Coherence Tomography Angiography. *OLSI Retina* **48**, 617–622 (2017).
 58. Kiuchi, K. et al. Mecamylamine suppresses Basal and nicotine-stimulated choroidal neovascularization. *Invest Ophthalmol Vis Sci* **49**, 1705–1711 (2008).
 59. Hoffman, E.C. et al. Cloning of a factor required for activity of the Ah (dioxin) receptor. *Science* **252**, 954–958 (1991).
 60. Reyes, H., Reisz-Porszasz, S. & Hankinson, O. Identification of the Ah receptor nuclear translocator protein (Arnt) as a component of the DNA binding form of the Ah receptor.

- Science* **256**, 1193–1195 (1992).
61. Takeuchi, A. et al. Effects of dioxin on vascular endothelial growth factor (VEGF) production in the retina associated with choroidal neovascularization. *Invest Ophthalmol Vis Sci* **50**, 3410–3416 (2009).
 62. Woodell, A. & Rohrer, B. A mechanistic review of cigarette smoke and age-related macular degeneration. *Adv Exp Med Biol* **801**, 301–307 (2014).
 63. Biswas, S.K. & Rahman, I. Environmental toxicity, redox signaling and lung inflammation: the role of glutathione. *Mol Aspects Med* **30**, 60–76 (2009).
 64. Rahman, I. Inflammation and the regulation of glutathione level in lung epithelial cells. *Antioxid Redox Signal* **1**, 425–447 (1999).
 65. Rom, O., Avezov, K., Aizenbud, D. & Reznick, A.Z. Cigarette smoking and inflammation revisited. *Respir Physiol Neurobiol* **187**, 5–10 (2013).
 66. Woodell, A. et al. A Targeted Inhibitor of the Alternative Complement Pathway Accelerates Recovery From Smoke-Induced Ocular Injury. *Invest Ophthalmol Vis Sci* **57**, 1728–1737 (2016).
 67. Bertram, K.M., Baglolle, C.J., Phipps, R.P. & Libby, R.T. Molecular regulation of cigarette smoke induced-oxidative stress in human retinal pigment epithelial cells: implications for age-related macular degeneration. *Am J Physiol Cell Physiol* **297**, C1200–1210 (2009).
 68. Masuda, T., Shimazawa, M. & Hara, H. Retinal Diseases Associated with Oxidative Stress and the Effects of a Free Radical Scavenger (Edaravone). *Oxid Med Cell Longev* **2017**, 9208489 (2017).
 69. Wang, A.L. et al. Changes in retinal pigment epithelium related to cigarette smoke: possible relevance to smoking as a risk factor for age-related macular degeneration. *PLoS One* **4**, e5304 (2009).
 70. Hajjar, D.P. & Gotto, A.M., Jr. Biological relevance of inflammation and oxidative stress in the pathogenesis of arterial diseases. *Am J Pathol* **182**, 1474–1481 (2013).
 71. Cano, M. et al. Cigarette smoking, oxidative stress, the anti-oxidant response through Nrf2 signaling, and Age-related Macular Degeneration. *Vision Res* **50**, 652–664 (2010).
 72. Moschos, M.M., Nitoda, E., Laios, K., Ladas, D.S. & Chatziralli, I.P. The Impact of Chronic Tobacco Smoking on Retinal and Choroidal Thickness in Greek Population. *Oxid Med Cell Longev* **2016**, 2905789 (2016).
 73. Saint-Geniez, M. & D'Amore, P.A. Development and pathology of the hyaloid, choroidal and retinal vasculature. *Int J Dev Biol* **48**, 1045–1058 (2004).
 74. Arjamaa, O. & Nikinmaa, M. Oxygen-dependent diseases in the retina: role of hypoxia-inducible factors. *Exp Eye Res* **83**, 473–483 (2006).

-
75. Khansari, M.M., Garvey, S.L., Farzad, S., Shi, Y. & Shahidi, M. Relationship between retinal vessel tortuosity and oxygenation in sickle cell retinopathy. *Int J Retina Vitreous* **5**, 47 (2019).
76. Grana, R., Benowitz, N. & Glantz, S.A. E-cigarettes: a scientific review. *Circulation* **129**, 1972–1986 (2014).
77. contributors, W. Electronic cigarette. Vol. 2021 (Wikipedia, The Free Encyclopedia, 2021).
78. England, L.J., Bunnell, R.E., Pechacek, T.F., Tong, V.T. & McAfee, T.A. Nicotine and the Developing Human: A Neglected Element in the Electronic Cigarette Debate. *Am J Prev Med* **49**, 286–293 (2015).
79. Mathur, A. & Dempsey, O.J. Electronic cigarettes: a brief update. *J R Coll Physicians Edinb* **48**, 346–351 (2018).
80. Farsalinos, K.E. et al. Nicotine absorption from electronic cigarette use: comparison between first and new-generation devices. *Sci Rep* **4**, 4133 (2014).
81. Meo, S.A. & Al Asiri, S.A. Effects of electronic cigarette smoking on human health. *Eur Rev Med Pharmacol Sci* **18**, 3315–3319 (2014).
82. Woodall, M. et al. E-cigarette constituents propylene glycol and vegetable glycerine decrease glucose uptake and its metabolism in airway epithelial cells in vitro. *Am J Physiol Lung Cell Mol Physiol* **319**, L957–L967 (2020).
83. Marshall, K., Liu, Z., Olfert, I.M. & Gao, W. Chronic electronic cigarette use elicits molecular changes related to pulmonary pathogenesis. *Toxicol Appl Pharmacol* **406**, 115224 (2020).
84. Cervellati, F. et al. Comparative effects between electronic and cigarette smoke in human keratinocytes and epithelial lung cells. *Toxicol In Vitro* **28**, 999–1005 (2014).
85. Fuoco, F.C., Buonanno, G., Stabile, L. & Vigo, P. Influential parameters on particle concentration and size distribution in the mainstream of e-cigarettes. *Environ Pollut* **184**, 523–529 (2014).
86. Moheimani, R.S. et al. Increased Cardiac Sympathetic Activity and Oxidative Stress in Habitual Electronic Cigarette Users: Implications for Cardiovascular Risk. *JAMA Cardiol* **2**, 278–284 (2017).
87. Hwang, J.H. et al. Electronic cigarette inhalation alters innate immunity and airway cytokines while increasing the virulence of colonizing bacteria. *J Mol Med (Berl)* **94**, 667–679 (2016).
88. Schweitzer, K.S. et al. Endothelial disruptive proinflammatory effects of nicotine and e-cigarette vapor exposures. *Am J Physiol Lung Cell Mol Physiol* **309**, L175–187 (2015).
89. Lerner, C.A. et al. Vapors produced by electronic cigarettes and e-juices with flavorings

- induce toxicity, oxidative stress, and inflammatory response in lung epithelial cells and in mouse lung. *PLoS One* **10**, e0116732 (2015).
90. Kyrou, I., Weickert, M.O., Gharanei, S., Randeva, H.S. & Tan, B.K. Fibroblast growth factors: new insights, new targets in the management of diabetes. *Minerva Endocrinol* **42**, 248–270 (2017).
 91. Ornitz, D.M. et al. Receptor specificity of the fibroblast growth factor family. *J Biol Chem* **271**, 15292–15297 (1996).
 92. Kelleher, F.C., O'Sullivan, H., Smyth, E., McDermott, R. & Viterbo, A. Fibroblast growth factor receptors, developmental corruption and malignant disease. *Carcinogenesis* **34**, 2198–2205 (2013).
 93. Schliermann, A. & Nickel, J. Unraveling the Connection between Fibroblast Growth Factor and Bone Morphogenetic Protein Signaling. *Int J Mol Sci* **19**, 3220 (2018).
 94. Ohta, H., Konishi, M. & Itoh, N. FGF10 and FGF21 as regulators in adipocyte development and metabolism. *Endocr Metab Immune Disord Drug Targets* **11**, 302–309 (2011).
 95. Itoh, N. FGF10: A multifunctional mesenchymal-epithelial signaling growth factor in development, health, and disease. *Cytokine Growth Factor Rev* **28**, 63–69 (2016).
 96. Katoh, M. & Katoh, M. FGF signaling network in the gastrointestinal tract (review). *Int J Oncol* **29**, 163–168 (2006).
 97. Bellusci, S., Grindley, J., Emoto, H., Itoh, N. & Hogan, B.L. Fibroblast growth factor 10 (FGF10) and branching morphogenesis in the embryonic mouse lung. *Development* **124**, 4867–4878 (1997).
 98. Torashima, Y. et al. Fgf10 overexpression enhances the formation of tissue-engineered small intestine. *J Tissue Eng Regen Med* **10**, 132–139 (2016).
 99. Sekine, K. et al. Fgf10 is essential for limb and lung formation. *Nat Genet* **21**, 138–141 (1999).
 100. Zinkle, A. & Mohammadi, M. Structural Biology of the FGF7 Subfamily. *Front Genet* **10**, 102 (2019).
 101. Yuan, T., Volckaert, T., Chanda, D., Thannickal, V.J. & De Langhe, S.P. Fgf10 Signaling in Lung Development, Homeostasis, Disease, and Repair After Injury. *Front Genet* **9**, 418 (2018).
 102. Dong, L. et al. FGF10 Enhances Peripheral Nerve Regeneration via the Preactivation of the PI3K/Akt Signaling-Mediated Antioxidant Response. *Front Pharmacol* **10**, 1224 (2019).
 103. Li, Y.H. et al. Neuron-derived FGF10 ameliorates cerebral ischemia injury via inhibiting NF- κ B-dependent neuroinflammation and activating PI3K/Akt survival signaling pathway in mice. *Sci Rep* **6**, 19869 (2016).

104. Gupte, V.V. et al. Overexpression of fibroblast growth factor-10 during both inflammatory and fibrotic phases attenuates bleomycin-induced pulmonary fibrosis in mice. *Am J Respir Crit Care Med* **180**, 424–436 (2009).
105. Mead, B., Logan, A., Berry, M., Leadbeater, W. & Scheven, B.A. Concise Review: Dental Pulp Stem Cells: A Novel Cell Therapy for Retinal and Central Nervous System Repair. *Stem Cells* **35**, 61–67 (2017).
106. Caprioli, A. et al. Wnt4 is essential to normal mammalian lung development. *Dev Biol* **406**, 222–234 (2015).
107. Seimetz, M. et al. Inducible NOS inhibition reverses tobacco-smoke-induced emphysema and pulmonary hypertension in mice. *Cell* **147**, 293–305 (2011).
108. Pichl, A. et al. Riociguat for treatment of pulmonary hypertension in COPD: a translational study. *Eur Respir J* **53**(2019).
109. Seimetz, M. et al. Cigarette Smoke-Induced Emphysema and Pulmonary Hypertension Can Be Prevented by Phosphodiesterase 4 and 5 Inhibition in Mice. *PLoS One* **10**, e0129327 (2015).
110. Wang, F. et al. Retinal tissue develops an inflammatory reaction to tobacco smoke and electronic cigarette vapor in mice. *J Mol Med* **99**, (2021) <https://doi.org/10.1007/s00109-021-02108-9>.
111. Röhl, D. 03.07.2014, Justus-Liebig-Universität Gießen (2014).
112. Wei, H., Xun, Z., Granado, H., Wu, A. & Handa, J.T. An easy, rapid method to isolate RPE cell protein from the mouse eye. *Exp Eye Res* **145**, 450–455 (2016).
113. El-Shazly, A.A.E., Farweez, Y.A.T., Elzankalony, Y.A., Elewa, L.S. & Farweez, B.A.T. Effect of smoking on macular function and structure in active smokers versus passive smokers. *Retina* **38**, 1031–1040 (2018).
114. Velilla, S. et al. Smoking and age-related macular degeneration: review and update. *J Ophthalmol* **2013**, 895147 (2013).
115. Miyashita, L. & Foley, G. E-cigarettes and respiratory health: the latest evidence. *J Physiol* **598**, 5027–5038 (2020).
116. McLeod, D.S. et al. Relationship between RPE and choriocapillaris in age-related macular degeneration. *Invest Ophthalmol Vis Sci* **50**, 4982–4991 (2009).
117. Pons, M. & Marin-Castaño, M.E. Nicotine increases the VEGF/PEDF ratio in retinal pigment epithelium: a possible mechanism for CNV in passive smokers with AMD. *Invest Ophthalmol Vis Sci* **52**, 3842–3853 (2011).
118. Iho, S. et al. Nicotine induces human neutrophils to produce IL-8 through the generation of peroxynitrite and subsequent activation of NF-kappaB. *J Leukoc Biol* **74**, 942–951 (2003).

119. Tierney, P.A., Karpinski, C.D., Brown, J.E., Luo, W. & Pankow, J.F. Flavour chemicals in electronic cigarette fluids. *Tob Control* **25**, e10–15 (2016).
120. Bekki, K. et al. Carbonyl compounds generated from electronic cigarettes. *Int J Environ Res Public Health* **11**, 11192–11200 (2014).
121. Higham, A. et al. Electronic cigarette exposure triggers neutrophil inflammatory responses. *Respir Res* **17**, 56 (2016).
122. Zhou, Y. et al. Voltage and e-liquid composition affect nicotine deposition within the oral cavity and carbonyl formation. *Tob Control* (2020) <https://doi.org/10.1136/tobaccocontrol-2020-055619>.
123. Nguyen, E. & Picklo, M.J., Sr. Inhibition of succinic semialdehyde dehydrogenase activity by alkenal products of lipid peroxidation. *Biochim Biophys Acta* **1637**, 107–112 (2003).
124. Liu, Z. et al. Hydroxytyrosol protects retinal pigment epithelial cells from acrolein-induced oxidative stress and mitochondrial dysfunction. *J Neurochem* **103**, 2690–2700 (2007).
125. Esterbauer, H., Schaur, R.J. & Zollner, H. Chemistry and biochemistry of 4-hydroxynonenal, malonaldehyde and related aldehydes. *Free Radic Biol Med* **11**, 81–128 (1991).
126. Facchinetti, F. et al. Alpha,beta-unsaturated aldehydes in cigarette smoke release inflammatory mediators from human macrophages. *Am J Respir Cell Mol Biol* **37**, 617–623 (2007).
127. Moretto, N. et al. Cigarette smoke and its component acrolein augment IL-8/CXCL8 mRNA stability via p38 MAPK/MK2 signaling in human pulmonary cells. *Am J Physiol Lung Cell Mol Physiol* **303**, L929–938 (2012).
128. Shi, H. et al. The Effect of Electronic-Cigarette Vaping on Cardiac Function and Angiogenesis in Mice. *Sci Rep* **9**, 4085 (2019).
129. Smith, C.J. & Hansch, C. The relative toxicity of compounds in mainstream cigarette smoke condensate. *Food Chem Toxicol* **38**, 637–646 (2000).
130. St Helen, G. et al. Comparison of Systemic Exposure to Toxic and/or Carcinogenic Volatile Organic Compounds (VOC) during Vaping, Smoking, and Abstinence. *Cancer Prev Res (Phila)* **13**, 153–162 (2020).
131. Reinikovaite, V. et al. The effects of electronic cigarette vapour on the lung: direct comparison to tobacco smoke. *Eur Respir J* **51**, 1701661 (2018).
132. Hom, S. et al. Platelet activation, adhesion, inflammation, and aggregation potential are altered in the presence of electronic cigarette extracts of variable nicotine concentrations. *Platelets* **27**, 694–702 (2016).
133. Lee, J. & Cooke, J.P. Nicotine and pathological angiogenesis. *Life Sci* **91**, 1058–1064

- (2012).
134. Zanardi, A., Leo, G., Biagini, G. & Zoli, M. Nicotine and neurodegeneration in ageing. *Toxicol Lett* **127**, 207–215 (2002).
 135. Tong, L. et al. Fibroblast Growth Factor-10 (FGF-10) Mobilizes Lung-resident Mesenchymal Stem Cells and Protects Against Acute Lung Injury. *Sci Rep* **6**, 21642 (2016).
 136. Chen, J. et al. Neuron and microglia/macrophage-derived FGF10 activate neuronal FGFR2/PI3K/Akt signaling and inhibit microglia/macrophages TLR4/NF- κ B-dependent neuroinflammation to improve functional recovery after spinal cord injury. *Cell Death Dis* **8**, e3090–e3090 (2017).
 137. Tan, X. et al. FGF10 Protects Against Renal Ischemia/Reperfusion Injury by Regulating Autophagy and Inflammatory Signaling. *Front Genet* **9**, 556 (2018).
 138. Dervişoğulları, M.S., Totan, Y., Tenlik, A. & Yuce, A. Effects of cigarette smoking on choroidal and retinal thickness and ocular pulse amplitude. *Cutan Ocul Toxicol* **34**, 217–221 (2015).
 139. Duman, R., Duman, R., Sabaner, M.C. & Çetinkaya, E. Effect of smoking on the thickness of retinal layers in healthy smokers. *Cutan Ocul Toxicol* **36**, 366–369 (2017).
 140. Sizmaz, S. et al. The effect of smoking on choroidal thickness measured by optical coherence tomography. *Br J Ophthalmol* **97**, 601–604 (2013).
 141. Ulaş, F., Çelik, F., Doğan, Ü. & Çelebi, S. Effect of smoking on choroidal thickness in healthy smokers. *Curr Eye Res* **39**, 504–511 (2014).
 142. Hart, W.E., Goldbaum, M., Côté, B., Kube, P. & Nelson, M.R. Measurement and classification of retinal vascular tortuosity. *Int J Med Inform* **53**, 239–252 (1999).
 143. Grisan, E., Foracchia, M. & Ruggeri, A. A novel method for the automatic grading of retinal vessel tortuosity. *IEEE Trans Med Imaging* **27**, 310–319 (2008).
 144. Aghamohamadian-Sharbat, M., Pourreza, H.R. & Banaee, T. A Novel Curvature-Based Algorithm for Automatic Grading of Retinal Blood Vessel Tortuosity. *IEEE J Biomed Health Inform* **20**, 586–595 (2016).
 145. Trucco, E., Azegrouz, H. & Dhillon, B. Modeling the tortuosity of retinal vessels: does caliber play a role? *IEEE Trans Biomed Eng* **57**, 2239–2247 (2010).
 146. Khansari, M.M., O'Neill, W., Lim, J. & Shahidi, M. Method for quantitative assessment of retinal vessel tortuosity in optical coherence tomography angiography applied to sickle cell retinopathy. *Biomed Opt Express* **8**, 3796–3806 (2017).
 147. Kylstra, J.A., Wierzbicki, T., Wolbarsht, M.L., Landers, M.B., 3rd & Stefansson, E. The relationship between retinal vessel tortuosity, diameter, and transmural pressure. *Graefes Arch Clin Exp Ophthalmol* **224**, 477–480 (1986).

148. Stanton, A.V. et al. Vascular network changes in the retina with age and hypertension. *J Hypertens* **13**, 1724–1728 (1995).
149. King, L.A., Stanton, A.V., Sever, P.S., Thom, S.A. & Hughes, A.D. Arteriolar length-diameter (L:D) ratio: a geometric parameter of the retinal vasculature diagnostic of hypertension. *J Hum Hypertens* **10**, 417–418 (1996).
150. Tapp, R.J. et al. Impact of size at birth on the microvasculature: the Avon Longitudinal Study of Parents and Children. *Pediatrics* **120**, e1225–1228 (2007).
151. McCormick, I.J. et al. Retinal vessel tortuosity in response to hypobaric hypoxia. *High Alt Med Biol* **13**, 263–268 (2012).
152. Tomita, Y. et al. Long-term in vivo investigation of mouse cerebral microcirculation by fluorescence confocal microscopy in the area of focal ischemia. *J Cereb Blood Flow Metab* **25**, 858–867 (2005).
153. Suñer, I.J. et al. Nicotine increases size and severity of experimental choroidal neovascularization. *Invest Ophthalmol Vis Sci* **45**, 311–317 (2004).
154. Dikalov, S. et al. Tobacco smoking induces cardiovascular mitochondrial oxidative stress, promotes endothelial dysfunction, and enhances hypertension. *Am J Physiol Heart Circ Physiol* **316**, H639–H646 (2019).
155. Sandborn, W.J. et al. Repifermin (keratinocyte growth factor-2) for the treatment of active ulcerative colitis: a randomized, double-blind, placebo-controlled, dose-escalation trial. *Aliment Pharmacol Ther* **17**, 1355–1364 (2003).

8 ACKNOWLEDGEMENTS

First and foremost, I would like to thank my supervisor Prof. Dr. Dr. Knut Stieger for providing me with this precious opportunity to work on this project. I truly appreciate the patience, geniality and confidence that my supervisor has always shown to me during the past four years. All of his advice, ideas, support and guidance through this project, were vital for me to grow as an independent researcher. His enthusiasm about this work and his wealth of knowledge in the field of retina has always inspired me. He is the investigator, mentor, and teacher that I hope to emulate in the future. Additionally, I would like to express my deepest gratitude to PhD Dr. Markus Preising for his constant scientific, technical assistance and guidance.

Secondly, I am extremely grateful to my colleague Baerbel Fuehler. She has provided me huge help on this project. Without her assistance and support, this project would not go deeper and even couldn't be successfully completed.

I sincerely appreciate the kind help from my colleagues Annabella Janise, Tobias Wimmer, for their patience and guidance and unfailing help during the course of my entire study. Furthermore, It is my pleasure to thank my other colleagues Franziska, Christin, Constanze, Dr. Brigitte Muller, Maria, Bettina, Kerstin and Fatimah for their friendly help and support.

I am really grateful to Prof. Dr. Norbert Weissmann and Dr. Stefan Hadzic from Excellence Cluster Cardio-Pulmonary Institute (CPI) of Justus Liebig University in Giessen, for their generously providing animal tissues and timely guidance and assistances.

I want to say thanks to my good friend Dr. Ming Wang. His encouragement and nice suggestions had provided me with the motivation to move forward and let me find the direction of strive.

In the end, it is a great opportunity to express my deepest gratitude and love to my husband Dr. Longcheng Hong. He has guided me to find the joy from the academic research and then love it deeply. He provided me firm encouragement when I was in

the most difficult time. My husband is the most strong backing of my life. A warm thank you to my sweet daughter Bao Hong, for her warm companionship as well as the unfavorable help at my work. Undoubtedly, she is the driving force for my struggle forever.

Furthermore, I would not be here today without the unconditional love and support from my parents and family, friends, and mentors, who have encouraged and motivated me all the time. Thank you all!

Der Lebenslauf wurde aus der elektronischen Version der Arbeit entfernt.

The curriculum vitae was removed from the electronic version of the paper.

10 LIST OF PUBLICATIONS

1. Publication originally from this thesis

- [1] **Feng Wang**, Stefan Hadzic, Elsa T. Roxlau, Baerbel Fuehler, Annabella Janise-Libawski, Tobias Wimmer, Bo Lei, Shao-Wei Li, Norbert Weissmann, Knut Stieger. Retinal tissue develops an inflammatory reaction to tobacco smoke and electronic cigarette vapor in mice. *J Mol Med.* **2021**, <https://doi.org/10.1007/s00109-021-02108-9>.
- [2] **Feng Wang**, Stefan Hadzic, Elsa T. Roxlau, Baerbel Fuehler, Annabella Janise-Libawski, Tobias Wimmer, Shao-Wei Li, Norbert Weissmann, Knut Stieger. Does Fgf10-overexpression have a protective effect on retinal tissue in mice exposed to smoke? (Under preparation).

2. Other publications


- [1] **Feng Wang**[†], Qiu-Mei Li[†], Zhe-Ming Wu, Zhen Liu, Chuan Zhan, Bing-Heng Chen, Jing Sima, Knut Stieger, Shao-Wei Li. Trifocal diffractive intraocular lens implantation in patients after previous corneal refractive laser surgery for myopia. *BMC Ophthalmol.* **2020**; 2020(20):293.
- [2] **Feng Wang**, Tao Zhang, Yan Wei Kang, Jing Liang He, Shi-Ming Li, Shao-Wei Li. Endothelial keratoplasty versus repeat penetrating keratoplasty after failed penetrating keratoplasty: A systematic review and meta-analysis. *PLoS ONE* **2017**, 12(7): e0180468.
- [3] Tao Zhang, Chang Liu, Jingliang He, Yanwei Kang, **Feng Wang**, Shaowei Li. Cornea guttate associated with special phenotypic variants of granular corneal dystrophy type 2 in a Chinese family. *Eur J Ophthalmol.* **2020**; 30(3); 469–474.

11 EHRENWÖRTLICHE ERKLÄRUNG

Ich erkläre: Ich habe die vorgelegte Dissertation selbständig und ohne unerlaubte fremde Hilfe und nur mit den Hilfen angefertigt, die ich in der Dissertation angegeben habe. Alle Textstellen, die wörtlich oder sinngemäß aus veröffentlichten oder nicht veröffentlichten Schriften entnommen sind, und alle Angaben, die auf mündlichen Auskünften beruhen, sind als solche kenntlich gemacht. Bei den von mir durchgeführten und in der Dissertation erwähnten Untersuchungen habe ich die Grundsätze guter wissenschaftlicher Praxis, wie sie in der „Satzung der Justus-Liebig-Universität Giessen zur Sicherung guter wissenschaftlicher Praxis“ niedergelegt sind, eingehalten.

I declare that I have completed this dissertation single-handedly without the unauthorized help of a second party and only with the assistance acknowledged therein. I have appropriately acknowledged and referenced all text passages that are derived literally from or are based on the content of published or unpublished work of others, and all information that relates to verbal communications. I have abided by the principles of good scientific conduct laid down in the charter of the Justus-Liebig-University of Giessen in carrying out the investigations described in the dissertation.

Giessen, den



Feng Wang